CNWRA 94-010

REVIEW OF DEGRADATION MODES OF ALTERNATE CONTAINER DESIGNS AND MATERIALS

Prepared for

Nuclear Regulatory Commission
Contract NRC-02-93-005

Prepared by

Center for Nuclear Waste Regulatory Analyses
San Antonio, Texas

April 1994

CNWRA 94-010

REVIEW OF DEGRADATION MODES OF ALTERNATE CONTAINER DESIGNS AND MATERIALS

Prepared for

Nuclear Regulatory Commission
Contract NRC-02-93-005

Prepared by

Narasi Sridhar, Gustavo A. Cragnolino
Darrell S. Dunn, and Hersh K. Manaktala

Center for Nuclear Waste Regulatory Analyses
San Antonio, Texas

April 1994

PREVIOUS REPORTS IN SERIES

Number	Name	Date Issued
CNWRA 91-004	A Review of Localized Corrosion of High-Level Nuclear Waste Container Materials—I	April 1991
CNWRA 91-008	Hydrogen Absorption and Embrittlement of Candidate Container Materials	June 1991
CNWRA 92-021	A Review of Stress Corrosion Cracking of High-Level Nuclear Waste Container Material—I	August 1992
CNWRA 93-003	Long-Term Thermal Stability of High-Level Nuclear Waste Container Materials—I Thermal Stability of Alloy 825	February 1993
CNWRA 93-004	Experimental Investigations of Localized Corrosion of High-Level Waste Container Materials	February 1993
CNWRA 93-014	A Review of the Potential for Microbially Influenced Corrosion of High-Level Nuclear Waste Containers	June 1993

ABSTRACT

Issues related to the performance of alternate container materials, including materials currently being considered for multipurpose canisters (MPCs), are reviewed in this report. The MPC is being considered to be a completely sealed canister containing spent fuel bundles that can be transferred within overpacks from the plants through intermediate storage sites to the eventual disposal site. Hence, the structural integrity of the MPC is important. The mechanical integrity of the MPC materials, especially in the welds, can be impaired due to embrittlement under long-term exposure to temperatures of 200–300 °C due to the precipitation of α' and σ phases. Currently, there are insufficient data to quantitatively predict the extent of the embrittlement. The issues related to the performance of disposal overpacks vary depending upon the class of materials. Carbon steel overpacks can suffer from embrittlement due to grain boundary segregation of phosphorus. Type 316L stainless steel (SS) and alloy 825 overpacks can be embrittled due to σ and Laves phase precipitation. These embrittlement kinetics can be accelerated by local plastic deformation or by welding-induced segregation. The near-field environment in the proposed repository at Yucca Mountain is uncertain, but may involve a wide range of chloride concentration through evaporative concentration of aqueous environment contacting the container. In aqueous environments and under mildly alkaline conditions, carbon steel can suffer from localized corrosion and stress corrosion cracking (SCC). Hydrogen generated from corrosion can cause embrittlement of carbon steel or cast iron due to either dissolved hydrogen directly or hydrogen reacting with carbides to form methane. Microbial action can be increased by the presence of carbon steel and may promote either localized corrosion or increased generation of hydrogen. The galvanic coupling between carbon steel and a corrosion resistant alloy, such as type 316L SS, can be beneficial in terms of the localized corrosion resistance of the latter. However, hydrogen embrittlement of the corrosion resistant alloy, especially the high-nickel alloys such as alloy C-4, is a possibility due to cathodic polarization. Specific areas that need further investigation are enumerated.

CONTENTS

CONTENTS (cont'd)

FIGURES

FIGURES (cont'd)

FIGURES (cont'd)

TABLES

ACKNOWLEDGMENTS

This report was prepared to document work performed by the Center for Nuclear Waste Regulatory Analyses (CNWRA) for the Nuclear Regulatory Commission (NRC) under Contract No. NRC-02-93-005. The activities reported here were performed on behalf of the NRC Office of Nuclear Regulatory Research, Division of Regulatory Applications. The report is an independent product of the CNWRA and does not necessarily reflect the views or regulatory position of the NRC. The authors acknowledge the critical reviews provided by F. Lyle, P. Nair, and B. Sagar, the editorial assistance of C. Cudd, C. Gray, and B. Garcia, and the work of A. Ramos throughout the preparation of the document.

EXECUTIVE SUMMARY

The list of candidate container materials for disposal of high-level nuclear waste (HLW) has undergone significant changes over the past 2 to 3 yr. In the Site Characterization Plan (SCP) of the U.S. Department of Energy (DOE), six metallic alloys were identified as candidate materials for single-wall containers. These alloys included three austenitic alloys and three copper-base alloys.The reference single-wall container concept identified in the SCP has been revised in the present Advanced Conceptual Design (ACD) phase to a multiwall concept in which a thin-walled corrosion resistant alloy is surrounded loosely by a thick-walled corrosion allowance material. The candidates for the corrosion resistant inner container are type 316L stainless steel (SS), alloy 825 (22 percent Cr, 42 percent Ni, 3 percent Mo, 2 percent Cu), alloy C-4 (62 percent Ni, 16 percent Cr, 16 percent Mo), and titanium (grade 12). The leading candidate for the corrosion allowance outer container is carbon steel, although no grade has been specified as yet. A more recent change in the DOE strategy with respect to spent fuel handling is the use of multipurpose canisters (MPCs) as the baseline design for waste package. The MPC is conceived to be a container made of an austenitic alloy, either type 316L SS or alloy 825, that will be loaded with spent fuel and seal welded at the plant site. The design is expected to minimize radiation exposure to workers during handling in the transportation, interim storage, and eventual disposal systems. The MPC will be placed in suitable overpacks depending upon the functions it has to perform during a particular stage in the HLW system. In the transportation and interim storage stages, the overpacks are conceived to be made of thick-walled steel or cast iron. In the disposal stage, the overpack could be either a thick steel, single-wall container or a multiwall container as discussed previously. As an alternative to the MPC, which will have the same overpack throughout the three stages are also under consideration. Currently, the MPC is the more vigorously championed of the two alternatives. The purpose of this report is to examine the issues related to the performance of candidate materials for these proposed alternative designs. While the focus is the performance in the repository, the possibilities of microstructural changes in the MPC prior to disposal are also considered, as they can influence the containment capabilities. In the current report, the performance of MPC internals such as the basket is not considered. Criticality conditions are also not considered in this report.

MECHANICAL PROPERTIES

The mechanical integrity of the MPC and overpack made from type 316L SS is dictated by the phase transformations in the weld metal ferrite. The ferrite in the weld metal can transform to α', a brittle, high-chromium intermetallic in the 200–300 °C temperature range. In cast SS components used in reactor systems, which possess higher ferrite content than weldments of type 316L SS, long-term aging in the range of 400–500 °C has been to shown to result in a reduction in fracture toughness. Similar data on type 316L weldments are not currently available. Long-term exposure of type 316L SS base metal to temperatures in the range of 500–700 °C can result in the formation of σ, χ, and Laves phases. Although these temperatures are higher than the maximum allowable temperature (350 °C) of the waste package, the storage and disposal time periods are much longer than the current reactor experience base. In the case of alloy 825, a potential embrittling mechanism is the formation of σ phase. However, insufficient data exist at present to draw any conclusions regarding the mechanical integrity of an MPC or overpack made from this alloy. The mechanical properties of the C-4 class of alloys, a distant possibility at this time for overpacks, can be affected by the precipitation of long-range ordered Ni_2Cr regions. While this is not expected to affect the properties of annealed alloys at repository temperatures for hundreds of years, it can be accelerated in welded regions or local regions of plastic deformation that can occur during repository operation.

In the case of carbon steel overpacks, the DOE currently has not specified a grade. However, pressure vessel grades of steel have been shown to embrittle upon exposure to temperatures in the range of 375–600 °C due to the segregation of phosphorus to the grain boundaries. This is exacerbated by large grains found in the heat affected zone (HAZ) of a weld. Since phosphorus (P) is present in most commercial grades of wrought and cast steels, this is a potential failure mode that deserves to be investigated in more detail. Of special importance in this regard is the tremendous variability in the fracture toughness reported for components made from the same nominal grade of pressure vessel steel. The weathering steels typically have higher P, and, hence the embrittlement due to P segregation may become even more significant than for the pressure vessel grades.

ENVIRONMENTAL EFFECTS

In terms of environmental effects, the disposal overpacks must be considered first as they form the primary barrier to groundwater contact with the spent fuel. The outer steel or cast iron overpack is nominally considered to be a corrosion allowance type of material with predictable uniform corrosion rates. However, under mildly alkaline conditions that may be present at the Yucca Mountain repository site, localized corrosion may occur. Current information suggests that the localized corrosion may broaden with time and not propagate deeply as in the case of the more corrosion resistant materials. Stress corrosion cracking (SCC) is another possibility in the presence of bicarbonate and carbonate and under mildly oxidizing conditions. However, if the formation of high-concentration brine due to evaporative processes is projected, the tendency toward localized corrosion and SCC will be mitigated. SCC of pressure vessel steels has also been shown to occur in high purity, oxygenated water in the temperature range of 100–288 °C, with the crack velocity decreasing to a low value at 100 °C. There is a lack of data for SCC in these environments at repository relevant temperatures and for microstructural conditions arising from castings and welds. Hydrogen induced cracking of the carbon steel is considered both in terms of lattice hydrogen (hydrogen embrittlement) and hydrogen reaction with carbon (hydrogen attack). The hydrogen embrittlement tendency decreases with an increase in temperature and may not be an important failure mode at repository temperatures, unless high hydrogen concentrations are shown to occur. The hydrogen attack, however, may be important because it does not require external stresses. Current data, which involve high hydrogen fugacities and durations of up to 10,000 hr, are inadequate to judge whether hydrogen attack can occur on a given grade of steel in the repository environment. The potential for hydrogen attack may be further enhanced in cast iron or ductile iron because of the higher carbon activity.

The localized corrosion of type 316L SS and alloy 825 overpacks can be predicted in terms of their repassivation potential in comparison to the corrosion potential. Several field and laboratory studies are cited which indicate the applicability of repassivation potential generated by short-term tests for longer-term prediction. If a concentrated brine is predicted to occur at the surface, alloy 825 may not be significantly better in localized corrosion resistance than type 316L SS. However, galvanic coupling with a carbon steel outer barrier may be beneficial to the localized corrosion resistance of the corrosion resistant alloys such as type 316L SS. C-4 type alloys are more resistant to localized corrosion than alloy 825, although concentrated $MgCl_2$ brine tests for long time periods indicate a possibility of localized corrosion in this environment. The repassivation potentials measured in the laboratory do not correspond to the ranking of these C-4 type alloys in long-term field performance. Hence, the technique of repassivation potential measurement for the C-4 type alloys will need to be evaluated further.

Type 316L SS is well known to undergo SCC in chloride containing environments. Alloys 825 and C-4 have significantly higher resistance to SCC due to their higher Ni content. However, there is insufficient data to eliminate SCC as a failure mode for these alloys. The high nickel alloys, such as alloy C-4, have been shown to fail by hydrogen embrittlement, especially when they have been aged at low temperatures (200–500 °C) to induce long-range ordering. Hydrogen embrittlement occurs more at low temperatures than at repository temperatures. Alloy 825 is more resistant to hydrogen embrittlement than alloy C-4. Hydrogen attack is less likely for these alloys than for carbon steel because of the stability of carbides.

Based on the review to date, recommendations for further study are made including: (i) evaluation of the low-temperature embrittlement of type 316L SS and alloy 825 due to intermetallic precipitation, (ii) evaluation of the embrittlement susceptibility of carbon-steel due to P segregation during storage and disposal, (iii) a determination of hydrogen concentration due to corrosion reactions as well as galvanic effects on both carbon steel and corrosion resistant alloys, (iv) evaluation of the potential for localized corrosion and SCC of carbon steel, (v) evaluation of the possibility of hydrogen induced cracking of carbon steel and corrosion resistant alloys under repository conditions, and (vi) investigations of the effect of high temperatures on the type and extent of microbial activity and the resultant influence on corrosion.

1 INTRODUCTION

One of the objectives of the Integrated Waste Package Experiments (IWPE) research project is to assist the Nuclear Regulatory Commission (NRC) in the assessment of waste package materials and designs selected by the U.S. Department of Energy (DOE), in terms of their compliance with the regulatory requirements set out in 10 CFR 60.112 and 60.113. Of special importance in the assessment of waste package designs and materials is the performance requirement for containment stated in 10 CFR 60.113(a)(ii)(A). In evaluating compliance with this performance requirement, several key technical uncertainties (KTUs) have been identified including: (i) prediction of criticality events in the waste packages; (ii) prediction of release path parameters (such as size, shape, and distribution of penetrations of waste packages); (iii) extrapolation of short-term laboratory and prototype test results to predict long-term performance; (iv) prediction of thermomechanical effects on the performance of waste packages; and (v) prediction of environmental effects on the performance of waste packages. Several of these KTUs are being addressed in the IWPE project for the candidate alloys cited in the DOE Site Characterization Plan (SCP) (U.S. Department of Energy, 1988). The SCP design consists of a single-wall container of 12.5 mm (0.5 in.) thickness placed vertically in a partially lined borehole with an air gap between the container and the borehole. The candidate container materials consist of three Fe-Ni-Cr-Mo alloys (types 304L and 316L stainless steel (SS), and alloy 825) and three copper-based alloys (oxygen-free copper, Cu-30 percent Ni, and Cu-8 percent Al bronze). The nominal chemical compositions of these alloys are shown in Table 1-1. Among the candidate alloys, alloy 825 has been considered to be the most promising (Farmer et al., 1988) for the proposed repository at Yucca Mountain.

1.1 ALTERNATE CONCEPTUAL DESIGNS & MATERIALS

Minimization of worker exposure to radiation during the overall waste handling process, consideration of longer-life containers, and the approaching deadlines for waste acceptance by the DOE have spurred alternate waste package conceptual designs (Short et al., 1992). In the Advanced Conceptual Design (ACD) phase, three alternate design concepts have been discussed:

- Robust container concept (Doering, 1993)
- Multipurpose canister (MPC) concept (U.S. Department of Energy, 1993a,b)
- Multipurpose unit (MPU) concept (Hollaway et al., 1993)

The robust container concept is shown in Figure 1-1. It consists of a 1.25-cm (0.5-in.) thick inner container encased in a 8.9-cm (3.5-in.) thick outer container. While the design shown in Figure 1-1 is visualized in terms of containing a large MPC, similar double-container designs can also be used to contain bare spent fuel assemblies inside a SS basket. The MPC is the current baseline design.

The MPC has been conceived in terms of two reference designs: (i) a large MPC shown in Figure 1-2 has an estimated total weight of 125 metric tons and can contain up to 21 pressurized water reactor (PWR) fuel assemblies or 40 boiling water reactor (BWR) fuel assemblies, and (ii) a medium MPC that has an estimated total weight of 75 metric tons with a maximum capacity of 12 PWR/24 BWR assemblies. Additionally, for reactor sites that are unable to handle the above weights, a small, 25-ton MPC, with a capacity for 2 PWR/4 BWR assemblies, has also been discussed. The current proposed design of the MPC consists of a SS canister 1.46 m (57.63 in.) in outer diameter (O.D.), 5 m (200.5 in.) long, and 3.5-cm (1.375-in.) wall thickness. These design details should be viewed as provisional, since

Table 1-1. Nominal chemical compositions of candidate container alloys in the DOE SCP design (U.S. Department of Energy, 1988)

Alloy	UNS No.	Weight Percent						
		C, max.	Cr	Cu	Fe	Mo	Ni	Others
304L SS	S30403	0.03	19.0	—	Bal.	—	10.0	Mn: 2.0 max. S: 0.03 max. P: 0.045 max.
316L SS	S31603	0.03	17.0	—	Bal.	—	12.0	Mn: 2.0 max. S: 0.03 max. P: 0.045 max.
Alloy 825	N08825	0.05	21.5	2.0	29.0	3.0	42.0	Ti: 1.0 max. S: 0.03 max. Mn: 1.0 max.
CDA 102	C10200	—	—	99.95 min.	—	—	—	—
CDA 715	C71500	—	—	Bal.	0.7	—	31	—
CDA 613	C61300	—	—	Bal.	2.5	—	—	Al: 6.8 Sn: 0.35

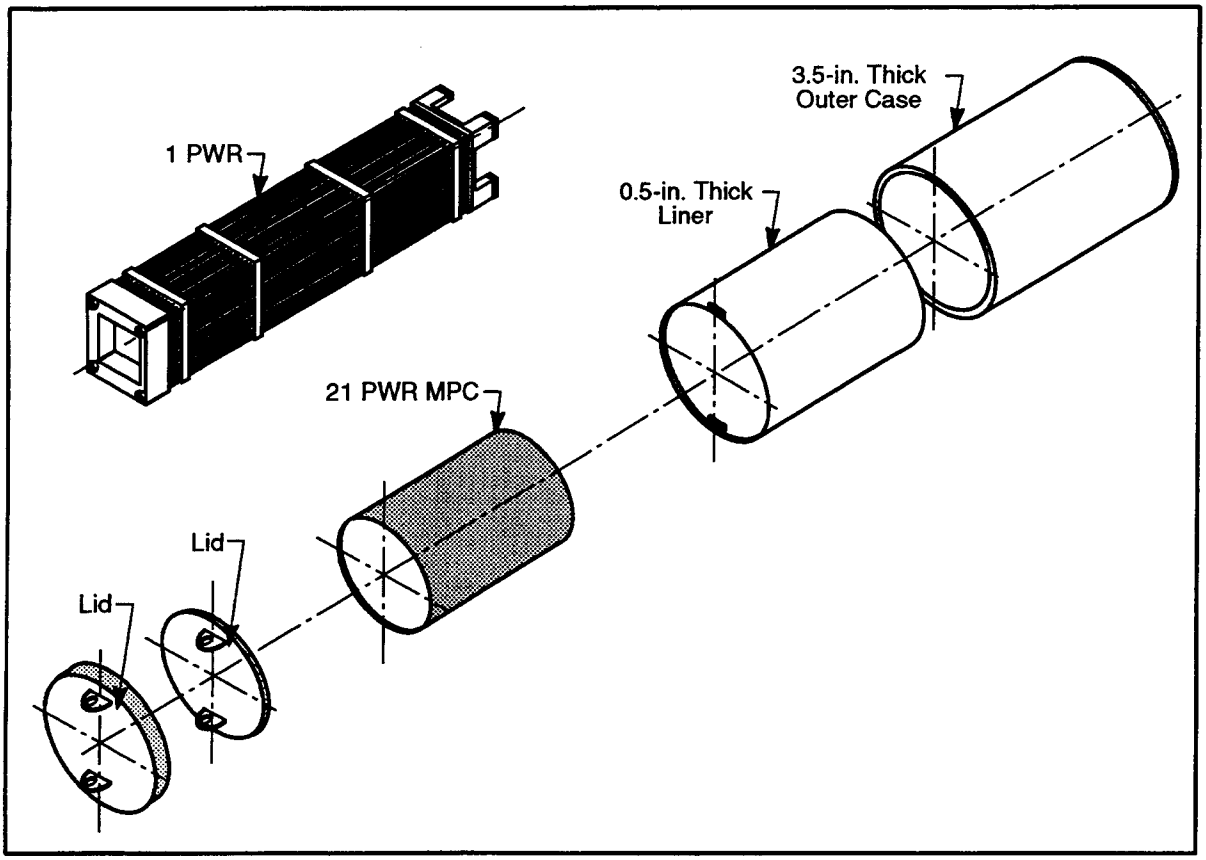

Figure 1-1. Schematic diagram of a proposed design for robust waste package as a standalone container or a disposal overpack for a large MPC containing 21 PWR assemblies (U.S. Department of Energy, 1993b)

detailed specifications may change as a result of a new request for proposal (RFP) that will be issued by DOE. While the details of the processing sequence by which the canister body will be manufactured are not available, one method of fabricating large-diameter vessels such as these is three-roll forming (ASM International, 1988).The combination of cylinder height and plate thickness involved in the MPC would require intermediate annealing operations (ASM International, 1988). The processing is usually completed by longitudinal welding and post-weld annealing. The ends of the canister consist of a thick steel shield plug, a SS cover plate, and a SS closure head. Automated welding has been chosen to be the closure method of choice for the canister ends (U.S. Department of Energy, 1993b). However, details of the closure technique in terms of welding process, welding parameters, and filler metal composition have not been presented. The spent fuel assemblies will be contained in baskets made of SS sheet with a neutron absorber such as borated aluminum sandwiched between the basket walls.

The MPU designs are much more preliminary in nature. The proposed MPU design (Hollaway et al., 1993; U.S. Department of Energy, 1993b) shown in Figure 1-3 consists of a 7.6-cm (3-in.) thick inner canister made of alloy 825 surrounded by a ductile cast iron outer container that is 25.4 cm (10 in.) thick. The large MPU, weighing 120 tons, is designed to contain 16 PWR/37 BWR assemblies. Alternatively, a small MPU, weighing 25 tons and containing 2 PWR/4 BWR assemblies, has also been proposed for those sites that cannot handle the large MPUs.

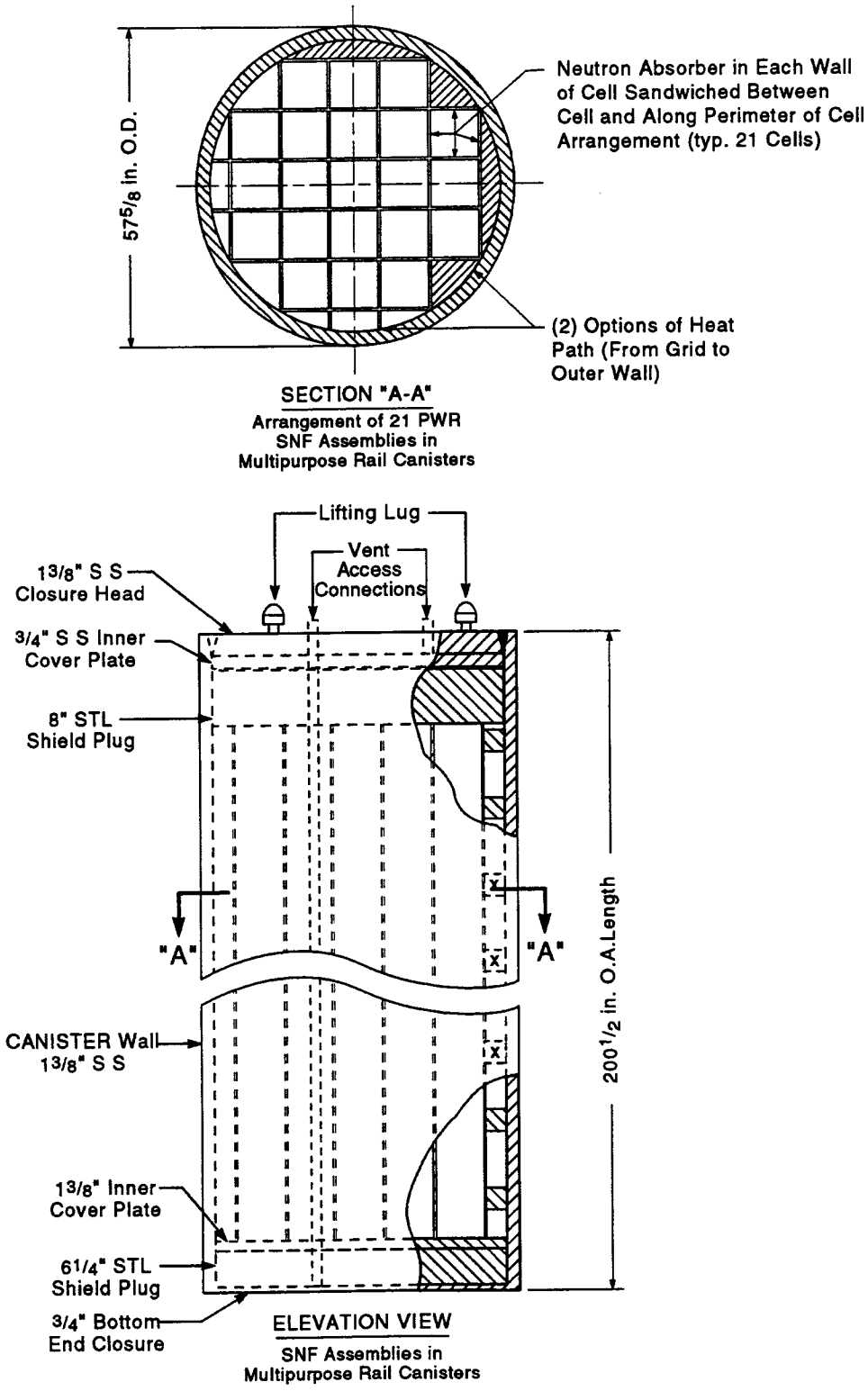

Figure 1-2. Schematic drawing of the currently proposed large MPC that can contain 21 PWR assemblies (U.S. Department of Energy, 1993b)

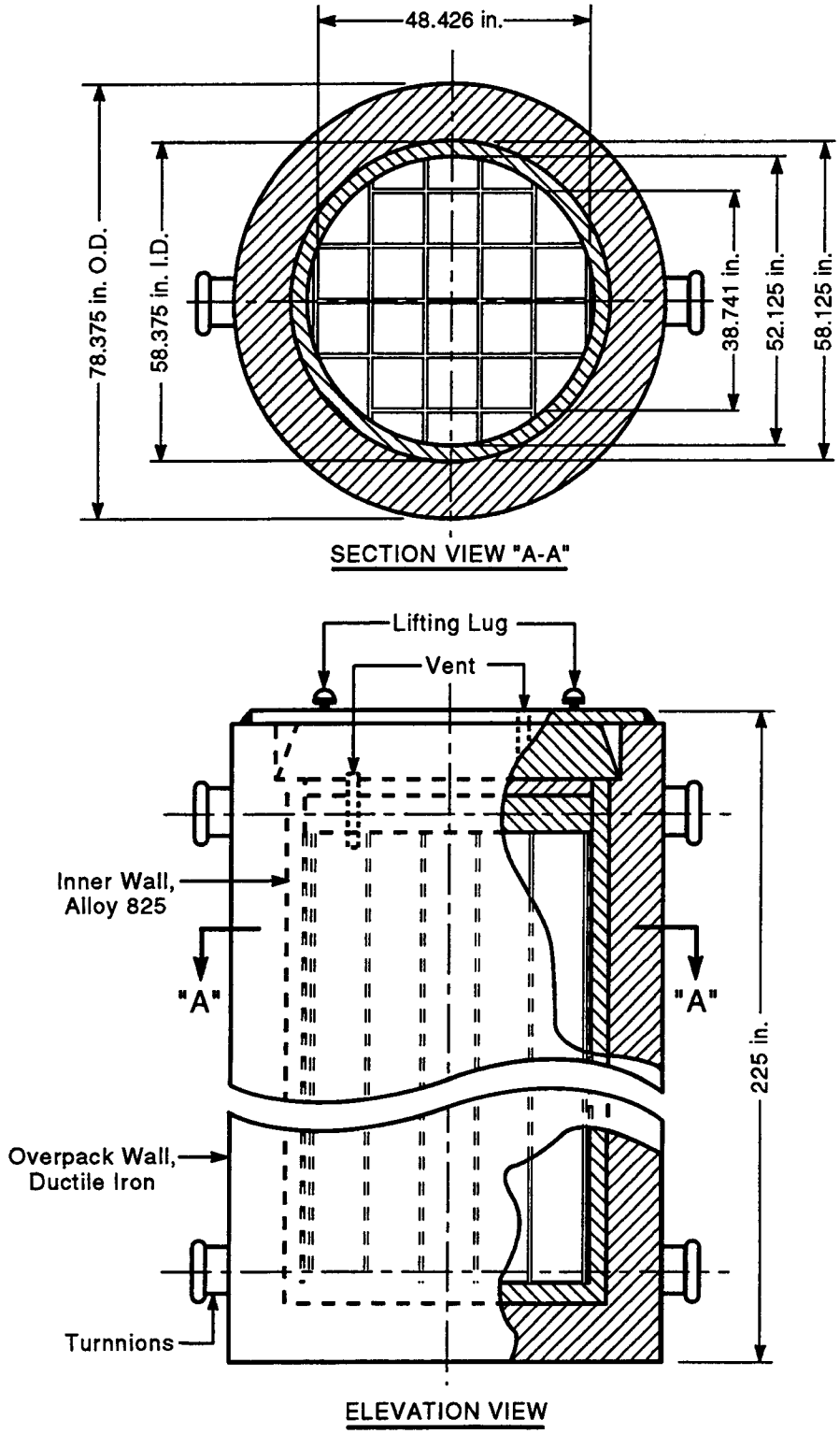

Figure 1-3. Schematic drawing of the currently proposed large MPU that can contain 16 PWR assemblies (U.S. Department of Energy, 1993b)

The list of candidate materials for these concepts is still evolving. The nominal compositions of the proposed materials for the various design concepts, which include some of the SCP alloys, are shown in Table 1-2. It must be emphasized that the list of materials shown in Table 1-2 for MPCs pertains only to the innermost canister that is transferred from the spent-fuel pool through the transportation and monitored retrievable storage (MRS) systems to the geologic disposal system. This canister is then proposed to be placed in suitable disposal containers for geologic disposal (U.S. Department of Energy, 1993a). In the evaluation of alternate concepts (U.S. Department of Energy, 1993b), the disposal container was conceived to be a double-wall construction of alloy 825 inner wall and carbon steel outer wall.

The focus of the IWPE research project is the evaluation of waste packages for disposal. It must also be noted that the DOEs waste package design is still evolving and contradictory information can be found in the published literature. For example, the MPU concept is discussed by Hollaway et al. (1993) as involving a thin, corrosion resistant inner barrier made of either type 316L SS or alloy 825 surrounded by a thick outer barrier of a corrosion allowance material such as ductile iron. In contrast, the MPU discussed as an alternative concept in the DOE report (U.S. Department of Energy, 1993b) depicts a four-layer structure consisting of an innermost container of type 316L SS (as in the MPC concept), a 0.375 in. alloy 825 container, an 8.375-in. third container of carbon steel, and a SS outermost structure for neutron absorption.

The alternate concepts also entail higher thermal loading, since 12–21 PWR or 24–40 BWR spent fuel bundles are planned to be contained in each waste package (U.S. Department of Energy, 1993b), depending on the burn-up credit for the time spent in the pool. This is in comparison to the SCP design involving 3–6 PWR or 7–14 BWR assemblies per container. Higher thermal loading is argued to result in extended dry conditions (< 10 percent saturation) (Buscheck and Nitao, 1992). Because of the proposed size of the disposal container, the emplacement concept has changed from vertical borehole to horizontal drift emplacement. Instead of an air gap between the container and the borehole wall proposed in the SCP design, crushed tuff backfill is proposed for the new emplacement configurations.

In evaluating the alternate container materials, the same systematic approach that was suggested (Sridhar et al., 1993a) for the analysis of SCP design material can be adopted. This approach consists of the following steps (Staehle, 1991):

(i)	Environmental description
(ii)	Material definitions
(iii)	Failure mode and submode definitions
(iv)	Determination of the occurrence of various failure mode/submode depending upon the environmental definitions
(v)	Failure criteria
(vi)	Statistical description of failure
(vii)	Accelerated testing
(viii)	Performance prediction
(ix)	Feedback from component performance during the monitoring period
(x)	Modification and optimization of design, materials, environment, operations based on the feedback

In this report, only steps (ii), (iii), and (iv) will be considered for the alternate materials. Step (i), a description of the near-field environment, is beyond the scope of the current document. However, various types of processes that can alter the near-field environment are described briefly.

Table 1-2. Nominal chemical compositions of candidate container alloys in alternate conceptual designs. For simplicity only, important alloying elements are listed.

Conceptual Design	Alloy	UNS No.	Weight Percent						
			C, max.	Cr	Cu	Fe	Mo	W	Ni
MPC[1] (Transportation and disposal outer cask materials not included)	316L SS	S31603	0.03	17.0	—	Bal.	—		12.0
	Alloy 825	N08825	0.05	21.5	2.0	29.0	3.0		42.0
MPU[2]	Alloy 825, inner wall	N08825	0.05	21.5	2.0	29.0	3.0		42.0
	Ductile Iron, outer wall	—	3.3	—	—	Bal. (Si:2.5)	—		—
Robust Waste Package[3] (only inner container materials shown)	Alloy 825	N08825	0.05	21.5	2.0	29.0	3.0		42.0
	Alloy C-276*	N10276	0.01	15.5		5.5	16.0	4.0	57.0
	Alloy C-4	N06455	0.01	16.0	—	3.0 max	15.5		64.5
	Alloy C-22*	N06022	0.015	21.5		3.0	13.0	3.0	56.0
	Ti-12 (Balance Titanium)	—	0.04	—	—	0.3 max	0.3		0.8

[1] — U.S. Department of Energy, 1993a; [2] — Holloway et al., 1993; [3] — Doering, 1993
* — Alloys reviewed here because of similarity to alloy C-4

1.2 ENVIRONMENTAL CONSIDERATIONS

It is well known that water extracted from the J-13 well located in the saturated zone of the Yucca Mountain site, has been used as the reference groundwater for experimental studies (Glassley, 1990), assuming that its composition is close to that of the vadose water in the unsaturated zone in the Topopah Spring tuff. However, the J-13 water has a range of composition for various species (Glassley, 1990) in which the prevailing ionic species are HCO_3^- and Na^+. Other anions, such as Cl^-, F^-, SO_4^{2-}, and NO_3^-, are present at lower concentrations. The silicon content of the water, in the form of silicic acid, is relatively high. Waters from other wells in the vicinity of Yucca Mountain have similar chemical compositions, but differences in pH and ion concentration ratios are considered to be significant (Kerrisk, 1987).

Of greater importance to all localized corrosion processes is the evolution of the environmental composition as a result of the emplacement of the waste packages in the repository. These changes in the environmental composition can occur by the following processes.

- **Rock-water interactions over long periods of time and modified by the increase in temperature**: Modeling efforts in this area (Pabalan and Murphy, 1991) have shown that, as the temperature increases, the bicarbonate concentration will decrease due to CO_2 volatilization resulting in a concomitant increase in pH. In many of the reported SCC experiments, J-13 water conditioned by contact with crushed tuff at the test temperature has been used. It can be presumed, however, that the concentration should be extremely dependent on the mineralogical composition of the rock and the temperature and also, unless equilibrium conditions were rapidly established, on the duration of the conditioning process and the volume ratio of the rock to the water. The evolution of J-13 water in contact with crushed tuff at 50 and 90 °C and under γ-irradiation was evaluated experimentally by Westerman et al. (1987). The autoclaves were continuously purged with air and were open to the atmosphere via 9 m of outlet tubing. After each period of testing, the solution was replaced with fresh J-13 water. Fresh rock was replaced after each test period up to 10 months and not thereafter. Unfortunately, no systematic variations in the concentrations of any species were found. The pH at the end of each period was higher than the initial pH of the J-13 water reported (7.1–7.6), which is consistent with the model predictions (Pabalan and Murphy, 1991). The Cl^- and SO_4^{2-}were generally much higher than found in the initial J-13 water that was used by the investigators. These results were corroborated by the measurement of high conductivity at the end of each period. The authors reported that the measurements of high ionic concentrations were reproducible.

  A further confirmation of the increase in concentration of ionic species due to rock-water interactions has been presented by Abraham et al. (1986). When synthetic J-13 water was heated in the presence of crushed tuff to boiling temperatures (100 °C) under refluxing conditions, it was shown (Abraham et al., 1986) that the concentration of several anions and cations, such as SO_4^{2-}, NO_3^-, Cl^-, Na^+, K^+, and Ca^{2+}, increases significantly with time. Detailed solution analyses were carried out after various time periods of testing. Interestingly, reaction of boiling distilled water with tuff produced an initial increase in Cl^- to about 160 ppm which, upon further treatment with new distilled water, decreased to a steady value of about 20 ppm, more than three times the 6-ppm concentration reported nominally for J-13 water.

In contrast to the above experiments, a review of rock-water interaction experiments performed at Lawrence Livermore National Laboratories (LLNL) (Knauss et al., 1990; Oversby, 1985; Glassley, 1990) indicated no significant changes from the initial J-13 values for chloride, fluoride, nitrate, and sulfate. These experiments were conducted as essentially closed systems. In the results reported by Oversby (1985), the pH increased to about 9 after 70 days at 150 °C, whereas, a slight decrease in the dissolved bicarbonate content was observed. This was attributed to the gradual exsolution of CO_2 from the solution through the pores in the polytetrafluoroethylene (PTFE) liner. Knauss et al. (1990) used an impermeable gold-bag, and, hence, did not observe any increase in pH during the course of their experiments. A slight decrease in the pH (measured at 25 °C) was noted and attributed to the precipitation of Ca and Mg carbonates which have retrograde solubility. The most significant compositional change was the dissolution of silicon from the tuff.

- **Changes due to occluded regions such as crevices**: It has been well established that concentration of anionic species such as chloride can increase greatly in regions such as crevices, while pH can decrease due to hydrolysis of cationic species such as Fe^{2+}, Cr^{3+}, and Ni^{2+} (Turnbull, 1983; Alavi and Cottis, 1987; Luo et al., 1992; Sridhar and Dunn, 1994). Additionally, highly reducing conditions may be created in occluded regions due to the rapid depletion of oxygen and slow rediffusion from the bulk. The radiolysis reactions in acidic reducing solutions may be significantly different from those in the bulk oxidizing solutions (Spinks and Woods, 1990).

- **Changes due to repeated/episodic evaporation and re-wetting of container**: This process has been modeled recently by Walton (1993), who predicted that a saturated salt solution layer can form on the container surface leading to a stabilization of aqueous conditions well above the boiling point of pure water. Experimental measurements of Beavers et al. (1992) have shown increases in anionic concentrations linearly proportional to the number of boil-down and refill cycles. However the relationship of these procedures to actual conditions in the repository is not clear. Westerman et al. (1987) performed boil-down tests in autoclaves at 200 °C and 1,000 psig with 7 days in liquid and 1 day under dry conditions. The dry period was achieved by reducing the pressure. The reported concentration of chloride and sulfate after 15 and 50 boil-down cycles were higher than initial values, but not high enough in proportion to the number of boil-down cycles if complete evaporation is assumed.

- **Changes due to radiolysis**: The γ dose rate from spent fuel containers is expected to be as high as 0.1 Mrad/hr and, typically, about 0.01 Mrad/hr (Reed and van Konynenburg, 1991). The dose rate from glass waste is expected to be somewhat less, about 0.005 Mrad/hr (van Konynenburg, 1986). Some of the early field evidences of the effects of radiolysis on corrosion and SCC were observed in the Spent Fuel Test—Climax Program (Patrick, 1986). Corrosion of the carbon steel liners exposed to spent-fuel containers and cracking of Ni-Fe extensometer connecting rods were noted. In the latter case, laboratory simulation of SCC of Ni-Fe specimens in groundwater environments was achieved only upon addition of an oxidizing salt, $CuCl_2$. In addition to galvanic effects due to coupling with copper components, it is possible that radiolysis of the groundwater environment increased the concentration of oxidizing species, thus raising the corrosion potential high enough to cause corrosion and cracking.

Experimental investigations of chemical and electrochemical effects of γ-radiation have been reported by van Konynenburg (1986), Glass et al. (1986), Kim and Oriani (1987), and Reed and van Konynenburg (1991). van Konynenburg (1986) interpreted the experimental results related to reaction of various types of glasses with water and water reacted with tuff. The major species present as a result of γ-radiation of water in contact with air were nitrite and nitrate. The ratio of nitrite to nitrate was dictated by the presence of catalytic surfaces such as tuff and ionic species in the water such as bicarbonate. In the absence of tuff rock and ionic species in water, the nitrite/nitrate ratio was close to 1. This is presumably due to the oxidation of nitrite to nitrate by the hydrogen peroxide that is formed in the water as a result of radiolysis. In the presence of catalysts that promote decomposition of hydrogen peroxide, the nitrite concentration increased. While the hydrogen peroxide concentration was not reported, van Konynenburg (1986) speculated that it would have been quite low. Reed and van Konynenburg (1990, 1991) reported that, in a moist-air system (at relative humidities of 15 percent at 90 °C), nitrites and nitrates were the main species as a result of radiolysis and copper specimens under these conditions formed hydrated cupric nitrates. In the 100 percent relative humidity environment, only Cu_2O and CuO were found on copper specimens. Irradiation experiments by Yunker (1990) on various copper alloys under 100 percent relative humidity conditions at 95 °C have resulted in the formation of mainly CuO. Yunker reported estimated concentrations of NO_2^- in the gas phase of moist air mixtures exposed to irradiation but did not report any observation of nitrate corrosion products on copper specimens. Colloidal Fe(III) compounds, thought to be from the reaction of SS vessels with the moist environment, have also been reported in these investigations (van Konynenburg, 1986). In situations where the aqueous phase is predominant (Glass et al., 1986) or where the aqueous phase is in contact with an inert gas such as argon (Kim and Oriani, 1987), the formation of H_2O_2 and O_2 in the solution is more likely, although only indirect evidence for this has been provided. Unfortunately, the effect of radiolysis on environments within occluded regions such as crevices and cracks has not been studied systematically.

- **Changes due to repository construction**: The presence of engine fluids and large amounts of grouting may cause formation of organic acids in the former case and alkaline conditions in the latter. Microbial colonies can either be introduced or promoted due to the presence of nutrients from repository construction (Geesey, 1993).

The foregoing discussion indicates that considerable uncertainty exists concerning the environment adjacent to the waste packages. Therefore, in discussing the performance of alternate waste package concepts and materials, a range of environmental conditions must be considered.

2 CARBON STEEL AND CAST IRON MATERIALS

2.1 THERMAL STABILITY

As mentioned in the previous chapter, carbon steel (either wrought or cast) and ductile cast iron are candidates for use as single-layer overpacks for the disposal of MPC or as part of a multibarrier disposal overpack. This section provides selected background information about carbon steels and ductile iron, chemical compositions, classification of the types of these materials, manufacturing/fabrication parameters affecting cast and wrought product properties, degradation modes relevant to the waste package performance under repository relevant conditions, and, to a lesser extent, issues related to welding of these materials.

Steels are the most widely used category of engineering materials, primarily because they can be manufactured inexpensively in large quantities. They also provide a wide range of mechanical properties from moderate yield strength levels of 200–300 MPa with excellent ductility to yield strengths exceeding 1,400 MPa, and fracture toughness levels as high as 110 $MPa \cdot m^{1/2}$. According to the American Iron and Steel Institute (AISI) (1985, 1986), steel is considered to be carbon steel when no minimum content is specified for chromium, cobalt, niobium, molybdenum, nickel, titanium, tungsten, vanadium, or zirconium, or any other element to be added to obtain a desired alloying effect; when the specified minimum for copper does not exceed 0.40 percent; or when the maximum content specified for any of the following elements does not exceed the percentages noted: [manganese, 1.65; silicon, 0.60; copper, 0.60 (American Iron and Steel Institute, 1985, 1986)]. There are two major groups of alloying elements, those that occupy interstitial sites and those that occupy substitutional sites in the crystal lattice of iron. Figure 2-1 indicates various elements in the periodic table that form substitutional- or interstitial-solid solution with iron.

Commercial plain carbon steels, which are in principle binary alloys of carbon and iron, always contain a large number of both types of alloying elements. Some are added intentionally to produce specific desired properties while others are introduced inadvertently via metal production and processing. Examples of undesirable elements are nitrogen (from air), sulfur (from coke), phosphorous (from ores), and hydrogen (from pickling during processing or moisture from rusted scrap). Steels can be classified by a variety of means depending on: (i) composition, (ii) manufacturing methods, (iii) finishing method, (iv) product form, (v) deoxidation practice, (vi) microstructure, (vii) required strength level, and (viii) quality descriptors. Low-carbon steels contain ≤ 0.30 percent carbon. The largest category of this class of steel is flat-rolled products (sheet or strip) usually in the cold-rolled and annealed condition. The carbon content for these high-formability steels is very low, typically 0.10 percent carbon, with ≤ 0.4 percent Mn. For structural plates and sections, the carbon content could be up to 0.30 percent, with manganese up to 1.5 percent. Medium-carbon steels are similar to low-carbon steels except that the carbon content is in the 0.30–0.60 percent range and the manganese from 0.60–1.65 percent. Increasing the carbon content to ~ 0.5 percent with increase in manganese content allows medium-carbon steels to be used in the quenched and tempered condition. High-carbon steels range in carbon from 0.60–1.00 percent and manganese from 0.30–0.90 percent.

2.1.1 Wrought Steels

At present, the DOE has not specified a particular grade of wrought carbon steel for overpacks. In the past, the AISI 1020 grade of plain carbon steel had been discussed as a likely candidate for

H 1																	He 3
Li 3	Be 2											B 1	C 1	N 1	O 1	F 3	Ne 3
Na 3	Mg 3											AL 2	Si 2	P 2	S 3	CL 3	Ar 3
K 3	Ca 3	Sc 3?	Ti 2	V 2+)	Cr 2+)	Mn 2+)	Fe	Co 2+)	Ni 2+)	Cu 2	Zn 2	Ga 2	Ge 2	As 2	Se 3	Br 3	Kr 3
Rb 3	Sr 3	Y 3?	Zr 2	Nb 2	Mo 2	Tc 2	Ru 2	Rh 2+)	Pd 2+)	Ag 3	Cd 3	In 3	Sn 2	Sb 2	Te 3	I 3	Xe 3
Cs 3	Ba 3	La 3?	Hf 2?	Ta 2	W 2	Re 2	Os 2	Ir 2+)	Pt 2+)	Au 2	Hg 3	Tl 3	Pb 3	Bi 3	Po 3?	At 3	Rn 3
Fr 3	Ra 3	Ac 3?	Th 3?	Pa 3?	U 3	Np 3?	Pu 3?	Am 3?	Cm 3?	Bk 3?	Cf 3?						

1 Interstitial Elements
2 Substitutional Elements
3 Practically No Solubility
+) Complete Solubility at Certain Temperatures.

Figure 2-1. Distribution of various elements in iron. Some of the industrially important alloying elements and impurities are indicated by shaded areas.

containers (McCright, 1988). In the basalt repository program, the American Society for Testing and Materials (ASTM) A216, grade WCA cast steel was examined (Ahn and Soo, 1984; Beavers et al., 1987b) as a candidate container material. Ductile iron has been proposed as a candidate transportation overpack (and possibly storage and disposal overpacks), although it has not been approved by the NRC for this purpose (U.S. Department of Energy, 1993b). If wrought steels are specified for overpacks, it may be one of a number of pressure vessel grades of steel because of the number of years of experience gained with these steels in the reactor pressure vessels and other components. Weathering steel (ASTM A242, A588) has also been discussed as a possible multibarrier waste package component (Van Luik et al., 1993). While weathering steels which contain some copper as an alloying element are superior to plain carbon steels in their resistance to atmospheric corrosion, they do not offer any particular advantage under conditions of total or partial immersion in an aqueous environment (Schumaker, 1979). Because of their higher P content certain grades of weathering steel (ASTM A242) maybe more susceptible to aging embrittlement. Hence, these steels are not considered further in this report.

Some of the pressure vessel grades that are currently used in the reactor pressure boundaries are listed in Table 2-1, along with the chemical composition limits for cast carbon steels and ductile iron. It must be noted that, for the ductile iron, ASTM does not list composition limits, letting the property specifications dictate the composition. The composition listed in Table 2-1 for the ductile iron is a typical composition for such a class. Typical mechanical properties of these steels are listed in Table 2-2.

Table 2-1. Composition ranges of some typical steel that may be used as overpacks in the multibarrier approach

Grade	Chemical Composition, Weight Percent							
	C*	Cr	Ni	Mo	Mn	P*	S*	Si*
A302-B[1]	0.25	—	0.4–0.7	0.45–0.6	1.15–1.5	0.035	0.035	0.15–0.40
A533-B[2]	0.25	—	0.4–0.7	0.45–0.6	1.15–1.5	0.035	0.035	0.15–0.40
A536[3]	3.6–3.8	0.03–0.07	0.05–0.2	0.01–0.1	0.15–1.0	0.03	0.002	1.8–2.8
A216-WCA[4]	0.25	0.5 max	0.5 max	0.2 max	0.7	0.04	0.045	0.6

* maximum
[1] Normalized
[2] Water quenched and tempered
[3] Ductile iron casting. Chemical composition not specified in ASTM.
[4] Carbon steel casting

Table 2-2. Typical range of mechanical properties of carbon steels and cast irons that are likely to be used as overpacks

Grade	Minimum Room Temperature Tensile Properties			
	Yield Strength MPa (Ksi)	Ultimate Tensile Strength MPa(Ksi)	Percent Elongation	Percent Reduction in Area
A302-B	310 (45)	515 (75)	19	—
A533-B, Class 1	345 (50)	550 (80)	18	—
A216-WCA	205 (30)	415 (60)	24	35
A536 Grade 60-40-18	276 (40)	414 (60)	18	—

Although, the discussion in this chapter is confined to plain carbon steels, references are made to other types of steels for comparison purposes.

Residual elements usually enter steel products from raw materials used to produce pig iron or from scrap steel used in steel making. Sulfur and phosphorus are usually considered deleterious to the mechanical properties of steels; therefore, for most grades restrictions are placed on the allowable amounts of these elements. The amounts of sulfur and phosphorous are invariably reported in the analyses of both carbon and alloy steels. Other residual elements typically exert a lesser influence than sulfur and phosphorus on the properties of steel. Generally, the intermediate phases that are of industrial significance in the Fe-base alloys are metastable phases. Some of the phases observed in Fe-C and Fe-N alloys are given in Table 2-3. Lowering of carbon content reduces the temperature at which the second phase precipitate start to form. Below 250 °C, relatively less stable ϵ-carbides or coherent α'-carbides are formed (Leslie, 1961a,b; Phillips, 1963).

Grain boundaries, dislocations, radiation defects in α-Fe, and stacking faults in γ-Fe are energetically favorable for segregation of alloying elements. Segregation of metalloid elements such as phosphorus to grain boundaries is important for the understanding of grain-size dependence of mechanical properties and temper embrittlement (Newhouse, 1972), while segregation of interstitials such as C and N to dislocations can explain strain age embrittlement. Of greatest importance to the mechanical stability of overpacks will be the temper embrittlement of steel due to repository thermal history. The closest analogy to this situation is the aging of reactor pressure vessels. The effect of thermal aging on the mechanical properties of pressure-vessel steels listed in Table 2-1 has been reviewed recently by Vatter et al. (1993) in relation to their performance as reactor pressure boundaries. The central issue is the increase in Charpy V-notch, ductile to brittle transition temperature (DBTT) as a result of long-term exposure to temperatures of about 300 °C during the operating life of the nuclear plants. The essential embrittling mechanism is the segregation of phosphorus to the prior austenitic grain boundaries. This is shown in Figure 2-2 for a model low-alloy steel doped with phosphorus, where the increase in DBTT, which is a measure of the embrittlement, is proportional to the grain boundary phosphorus concentration.

The deleterious effects of phosphorus are enhanced by large grain sizes such as those found in the heat affected zones (HAZs) of weldments, quenching temperature, and the presence of other alloying elements, notably copper (Vatter et al., 1993). Sulfur did not have an effect similar to that of phosphorus. These authors emphasize the paucity of long-term data (most current data on the embrittlement have been arrived at by aging for a maximum of 20,000 hr at higher-than-service temperatures). They have also attempted modeling the aging process in terms of equilibrium segregation of phosphorus to the grain boundaries. Since phosphorus will be present in all steels including the non pressure vessel grades, and the steel overpacks are expected to experience temperatures in the 200–300 °C for much longer periods than present-day nuclear reactor vessels, this phenomenon is of great importance in the performance of waste packages. A particularly important question in this respect is the tremendous variability in the impact properties of fabricated components cited by Vatter et al. (1993). This is due to variations in minor alloying elements, and the range of microstructures (e.g., grain sizes) that can be produced by fabrication and post-weld heat treatment operations.

Strain aging occurs in low-carbon steels deformed certain amounts and then aged, which produces an increase in strength and hardness but a loss in ductility (Baird, 1963; Garofalo and Smith, 1955; Wilson and Russell, 1960; Sridhar et al., 1993c; Kim and Kang, 1993). The degree of deformation, or cold work, is important. Generally, about a 15 percent reduction in thickness provides the maximum effect. The resulting brittleness varies with the aging temperature and time. Aging at room

Table 2-3. Typical secondary carbides and nitrides formed in plain carbon steels at low temperatures

Phase	Composition	Nucleation Sites	Formation Temperatures
cementite	Fe_3C	dislocations, grain b.[1]	>200 °C
ϵ-carbide[2]	$Fe_{2-3}C$	matrix, dislocation	<250 °C
α'-carbide[2]	Fe_8C	matrix	<100 °C
γ'-nitride[3]	Fe_4N	dislocations, grain b.[1]	>250 °C
α'-nitride	Fe_8N	matrix	<300 °C

[1] only at high temperatures
[2] there is not complete certainty about these structures
[3] in stable equilibrium with γ'Fe

temperature is very slow, requiring several months to obtain maximum embrittlement. As the aging temperature is increased, the time for maximum embrittlement decreases. In low-carbon steels, strain aging is caused by the interstitial solute atoms, namely. carbon and nitrogen. These interstitial atoms have high diffusion coefficients in iron and high interaction energies with dislocations. Strain aging below 100 °C is due to carbon, because of the higher solubility of nitrogen (Stephenson and Cohen, 1961). Strain aging due to nitrogen is a result of the nitrogen which is not tied up with strong nitride formers, (i.e., aluminum, titanium, zirconium, vanadium, or boron). The strain-age embrittlement degradation mode could be relevant to the high-level nuclear waste (HLW) package in the areas of local deformation such as due to rock fall. In the reactor pressure vessel area, strain-aging of quenched and tempered A508 class 3 steel in the temperature range of 150 to 340 °C has been shown to reduce fracture toughness in the upper shelf region (Sridhar et al., 1993c; Kim and Kang, 1993). However, this embrittlement mode is not considered a life-limiting failure mechanism for the waste package. On the other hand, the effect of plastic deformation on the kinetics of phosphorus segregation to grain boundaries and eventual temper embrittlement may be important and needs further consideration.

Welding of low-carbon steels is readily achieved using most commercial techniques. Preheating and, less frequently, post-weld stress relieving may be necessary, particularly for large section sizes (>25 mm thickness), depending on the carbon content. The final microstructure of the weldment in carbon steels is determined by the cooling rate from the peak temperature. Because the alloy level in carbon is low, the major physical properties of the steel are not affected by welding. Therefore, the temperature gradient (base metal preheat, interpass temperature control) and heat input become the major parameters in weld metal microstructural evolution. A slower cooling rate decreases shrinkage stress, prevents excessive hardening, and allows time for hydrogen diffusion. However, slower cooling tends to increase grain size and later temper embrittlement (Vatter et al., 1993).

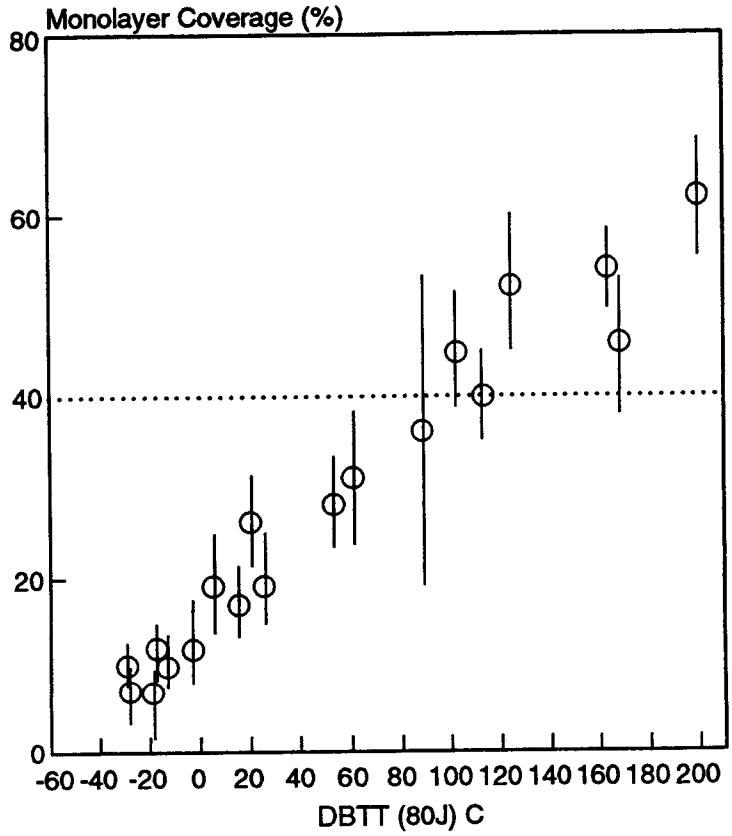

Figure 2-2. Dependence of DBTT at 80 Joules as a function of grain boundary P. A model alloy with nominal composition of A533–B was aged at temperatures 375 to 600 °C (Vatter et al., 1993).

2.1.2 Ductile Iron

The term cast iron identifies a large family of ferrous alloys. Cast irons are multicomponent ferrous alloys that solidify with a eutectic. They contain major (iron, carbon, silicon), minor (<0.1 percent), and often alloying (>0.1 percent) elements. Cast iron has higher carbon and silicon contents than steel. The high silicon content stabilizes the graphite rather than the metastable cementite. In ductile cast iron, also known as nodular iron or spheroidal-graphite (SG) iron, graphite is present as spheres (nodules). The additives, such as cerium, introduced in the molten iron before casting lead to the development of graphite spheres rather than flakes. The spherical shape is beneficial in terms of increasing the ductility because of the minimization of stress raisers. The correspondence between commercial and microstructural classification, as well as the final processing stage in obtaining common cast irons, is given in Table 2-4.

Typical compositions of unalloyed ductile iron are shown in Table 2-5. Ductile iron can also be alloyed with small amounts of nickel, molybdenum, or copper to improve its strength and hardenability. Larger amounts of silicon, chromium, nickel, or copper can be added for improved resistance to corrosion, oxidation, or abrasion, or for high-temperature applications. The discussion in this chapter is confined to unalloyed ductile cast iron. In cast irons the principal alloying element are carbon and silicon.

Table 2-4. Typical microstructures of various cast irons as a function of grade and processing history

Commercial Designation	Carbon-Rich Phase	Matrix[a]	Fracture	Final Structure
Gray iron	Lamellar graphite	P	Gray	Solidification
Ductile iron	Spheroidal graphite	F, P, A	Silver-gray	Solidification or Heat Treatment
Compacted graphite iron	Compacted vermicular graphite	F, P	Gray	Solidification
White iron[b]	Fe_3C	P, M	White	Solidification and Heat Treatment
Mottled iron	Lamellar graphite + Fe_3C	P	Mottled	Solidification
Malleable iron	Temper graphite	F, P	Silver-gray	Heat Treatment
Austempered ductile iron	Spheroidal graphite	At	Silver-gray	Heat Treatment

[a] F, ferrite; P, pearlite; A, austenite; M, martensite; At, austempered (bainite);
[b] White iron is not usually heat treated, except for stress relief and to continue austenite transformation

A number of processing and post-casting heat treatments alter the properties of ductile iron and could have considerable influence on the design of the waste package for HLW. These parameters, discussed in this section, include chemical composition, graphite shape (morphology), section size, cooling rate, post-casting heat treatment, and welding (Jenkins and Forrest, 1990).

Carbon, silicon, and manganese have the most significant influence on the properties of cast irons. Carbon influences the fluidity of the molten iron and controls the shrinkage characteristics of the cast metal. The size and number of graphite nodules formed during solidification are also influenced by the amount of carbon, the number of graphite nuclei, and the choice of inoculation practice. Silicon is a powerful graphitizing agent and increases the fluidity of the melt. Within the normal composition limits, increasing amounts of silicon promote structures that have progressively greater amounts of ferrite. Increasing the amount of ferrite reduces the yield strength and tensile strength but increases the elongation and impact strength. Manganese acts as a pearlite stabilizer and increases strength, but reduces ductility and machinability. Nickel is frequently used to increase strength by promoting the formation of fine pearlite and to increase hardenability, especially for surface-hardening applications or for producing austempered ductile iron. Copper is used as a pearlite former for high strength with good toughness and machinability. Molybdenum is used to stabilize the structure at elevated temperatures. The amount must be controlled because of the tendency of molybdenum to segregate to the cell boundaries as stable carbides.

Table 2-5. Typical compositions of cast irons

Type	Composition, Percent										
	TC[a]	Mn	Si	Cr	Ni	Mo	Cu	P	S	Ce	Mg
Gray iron	3.25–3.50	0.50–0.90	1.80–2.30	0.05–0.45	0.05–0.20	0.05–0.10	0.15–0.40	0.12 max	0.15 max	—	—
Malleable iron	2.45–2.55	0.35–0.55	1.40–1.50	0.04–0.07	0.05–0.30	0.03–0.10	0.03–0.40	0.03 max	0.05–0.07	—	—
Ductile iron	3.60–3.80	0.15–1.00	1.80–2.80	0.03–0.07	0.05–0.20	0.01–0.10	0.15–1.00	0.03 max	0.002 max	0.005–0.20[b]	0.03–0.06

[a] TC, Total carbon
[b] Optional

The presence of graphite in ductile cast iron in the shape of spheroidal nodules instead of sharp flakes such as those found in gray cast iron is caused by the addition of magnesium (or magnesium and cerium) to the molten iron, resulting in a fivefold to sevenfold increase in the strength of the cast metal. Figure 2-3 shows the influence of graphite morphology on the stress-strain curve of several types of irons. Shapes that are intermediate between a true nodular form and a flake form yield mechanical properties that are inferior to those of ductile iron with a true nodular graphite. The size and uniformity of distribution of graphite nodules also influences properties, but to a lesser degree than graphite shape.

2.1.3 Section Size

The variable chiefly affected by section size is the cooling rate—which in turn affects both the size of the graphite nodules and the microstructure of the matrix. Heavier sections cool at a slower rate leading to the formation of larger and fewer graphite nodules during solidification. Bainite and martensite are not typically found in as-cast structures, but can be introduced by heat treatment subsequent to the casting. The resulting product, Austempered Ductile Iron (ADI), has a matrix that exhibits a combination of acicular (bainitic) ferrite and stabilized austenite. In order to minimize the deleterious effects of segregation in medium- and thick-section ADI castings, the graphite nodules count must be maintained as high as possible, ideally at a level > 150 nodules/mm^2. Like the chemical composition, the cooling rate can significantly influence the as-cast structure and therefore the mechanical properties. The cooling rate of a casting is primarily a function of its section size. Increasing the cooling rate will: (i) refine both graphite size and matrix structure leading to increase in the strength and hardness, and (ii) increase the chilling tendency which will also result in an increase in hardness, but will decrease the ductility. However, ductile iron exhibits significantly lower section size sensitivity compared to gray iron, because SG is less affected by cooling rate than flake graphite.

It is anticipated that if ductile iron is used for fabricating waste packages it will be cast into the shape of the waste package and then given appropriate post-casting heat treatment to tailor the properties to the design specification. Factors that are likely to have significant effect on the mechanical and physical properties of the waste package include the chemical composition, graphite shape, section size, cooling rate, heat treatment, and welding. Sufficient information exists in the literature to assess qualitatively the influence of these variables on the design parameters, but more detailed information related to the chemical composition of the steel and its fabrication history would be necessary to assess their effects on performance under repository conditions.

A difficulty, related to the use of ductile iron for waste packages envisioned at this time is the heat-to-heat variability. Therefore, the use of commercial grade ductile iron could lead to waste package containers with widely variable characteristics that may eventually result in an extremely wide range in the failure times of the waste package. This situation, therefore, calls for use of a waste package grade ductile iron with very tightly controlled composition. The fabrication of such iron would also require a very tight process control to keep the performance variability in an anticipated quantity of 70,000 waste packages to within the design requirements. The potential design-life limiting degradation modes that need to be addressed for ductile iron are phosphorus segregation induced embrittlement, graphite morphology changes leading to mechanical and physical property changes, and hydrogen damage both due to the high solubility of hydrogen in iron and the possibility of interaction of the gas with carbon.

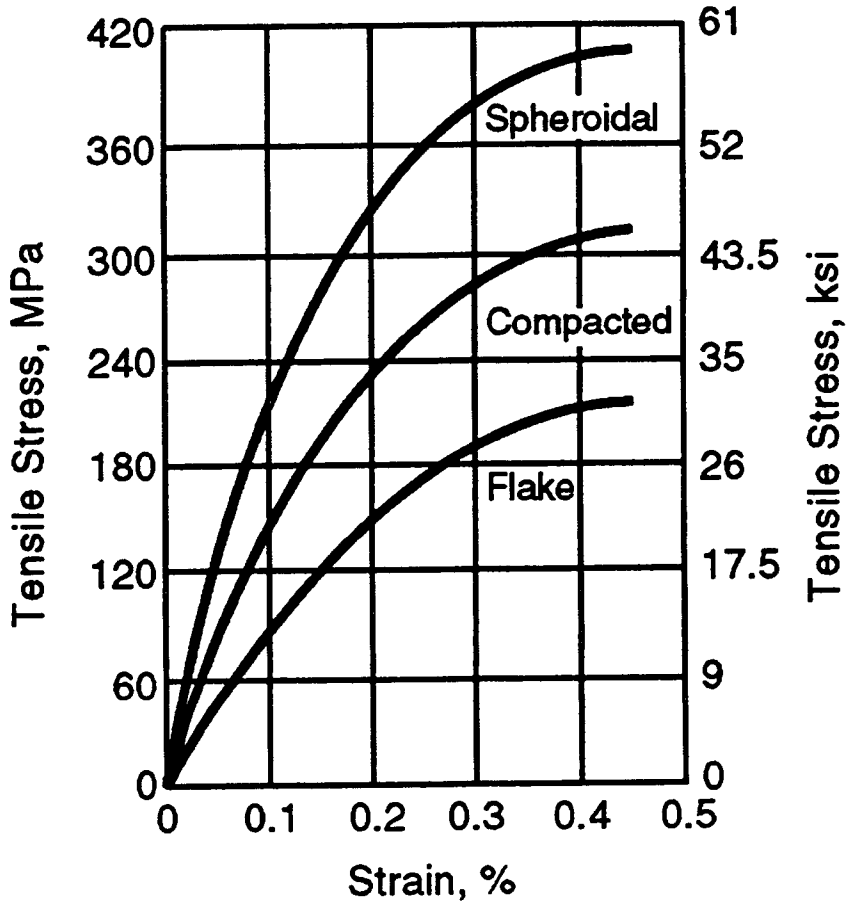

Figure 2-3. Effect of graphite shape on the mechanical properties of cast irons

2.2 CORROSION

The corrosion of carbon steels and cast irons in many environments has been extensively studied. Most investigations pertaining to the corrosion of these materials are application specific and not directly useful in predicting the long-term performance of steels and cast irons in a HLW repository. Despite this limitation, some of these investigations can provide useful information such as oxidation rates as a function of temperature. Uniform corrosion rates, gathered by atmospheric corrosion testing, are only useful in predicting the minimum corrosion rate in the absence of aggressive environmental conditions. Investigations carried out in marine environments can be useful for making predictions under less favorable conditions. However, key differences between marine applications and HLW disposal such as temperature, radiation, and biological activity again limit the use of this data for long-term prediction in a repository environment.

Within the last 10–12 yr, investigations have been conducted to evaluate the use of carbon steels and cast irons for HLW containers. Long-term experimental data, which have previously been used to evaluate the accuracy of atmospheric corrosion model predictions, are lacking for repository environments. The effect of environmental variables, such as groundwater composition, temperature, and degree of aeration, on the type and rate of corrosion have only been investigated in short-term tests.

These short-term studies have been conducted for proposed repositories in basalt, salt, granite, and tuff environments. Many attempts of long-term prediction have been made as a result of these investigations.

The most important factor in making long-term performance predictions is correctly identifying whether the material will undergo uniform or localized corrosion. In the case of uniform attack, if the corrosion rate can be measured in relatively short-term tests, then long-term performance prediction may be straightforward. However, due to the extremely long time frames involved, a high degree of caution should be exercised in ruling out the possibility of localized corrosion. Performance predictions for combinations of materials and environments leading to localized attack are considerably more difficult. Under these conditions, successful lifetime estimation requires knowledge of the localized corrosion propagation rates, as well as relatively accurate estimations of the initiation times.

2.2.1 Effect of Environmental Factors on Uniform Versus Localized Corrosion

The range of possible repository environments makes it necessary to determine under which conditions a container will undergo uniform corrosion or localized attack. Uniform corrosion rates for cast irons and steels in neutral and slightly alkaline water are dependent on the rate of reduction of oxygen in aerated solutions, shown as Eq. (2-1), and the rate of reduction of hydrogen ion, Eq. (2-2), in deaerated acidic solutions. In aerated acidic solutions the corrosion rate is controlled by the reduction of hydrogen ion Eq. (2-2) and dissolved oxygen shown as Eq. (2-3).

$$O_2 + 2H_2O + 4e^- \rightleftarrows 4OH^- \tag{2-1}$$

$$2H^+ + 2e^- \rightleftarrows H_2 \tag{2-2}$$

$$4H^+ + O_2 + 4e^- \rightleftarrows H_2O \tag{2-3}$$

The limiting current density, $i_L^{O_2}$, which defines the maximum uniform corrosion rate (Akashi et al., 1990) of iron in aerated solutions where reaction Eq. (2-1) limits the corrosion rate may be calculated by:

$$i_L^{O_2} = \frac{zFD_{O_2}C_{O_2}}{d} \tag{2-4}$$

where z is the number of electrons transferred in the reaction, F is the Faraday constant (96,500 coulombs/equivalent), D is the diffusion coefficient of dissolved species, C is the bulk concentration of dissolved species, and d is the thickness of the diffusion layer. At 25 °C with 8.1 ppm O_2, the corrosion rate is 0.2 mm/yr. The rate is observed to decrease with time to 0.1 mm/yr or less due to the formation of a corrosion product film limiting the diffusion of O_2. The accessibility of oxygen to the metal surface and therefore, the area available for the cathodic reaction is one of the main factors limiting the corrosion rate, as well as the conductivity of the aqueous solution.

In the absence of dissolved O_2 in solutions where the pH is <5, the equation becomes:

$$i_L^{H^+} = \frac{zFD_{H^+}C_{H^+}}{d} \tag{2-5}$$

Under these conditions, the corrosion rate increases as the pH of the solution decreases. In deaerated solutions having a pH above 5, the cathodic reaction is the reduction of water (Turnbull and Gardner, 1982), shown as Eq. (2-6).

$$2H_2O + 2e^- \rightarrow H_2 + 2OH^- \tag{2-6}$$

At lower pH values, the corrosion rate of iron increases as a result of the dissolution ferrous oxide film, leaving the iron surface in direct contact with the acid environment. In terms of Eq. (2-4), of the decreasing the pH increases the dissolution of the ferrous oxide film which, in turn, results in a decrease in *d*, the thickness of the diffusion layer. In acidic solutions, the reduction of hydrogen ions also occurs at a rapid rate. Thus, in aerated acidic solutions the corrosion rate of steels and cast iron is very high. At 25 °C, increasing the pH to values between 10–14 results in a decrease in the corrosion rate due to the onset of passivity. In this pH region, the formation of protective oxide film is favored. Investigations of oxides on mild steel in oxygenated water (Misawa et al., 1971; Szklarska-Smialowska, 1986) have shown that γ-FeOOH initially formed on the surface at room temperature. With time, this film is converted to a mixture of γ-FeOOH and Fe_3O_4. In addition, $Fe(OH)_2$ has also been reported to form under these conditions. Increasing the temperature to 50–100 °C favors the formation of Fe_3O_4, since at temperatures around 100 °C, $Fe(OH)_2$ decomposes to $Fe_3O_4 + H_2$. In concentrated alkali solutions (pH > 14) at room temperature, the passivity is disrupted due to the formation of soluble $HFeO_2^-$, resulting in an increased corrosion rate (Pourbaix, 1974).

The uniform corrosion rate is also a function of temperature (Uhlig and Revie, 1985). Increasing the temperature causes a linear increase in the corrosion rate of iron in water. Beyond 75 °C, the corrosion rate in an open system decreases in the temperature range of 75–100 °C. The observed decrease in the corrosion rate at elevated temperatures is a result of the decreased solubility of oxygen in solution as the temperature is increased. On the other hand, in a closed system, where the oxygen concentration is not allowed to decrease, the corrosion rate continues to increase with temperature. A plot of corrosion rate as a function of temperature for open and closed systems is shown in Figure 2-4.

In natural groundwater, the composition of the dissolved species along with the temperature and material characteristics will determine both form and rate of corrosion. For groundwater in the pH range of 4–10, sodium chloride and calcium carbonate can have an important effect on the uniform corrosion rate which is controlled by the reduction reaction kinetics. As the sodium chloride concentration is increased, the solubility of O_2 decreases and the amount of dissolved oxygen in solution is reduced. The relative uniform corrosion rate of iron as a function of sodium chloride concentration is shown in Figure 2-5 (Uhlig and Revie, 1985). Initially, the corrosion rate is shown to increase with the salt concentration. The maximum uniform corrosion rate occurs at approximately 3-percent sodium chloride. The initial increase in the corrosion rate in spite of the decrease in the concentration of dissolved oxygen is believed to be a result of a change in the protective properties of the oxide film. In low conductivity solutions the reduction of oxygen and the subsequent formation of OH^- occur very close to the location of the anodic reaction producing Fe^{2+}. The close proximity of the anodic and cathodic reactions results in the formation of $Fe(OH)_2$ on the surface of the metal which acts as a diffusion barrier for oxygen. Greater solution conductivity caused by the addition of sodium chloride allows for a larger separation of

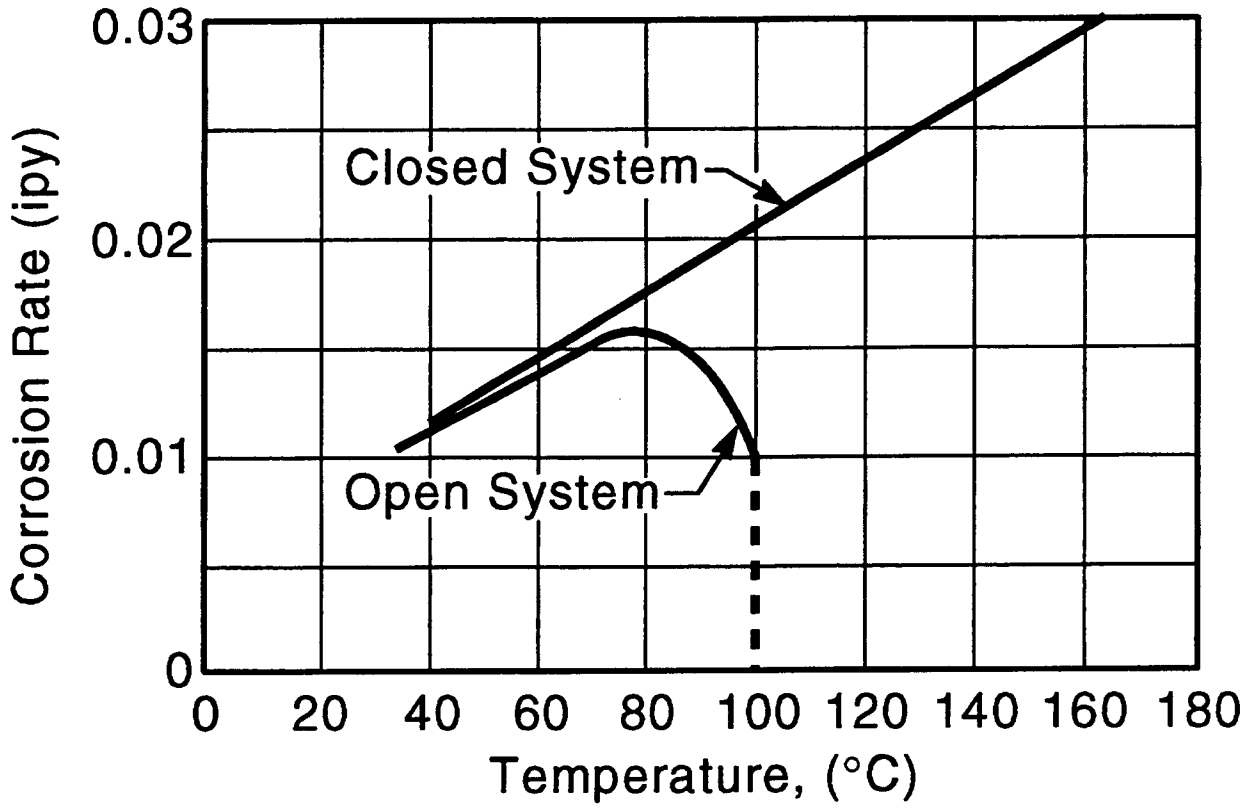

Figure 2-4. Effect of temperature on the corrosion rate of iron in water containing dissolved oxygen in open and closed systems (Speller, 1951)

anodic and cathodic sites. The increased distance required for the subsequent reaction results in some portion of the $Fe(OH)_2$ actually being formed in solution instead of on the metal substrate. Further increases in the sodium chloride concentration sufficiently reduce the concentration of dissolved oxygen to cause a decrease in the corrosion rate.

In addition to an oxide film, another effective dissolved oxygen diffusion barrier can be created by the formation of a $CaCO_3$ scale on the metal surface. The conditions under which such scales can form are defined by the saturation index (Langelier, 1936). Precipitation of calcium carbonate scales can also occur on nonmetallic surfaces such as colloidal silica and organic particles (Uhlig and Revie, 1985). Scales formed on these other surfaces will not provide a diffusion barrier for oxygen transport to the metal.

Localized corrosion of steels can occur when the environmental conditions allow breakdown of a passive film formed on the metal surface. The formation of a passive film on iron and carbon steels is favored at alkaline pH values. Other species in solution such as carbonate and bicarbonate can also promote passivation at near neutral pH values. Aggressive ions such as halides (X^-) and sulfate, when present in sufficient quantity, induce breakdown of the passive film and thus initiate localized corrosion. The breakdown potential, E_{br}, in alkaline environments has been related (Davies and Brook, 1992; Bird et al., 1988) to a competitive adsorption of hydroxyl and halide ions present described by the equation:

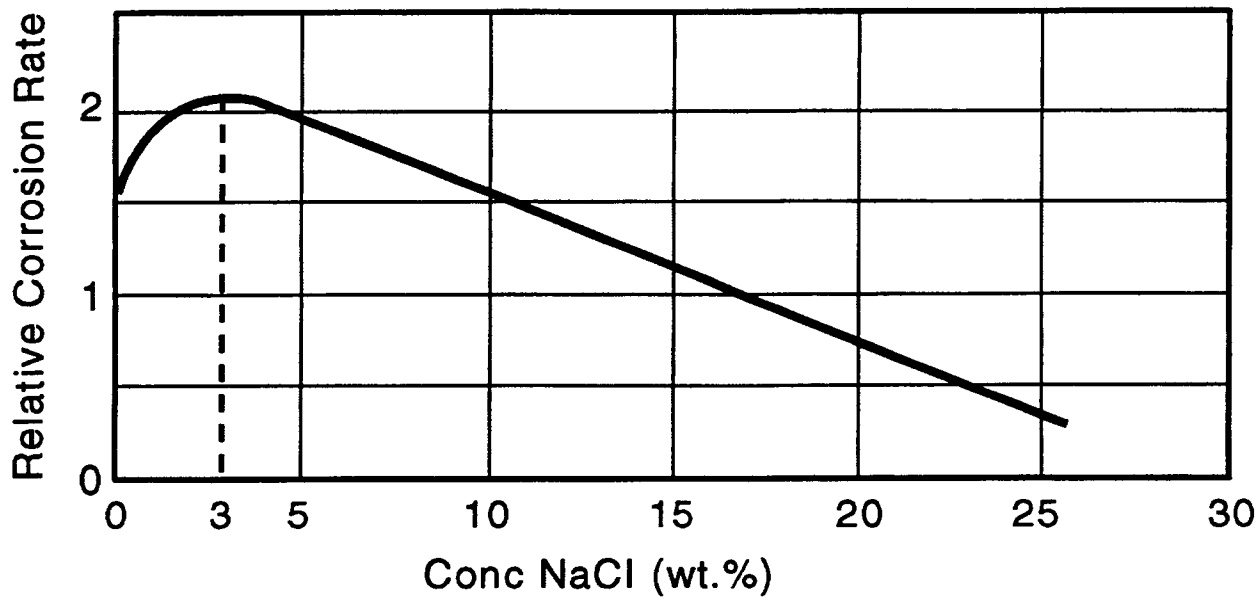

Figure 2-5. Corrosion rate of iron as a function of sodium chloride concentration at ambient temperature (Uhlig, and Revie 1985). IPY = Inch per year.

$$E_{br} = A + B\log\left(\frac{[X^-]}{[OH^-]}\right) \tag{2-7}$$

For constant pH, oxidizer concentration, and halide concentration, the breakdown potential increases as the halide species changes from chloride to bromide to iodide. The presence of other ions such as sulfate can also decrease the pit initiation potential while anions such as borate inhibit pitting and increase the pitting potential.

In addition to the environment, alloying additions to the material have a pronounced effect on the formation and stability of the passive films. A study of localized corrosion potentials with experimental heats of steel alloyed with Ni, Cr, Cu, and Al was conducted to determine the mechanism by which these alloying additions alter the corrosion behavior of steels (Gainer and Wallwork, 1980). A potentiometer was used to measure the corrosion potential at multiple locations on the steel surface and Energy Dispersive X-ray (EDX) analysis was used to determine the distribution of the alloying additions. The results indicated that the alloying additions act either to decrease the activity of pit initiation sites or increase the corrosion activity of nonactive regions, eliminating cathodic sites and thereby promoting uniform attack. All steels contained pearlite, the amount of which depended on the carbon content and alloying additions. However, carbon did not influence the pitting behavior of the materials. Additions of Cr and Al were found to reduce the mean potential resulting in a lower uniform corrosion rate, but localized attack was observed. Copper and nickel additions reduce the magnitude of the potential range measured on the surface of the material in different ways. The addition of nickel increased the potential

of the matrix resulting in larger uniform corrosion rates but reduced the tendency of pitting compared to mild steel. In contrast, copper reduced the sulfide activity and to a lesser extent the matrix activity. The reduction of the anodic potential levels of the sulfide inclusions reduces the possibility of pitting attack. Thus, compared to mild steel, the degree of pitting attack increases with the addition of Cr and Al and decreases with the addition of Ni and Cu.

The presence of a well formed oxide tends to delay the onset of pitting (Szklarska-Smialowska, 1986). It should be noted, however, that pitting will eventually occur at potentials above a critical potential if the appropriate concentration of chloride or some other aggressive species is available. On the other hand, a poorly formed oxide film and the presence of inclusions at the surface of the material provide the necessary pit nucleation sites. Inclusions may also contribute to growth provided they are not etched out in the process. Spherically shaped inclusions can easily be etched out during corrosion leaving a relatively large open depression incapable of functioning as an occluded cell. For this reason, spherically shaped inclusions are less detrimental than irregularly shaped inclusions (Szkarska-Smialowska, 1986; Ives and Srivastava, 1987). Four categories of inclusions have been identified. Type I inclusions, such as homogeneous sulfides, are anodic to the steel matrix and hence are attacked selectively. Type II inclusions are multiphase inclusions in which one of the phases is selectively attacked and the metal is cathodic. Type III inclusions are cathodic to the metal matrix. Type III inclusions are not attacked but the metal matrix surrounding the inclusion is anodic and is locally attacked, nucleating a potential pit site. The type IV inclusion is neither anodic nor cathodic to the metal matrix in the bulk solution. However, a poor mechanical bond between the inclusion and the metal matrix results in the formation of a crevice during heating and cooling cycles or metal working operations. Localized corrosion occurs as a result of this crevice formed between the inclusion and the metal matrix. For iron base materials, the Type I and Type II inclusions are the most common.

The galvanic corrosion of mild steel coupled to platinum, copper, brass, or 304 SS in 0.001–25-percent sodium chloride solutions at ambient temperature has been shown (Tsujino and Miyase, 1982) to follow the equation:

$$P = P_0 \left[1 + \frac{A_c}{A_a} \right] \tag{2-8}$$

where P is the corrosion rate with coupling, P_0 is the corrosion rate without coupling, A_c is the area of the cathode, and A_a is the area of the anode. The maximum corrosion rate was found to occur at a concentration of 1 percent NaCl. The addition of NaCl increases the conductivity of the solution which, in turn, tends to increase the corrosion rate. Lower penetration rates at higher concentrations of NaCl are due to the decrease in the dissolved oxygen concentration. The current density for the cathode approaches the limiting current density for the reduction of oxygen and is independent of the area ratio. Crevice corrosion rates of galvanically coupled mild steel and alloy 600 in 0.001-M HCl have also been shown to be dependent on the reduction of oxygen (McKubre et al., 1983). Galvanic corrosion currents as high as 12–14 $\mu A/cm^2$ have been recorded (Kolts et al., 1987) in CO_2 environments between steels with slightly different compositions.

Passivation of steel is possible in aerated environments and environments containing CO_2 (Kolts et al., 1987). However, in deaerated environments, passive films on iron can be reduced allowing the metal to undergo active corrosion. The presence of hydrogen at high pressures has been shown to lower the pitting potential of the passive films (Pyun et al., 1992). Hydrogen in the oxide is believed to combine with the oxygen and form hydroxyl ions which are more easily displaced by aggressive ions such

as Cl^-. Aging of the hydrogen charged passive films results in an increase in the pitting potential, approaching that of uncharged passive films, due to an egress of the hydrogen from the oxide. This observation has been compared to the observed increase in the pitting potential when passive films grown in the absence of Cl^- are aged.

Localized corrosion of low carbon steels can also have detrimental secondary effects such as the production of hydrogen. While hydrogen can be liberated during uniform corrosion, the presence of localized corrosion increases the rate of hydrogen generation due to local acidic conditions (Simpson et al., 1985). The hydrogen produced may then promote other forms of material degradation such as cracking or reduce the stability of passive films. Pits initiating from MnS inclusions have been shown to initiate cracks in ASTM A502 Cl2 carbon steel in water with dissolved O_2 at 100–150 °C (Choi et al., 1982). Cracks initiating from smooth unpitted regions of the samples were only observed at higher temperatures.

2.2.2 Atmospheric Corrosion Studies

Atmospheric corrosion studies of carbon steels and cast iron materials are typically carried out under ambient conditions. The location in which the study is conducted dictates the severity of the test. Coastal environments with high average relative humidities combined with the presence of chloride, and industrial environments, which often experience acidified precipitation as a result of airborne pollution, are more corrosive than rural environments. The results of 8-yr (Townsend and Zoccola, 1982) and 16-yr (Shastry et al., 1988) atmospheric corrosion studies for copper bearing low alloy steels ASTM A-242 Type-1 and ASTM A 588-grade B have shown that the corrosion loss of the materials followed the equation:

$$C = At^B \tag{2-9}$$

where C is the corrosion loss, t is time, and A and B are constants that depend on the location and material. Another study (Legault and Preban, 1975) of Mo, Cu, and Ni additions also found this equation to describe the corrosion rate of the materials. The value of A was the deciding factor in determining the short-term performance whereas B was significant for long-term exposures. In a study of welded and unwelded specimens in industrial plant atmospheres (Mishra and Das, 1987), A, again identified as the significant short-term parameter, was described as a measure of the inherent reactivity of the metal surface to produce an oxide corrosion product in a short-term exposure. The value of B, on the other hand, was determined to be a measure of the oxide film properties to resist transport processes within the corrosion product film.

Additional results of this study indicate that welded specimens, corroded faster in the welded areas than on unwelded areas. The method of welding was also found to significantly alter the corrosion rates of the materials. Gas welded (probably oxyfuel gas welded) specimens corroded at a faster rate than specimens welded using a shielded metal arc method. This result was thought to be due to the increased inclusion content of the gas welds. Cold rolled specimens corroded at a faster rate than hot rolled material of the identical composition due to the increased dislocation density and an increase in the number of point defects.

An analysis of 38 atmospheric corrosion tests (McCuen, and Albrecht, 1994) conducted in rural, marine, and industrial environments for periods ranging from 3.5–23 yr indicated that the logarithmic

power model, shown as Eq. (2-9), tends to underpredict the short-term and long-term corrosion penetration and overestimate the corrosion at intermediate times. Numerical power models are of the same form as Eq. (2-9) with the exception that the coefficients are fitted numerically with a nonlinear least squares method directly to the actual values of the variables and not the logarithm of the variables. The solutions are optimized until the overall bias becomes zero. These models performed somewhat better than the logarithmic power models but still tended to underpredict the long-term corrosion damage. Constant intercept power-linear models of the form:

$$p_1 = b_0 t^{b_1} \qquad \text{for } t \leq t_c \tag{2-10}$$

$$p_2 = b_2 + b_3 t \qquad \text{for } t \geq t_c \tag{2-11}$$

were no worse than the logarithmic power and numerical power models and were usually found to fit long-term data better than the previous models. Predictions of the corrosion damage using a constant intercept power-linear model are much greater than the damage predicted by the power models even for times as short as 10 yr in aggressive environments. Extrapolations to longer times resulted in much larger differences in the predictions from each of the models.

The corrosion product film formed in atmospheric corrosion has been characterized in order to determine why some films are apparently more protective than others. The composition of the corrosion product films are similar for atmospheric and aqueous conditions. Differences in the corrosion protection provided by the surface films are apparently related to the adhesiveness of the films to the metal substrate. Steels containing Cu or P (Misawa et al., 1971) tend to form a continuous Δ-FeOOH layer. Mild steels without these alloying additions tend to form a mixed oxide containing Δ-FeOOH and also Fe_3O_4 with α, β, or γ-FeOOH. The α and γ forms of FeOOH have large needle shaped grains and, as a result, the oxide contains many pores that serve as paths for water and O_2. Later investigations (de Meybaum and Ayllon, 1980) confirmed that the composition of the corrosion product films was secondary in importance to the uniformity of the corrosion product layer.

The rate of thermal oxidation at various temperatures has also been investigated (Szklarska-Smialowska and Jurek, 1976) for iron-base materials. For films formed below 200 °C, the rate of oxidation follows the logarithmic law. The film formed under these conditions is predominantly magnetite (Fe_3O_4). At temperatures above of 250 °C, the rate of oxidation becomes parabolic. Under these conditions the film formed near the oxide metal interface is magnetite with an outer layer of hematite ($\alpha - Fe_2O_3$). The hematite layer formed under these conditions is not homogeneous and consequently provides little protection to the underlying metal from further oxidation. Graphical representations of thermal oxidation rates under logarithmic and parabolic control are shown in Figures 2-6 and 2-7.

2.2.3 Corrosion in Seawater

The corrosion of steels and cast iron materials in seawater has also received considerable attention. Typically these tests are carried out for several months to many years. The overall corrosion rate is usually highest during the initial exposure and then decreases for long-term exposures. A study of carbon steel in Cochin Harbor (Ravindran and Gopalakrishna Pillai, 1984) reported the initial corrosion rate to be 0.41 mm/yr, but this decreased to 0.10 mm/yr after 270 days. Corrosion rates for grey and

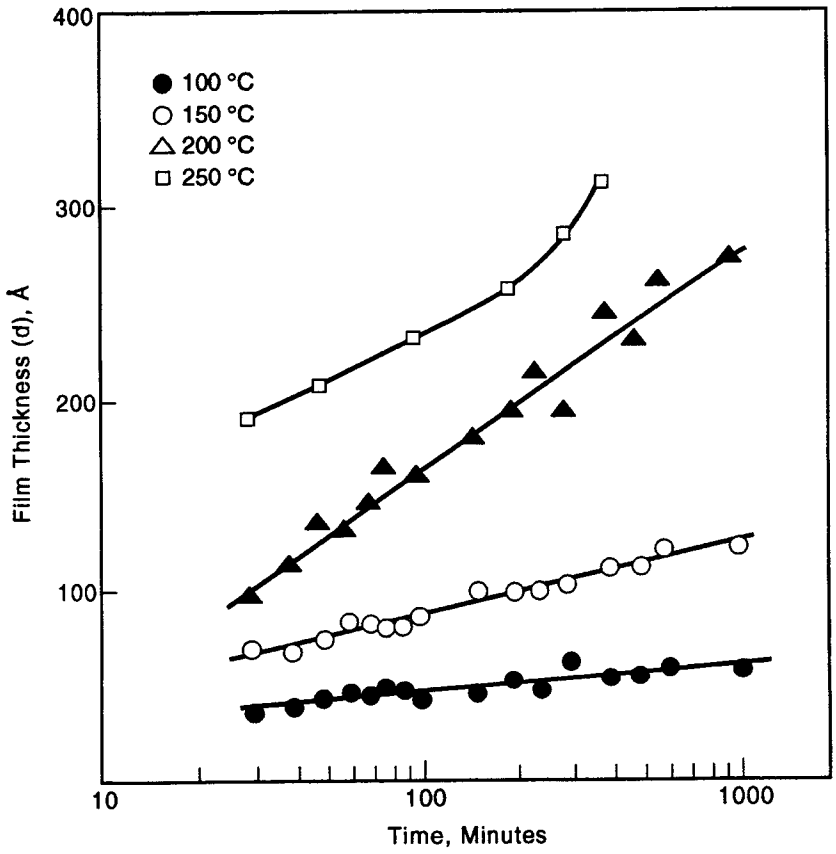

Figure 2-6. Oxide film thickness on low carbon steel as a function of time at 100, 150, 200, and 250 °C (Szklarska-Smialowska and Jurek, 1976)

nodular cast iron fall in the range of 0.06–0.2 mm/yr depending on the time and location of exposure (El-Dahshan et al., 1988; Escalante and Iverson, 1978; Shalaby et al., 1992). High silicon cast iron has been shown to suffer from pitting and interdendritic attack in stagnant water (Shalaby et al., 1992). Similar measurements for carbon steels have yielded corrosion rates of 0.08–0.3 mm/yr (El-Dahshan et al., 1988; Escalante and Iverson, 1978; Shalaby et al., 1992). Pitting penetration rates for these materials have been determined in a case study of desalination plants (El-Dahshan et al., 1988). For clean carbon steel, the penetration rate was 0.4–0.8 mm/yr. The presence of a mill scale increased the penetration rate to 0.5–1.0 mm/yr. Cast iron materials performed better with penetration rates of 0.1–0.3 mm/yr.

Several factors have been shown to alter the corrosion rate of carbon steels and cast irons during exposure in seawater. Corrosion rates tend to increase with flow velocity (Shalaby et al., 1992). The increased corrosion rate under flowing conditions are a result of increased oxygen transport to the metal surface and abrasion by particles in solution (Uhlig and Revie, 1985). Corrosion rates for carbon steel piles were found to be greater by a factor of two on areas of the test pile that were continuously above water compared to the region always below water (Escalante and Iverson, 1978). Similarly, the region of the pile continuously below the sea floor was found to have the lowest corrosion rate by a factor of 5. These results are not surprising since the rate of oxygen reduction is dependent on the concentration of oxygen in the system. The concentration of dissolved oxygen in seawater is highest in the thin water films that form on the steel piles above the splash zone and lowest in sub sea bed location.

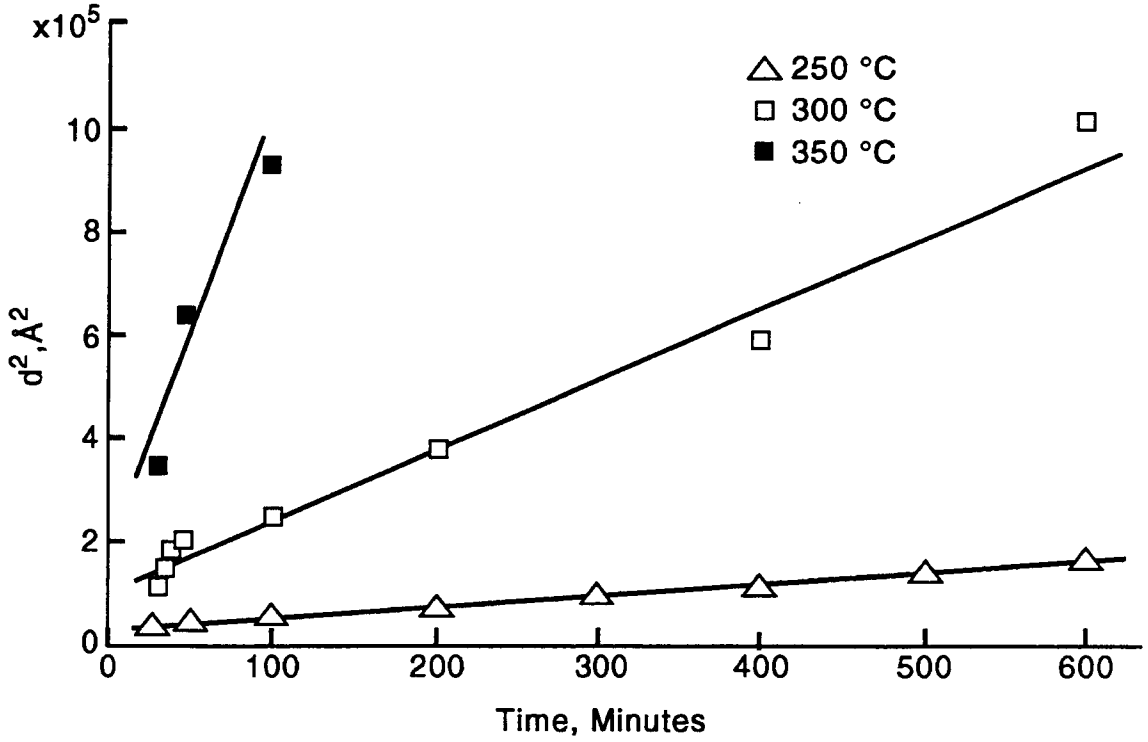

Figure 2-7. Parabolic growth of oxide film thickness for low carbon steel at 250, 300, and 350 °C (Szklarska-Smialowska, and Jurek, 1976)

X-ray diffraction (Sasaki et al., 1992) of corrosion products formed on low carbon steel in aerated and deaerated synthetic seawater at 80 °C indicated that for both cases $Mg_6FeCO_3(OH)_{16} \cdot 4H_2O$ is formed. With increased time the corrosion products change to Fe_3O_4. Pitting-like corrosion was observed to occur with prolonged exposure in deaerated conditions. Localized corrosion increased with the degree of aeration.

The results of galvanic studies (Scully and Hack, 1984) using HY-80 steel and alloy 625 indicated that the couple potential was -640 to -680 mV_{SCE}. The corrosion current was 7–9 $\mu A/cm^2$ giving a carbon steel corrosion rate of 0.17–0.19 mm/yr. The results of another test (Hack and Taylor, 1979) using HY-130 steel and a variety of cathode materials such as Ti alloys, 304, and 316 SS concluded that the corrosion rate of steel coupled to these materials was unacceptably high even for short durations. Tests conducted using a medium carbon chromated steel bolt in a HY-130 steel panel suggested that steel was unacceptable for long-term exposures.

2.2.4 Corrosion in Repository Environments

The corrosion of carbon steel and, to a lesser extent, cast iron, under simulated repository conditions, has received limited study. The conditions encountered by the waste package in a nuclear

waste repository are greatly dependent on the location and design of the facility. The anticipated nominal groundwater composition for repository sites in the United States in basalt, granite, salt, and tuff environments are summarized in Table 2-6. European repository programs have also identified and characterized the groundwater most likely to intrude into various repository sites (Accary, 1985). As discussed in the previous section, the concentration of dissolved species in groundwater may become greater due to evaporation of the water on the container surface. Increasing the number of fuel assemblies within each waste package or raising the areal power density within the repository will further increase the evaporation rate. Containers that are not shielded may also alter the groundwater by radiolysis. Therefore, for a given repository location, the conditions to which the waste package will be exposed may vary with time. Initially the conditions may be hot and dry causing the surface of the waste package to oxidize. Wet oxidation or corrosion in a steam environment may occur if water intrudes into the repository and then evaporates. With time, the waste container surface will cool to below the boiling point of water increasing the possibility of aqueous corrosion.

As mentioned in Chapter 1, all of the repository studies have indicated that the groundwater most likely to contact the waste package contains varying amounts of aggressive species such as chloride and sulfate. The concentration of these species is highest in salt repositories and lowest in the groundwater associated with tuff repositories. In addition to the aggressive species, there are also passivating species such as carbonate and bicarbonate. In the passive state, the corrosion rate of steel and cast iron materials decreases by several orders of magnitude. However, localized corrosion such as pitting or crevice corrosion is possible in the presence of chloride, when iron based materials are in the passive state. Borate, a known inhibitor of localized corrosion of steels in chloride environments, may possibly be present in significant concentrations in a salt repository.

2.2.4.1 Uniform Corrosion Studies

Investigations of the corrosion rates of unalloyed steels and cast irons in reducing granitic groundwaters (Simpson et al., 1985) have indicated that, without the presence of bicarbonate, the uniform corrosion rate of these materials decreased with time. The highest corrosion rate reported, measured by hydrogen generation, was 0.0065 mm/yr at 50 °C. A decrease in the corrosion rate was observed at 80 and 140 °C. Since the system used in these tests was closed, the authors speculated that a change in the nature of the oxide film was the reason for the decrease in the corrosion rate.

Statistically designed autoclave tests (Anantatmula, 1985) in simulated Grande Ronde basalt groundwater with 75 percent basalt and 25 percent bentonite indicated that the corrosion of AISI 1020 steel was lower at 250 °C than at 100 °C. The lower corrosion rate was attributed to the formation of an iron- and silicon-rich clay on the surface of the steel. This strongly adherent layer was formed by a reaction between the steel surface and the basalt-bentonite packing material. No localized corrosion was observed. The pH at the end of testing was measured to be in the range of 6.7–8.8. The corrosion rate under oxic conditions was 0.23 mm/yr and under anoxic conditions was 0.024 mm/yr.

Polarization tests conducted at 95 °C in simulated J-13 water have shown that if the chloride concentrations are increased by a factor of 1,000, carbon steel and other SS can undergo localized corrosion. However, the results of tests (Wilde and Wilde, 1993) in simulated J-13 water with 1,000 times the concentration of all the constituents evaporated to dryness, baked for 24 hr and then rehydrated, indicated that the polarization behavior of AISI 1020 steel, 316L SS, alloy C-22, and platinum was similar. A breakaway potential of 600 mV_{SCE} was observed for all materials. This was attributed to the oxidation of some dissolved species (presumably oxygen evolution) in solution. Post-test

Table 2-6. Composition of groundwaters used for material evaluation in different repository sites

Species	J-13, ppm	Basalt, ppm	Brine A, ppm	Grande Ronde Basalt, ppm	Permian Basin Brine PBB1, ppm	Q-Brine, mg/l at 55 °C	Permian Basin Brine PBB3, ppm
Na^+	51	360	42,000	25	123,000	7,100	23,000
K^+	4.9	3.4	30,000	1.9	40	31,800	10,000
Ca^{2+}	14	2.8	600	1.3	1,600	—	15,000
Mg^{2+}	2.1	0.03	35,000	0.4	130	91,900	53,000
Ba^{2+}	0.003		400			—	
HCO_3^-	120	[a]	700	70	30	-	
SO_4^{2-}	22	175	3,500	108	3,200	14,400	160
Cl^-	7.5	310	190,000	148	191,000	297,300	210,000
NO_3^-	5.6					—	
F^-	2.2	33.4		37		—	
SiO_2	66.4	[b]		65.1		—	
Other	PO_4^{3-}: 0.12 Sr^{2+}: 0.05	BO_3^{3-}: 1,200	Sr^{2+}: 5	CO_3^{2-}: 0.27	Br^-: 32	Satd. O_2: 3.7	Br^-: 2,400
pH	7.1	9.8	6.5	9.8–10		4.9	

[a] 18.1 PPM total organic carbon as HCO_3^- and CO_3^{2-}
[b] 35.5 mg/l Si

examination revealed the presence of a $CaCO_3$ film on the surface of all specimens and no localized corrosion. The formation of the calcium carbonate scale was believed to protect the underlying material from localized corrosion. The authors point out that arbitrarily increasing the concentration of chloride in order to simulate the effects of evaporation concentration without increasing the concentration of the other components in this groundwater may lead to results inconsistent with actual repository conditions.

Autoclave tests (Westerman et al., 1984) of 1025 wrought steel, cast mild steel, ductile cast iron, as well as low alloy steels containing chromium and molybdenum have been conducted in a simulated permian basin salt brine containing high chloride concentrations at a pH of 7.0. The results of these tests indicated that the uniform corrosion rate increased for specimens held at 150 °C versus specimens at 110 °C. The corrosion product film in these tests was determined to be Fe_3O_4. Anhydrite, (Anhydrous $CaSO_4$) was also found on the specimen surfaces. Spalling of the corrosion product films was also observed. The corrosion rate of all specimens, determined by weight loss measurements, was observed to decrease with time of exposure in the range of 3–7 months. The maximum corrosion rates at 3 and 7 months were 0.028 and 0.012 mm/yr, respectively, under oxic conditions where the brine contained 1.5-ppm dissolved oxygen. Under an anoxic condition in which the brine contained 0.5-ppm dissolved oxygen, the corrosion rates were 0.008 and 0.005 mm/yr at 3 and 7 months, respectively. Extension of these data to 1,000-yr results in a corrosion penetration of 25 mm. This extrapolation assumes that localized corrosion does not occur and any time dependent changes in the conditions of exposure do not cause large increases in the corrosion rate in the 1,000 yr after emplacement. For irradiation levels of 2×10^3 rad/hr, the corrosion rate in anoxic brine at 150 °C is equivalent to unirradiated conditions. Increasing the irradiation levels to 1×10^5 rad/hr resulted in corrosion rates of 0.125 mm/yr after 7 months exposure.

A later series of tests (Westerman et al., 1984; Westerman et al., 1986) in brines using 1025 and ASTM A216 grade WCA steel indicated that the corrosion rate was strongly dependent on the concentration of Mg^{2+} in the brine. The uniform corrosion rate was observed to increase from <0.025 to >0.40 mm/yr by increasing the Mg^{2+} concentration from 0–0.46 percent. Additional increases in the Mg^{2+} concentration did not result in such sharp increases in the corrosion rate. Further examination revealed that, in solutions containing 1.5 percent Mg^{2+}, the corrosion product formed on ASTM A216 grade WCA steel contained 5–7 percent Mg and was an Fe-Mg hydroxide. The resulting film was an ineffective oxygen diffusion barrier resulting in increased attack. Apparently, Mg interfered with the $Fe(OH)_2$ to Fe_3O_4 conversion (Westerman and Pittman, 1985). The pH of the Mg^{2+}-containing brines is lower than brines that do not contain Mg^{2+} due to hydrolysis. While it is possible that the increase in acidity may be a factor in the observed increased corrosion rate, no control tests using acidified brines without Mg^{2+} were conducted. The evaluation of several heat treatment schedules indicated that the corrosion rates increased to 0.75 mm/yr when austenized and then exposed to a high-Mg brine environment. This suggests that welding operations may decrease the corrosion resistance in these environments.

European studies (Smialos et al., 1990) have also investigated the corrosion performance of low carbon steel, cast steel, nodular cast iron, and high silicon cast iron in brines with low- and high-Mg contents. Corrosion rates for low carbon steel and cast steel in low-Mg brines were reported to be 0.005–0.020 mm/yr at 90 °C and 0.025–0.040 mm/yr at 170 °C. For high-Mg brines the corrosion rate increased to 0.050–0.060 mm/yr at 90 °C and 0.100–0.130 mm/yr at 170 °C.

2.2.4.2 Localized Corrosion

Localized corrosion of low carbon steels, mild steels, and cast iron materials has been reported as a possibility in salt, basalt, granite, and tuff repositories should the waste containers come in contact with the groundwater closest to the repository horizon. The initiation and propagation of localized corrosion have been examined in simulated repository environments. Detailed studies have been conducted on several materials in order to determine the effect of each of the different species dissolved in the groundwaters.

Results of 5-yr tests of A216/WCA steel exposed to a high Mg-Na-K chloride concentrated brine [Waste Isolation Pilot Plant (WIPP) brine A] at 80–100 °C indicated that all specimens of this material underwent significant uniform corrosion (Sorensen and Molecke, 1992). In addition, many of the specimens suffered severe localized attack in the form of crevice corrosion. The frequency of attack for the welded specimens was reported to be much higher than for unwelded specimens. The authors indicated that with time, sodium chloride and some other unnamed minerals would precipitate out leaving an increasingly magnesium rich brine. Within months, the specimens would be exposed to a near-solid hot salt instead of brine. In addition to some ambiguity with regard to the test environment, there are insufficient data given to calculate the corrosion rate or the penetration depth of the localized attack.

Carbon steels and cast irons have been observed to undergo localized corrosion in the low-Mg brine at a pH of 6 (Smialos et al., 1990). The localized corrosion observed here was not in the form of pits in the classic sense of passive film breakdown but rather preferential attack on various areas of the specimen that were attributed to imperfections in the steel. Maximum penetrations in low-Mg brines were 0.030–40 mm/yr at 90 °C and 0.120–0.150 mm/yr at 170 °C. This preferential attack was not observed in high-Mg brines. The corrosion rate was not affected by welding or exposure to radiation sources.

Cast steel containing Cr and Mo, as well as ductile iron specimens, have been shown to undergo crevice attack in Grande Ronde basalt groundwater at 150 and 250 °C (Nelson et al., 1984). Under a dose rate of 3×10^5 rad/hr the corrosion rate was reported to increase 2–3 times with respect to that of nonirradiated conditions. Studies (Thompson, and Beavers, 1990; Beavers et al., 1987b) investigating the effects of the different dissolved species of groundwater present in basalt repositories have indicated that carbon steel had an active-passive behavior in this environment. An increased chloride concentration tended to decrease the pitting and repassivation potentials indicating more severe pitting conditions. Conversely, increasing the carbonate concentration shifted E_p and E_{rp} to more noble values indicating a region of increased passivity. The corrosion potential was shown to shift to more active values with the addition of nitrate.

Pitting corrosion of carbon steels and cast iron materials has been observed under conditions possible in granite repositories (Simpson et al., 1985; Marsh et al., 1985). Several studies have developed experimentally determined potential-pH diagrams to define areas in which the localized corrosion of these materials can occur. The regions of passivity, pitting, and uniform corrosion have been shown in these diagrams to be dependent on the concentration of bicarbonate and chloride. The potential-pH diagrams developed by Marsh et al. (1985) are shown in Figure 2-8. It may be seen from Figure 2-8 determined by cyclic polarization tests at 50 °C, that at low bicarbonate concentrations the corrosion of carbon steel is uniform. A region of passivity was observed after the bicarbonate concentration was increased by a factor of 10. Pitting of the material was observed in 0.001 M HCO_3^-/CO_3^{2-} + 10 ppm Cl^- at a pH of 9.2 and a potential of -600 mV_{SCE}. Increasing the chloride concentration shifted the regions of passivity and pitting to lower potentials and higher pH values. For well buffered systems, the type of

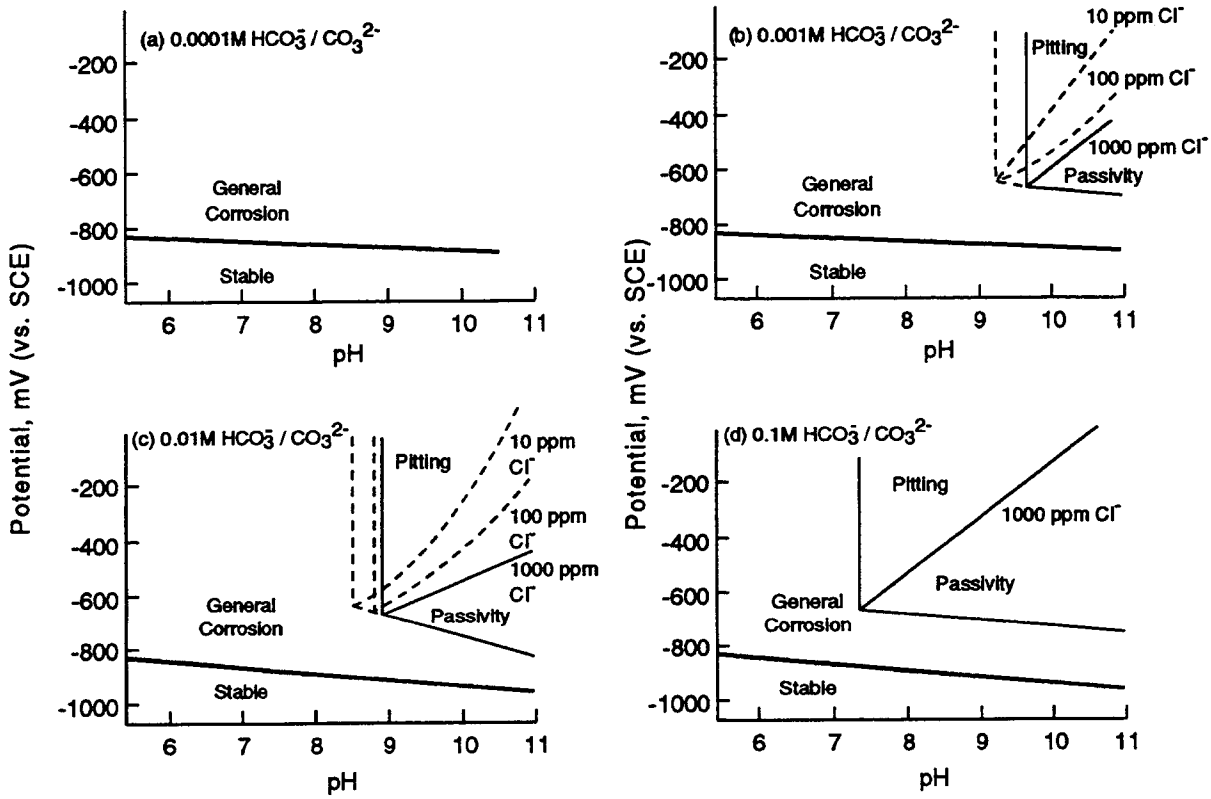

Figure 2-8. Potential pH diagrams determined by cyclic polarization of carbon steel at 50 °C (Marsh et al., 1985)

corrosion may shift from localized attack to uniform corrosion as the chloride concentration is increased. Such observations have been reported by Simpson et al. (1985) who observed localized attack at pH 8.5 and pH 10 in 80–800 ppm Cl^- but uniform corrosion in 8,000 ppm Cl^- in the same pH range. A similar study (Kosaki and Komada, 1993) has reported that steel is in the passive state in 1 mM HCO_3^-, but the pitting potential was above the stability line of water corresponding to oxygen evolution. Increasing the Cl^- concentration was observed to lower the pitting potential within the stability limits for water. Increasing the temperature reduced the pH for passivity. Low-carbon steel was found to be passive at 80 °C, in the presence of 10 ppm Cl^- but at pH 8.6; at 50 °C the minimum pH for passivity was 9.5. The presence of bicarbonate and chloride may also be relevant to groundwaters in tuff and basalt repositories.

Investigations by Nakayama and Akashi (1992a,b), using mild steel in solutions containing 1 mM HCO_3^- + 10 ppm Cl^-, showed that the addition of bentonite as a buffer material could alter the pH of the groundwater. They reported a critical pH for passivity of 9.4 at 20 °C. This value was observed to decrease with increasing temperature and increase with higher chloride concentrations. The repassivation potential for crevice corrosion was measured in these solutions by first initiating crevice corrosion and then reducing the potential at a rate of 0.167 mV/s until passivation for a minimum of 2 hr was observed. The results indicated that, in the pH range of 10–11 without the addition of bentonite, the repassivation potential for crevice corrosion, $E_{r,crev}$, was in the range of −0.8 to −0.6 V_{SCE}. This was

well below the pit initiation potential, E_p, of $-0.2\ V_{SCE}$. A similar value of $E_{r,crev}$ was obtained (Kosaki and Komada, 1993) under comparable conditions. The addition of bentonite was observed to lower the pit initiation potentials to $-0.7\ V_{SCE}$. Bentonite-solution ratios had less of an effect on the $E_{r,crev}$. A decrease of 80 mV was observed for $E_{r,crev}$ as the bentonite solution ratio was changed from 0 to 0.1. The decrease in the E_p was believed to be a result of the bentonite particles acting as crevice formers. Similar observations were also made in seawater/bentonite systems (Sasaki et al., 1992). The critical potentials were approximately the same for both aerated and deaerated conditions (Nakayama and Akashi, 1992b). No crevice corrosion was initiated on specimens potentiostatically held at $E_{r,crev}$ for times up to 4×10^6 sec. However, crevice corrosion was initiated within 10^6 sec on specimens held 50 mV anodic to $E_{r,crev}$. Increasing the potential resulted in faster initiation times.

The corrosion behavior of several steels including AISI 1020, ASTM A-36, 9Cr-1Mo, and nodular cast iron, has been investigated for use as borehole liners in water representative of a tuff repository (McCright and Weiss, 1985). All of the materials showed some evidence of crevice attack and several specimens showed localized attack on uncreviced regions as well. The maximum corrosion rate for a 1,500-hr test was found to occur at 70–80 °C, where the concentration of dissolved oxygen was between 4.5 and 3.3 ppm. For AISI 1020 carbon steel, the maximum corrosion rate, determined by weight loss for a 1,500-hr test, was 0.53 mm/yr. In comparison, the corrosion rate measured by polarization resistance was 0.84 mm/yr. The highest pitting corrosion rate was measured to be 1.0 mm/yr at 90 °C. The highest measured crevice corrosion rate was 0.6 mm/yr at 100 °C, corresponding to a crevice factor of 1.98. The corrosion rates measured in long-term boiling J-13 water without air sparging were reported to decrease with time. At 3,000 hr, the general corrosion rate was 0.042 mm/yr in the liquid phase and 0.026 mm/yr in the vapor phase. However, the maximum crevice corrosion rates were found to be 0.26 mm/yr in solution and 0.331 mm/yr in the vapor phase giving crevice factors of 6.25 and 16.3, respectively. Similar observations were reported for a 5,000-hr test for both AISI 1020 and ASTM A-36. Crevice corrosion rates in the vapor phase are quite significant since, a repository is expected to have a mean temperature above the boiling point of water for several hundred years. It is possible that groundwater coming in contact with the waste containers will evaporate and produce a significant amount of vapor in this time frame.

The effect of oxidation of container materials in a dry environment on the corrosion performance in aqueous conditions is also of significance in an unsaturated hot repository. One study (Jurek and Szklarska-Smialowska, 1976) indicated that the pitting potential for specimens oxidized at different temperatures did not change. However, the number of pits for specimens oxidized and subsequently held above the pit initiation potential in a borate buffer with 0.1 M Cl^- at 20 °C for 20 min decreased with the time of oxidation up to 150 °C. At 200 °C, the number of pits was not found to be a function of oxidation time. At 250 °C, hematite forms over the magnetite film and the number of pits increases rapidly. For specimens thermally oxidized at 300–400 °C, the number of pits decreases with oxidation time and the pits observed are very shallow. There was no relationship between the electronic properties and the corrosion behavior of the films. Instead, it was determined that breakdown mainly depends on the structure of the films. The outer layer of the film was determined to be more important than the inner layer. If the outer film is discontinuous or has cracks, then Cl^- and H^+ can concentrate within the defects of the outer layer and promote breakdown of the inner film. Oxide films formed at 250 °C were found to be more susceptible to breakdown in the aqueous environment. Films formed at 100–200 °C were less susceptible to breakdown as evidenced by the fewest number of pits. However, the pits on these specimens, which were covered with a magnetite film, were the largest and deepest. For high temperature oxides formed at 300–400 °C, the breakdown of the porous film tends to result in general corrosion rather than pitting corrosion.

The formation of pits and crevice corrosion on low carbon steel and cast iron materials in simulated repository environments means that the container lifetime will depend upon the time required for the localized attack to penetrate the container wall. An investigation (Beavers et al., 1987) into the pit propagation rate for AISI 1020 steel in basalt groundwater at 25 °C was conducted using reactive and nonreactive wall geometries, schematically shown in Figure 2-9. These tests were conducted by constructing artificial pits of different aspect ratios and measuring the current with a zero resistance ammeter. The pits were filled with a 0.1-N $HCl^{-}Fe_3O_4$ paste on the basis that after 6-month exposures of carbon steel to basalt groundwater, pits were found to contain Fe_3O_4 and had a pH of <3. After 130 hr the current density of the nonreactive wall geometry had reached a steady value of 40 $\mu A/cm^2$ which corresponds to a corrosion rate of 0.470 mm/yr. For the reactive wall pits, the current density decreased from 12 to 0.4 $\mu A/cm^2$ corresponding to 0.0047 mm/yr. The uncoupled potential between the reactive wall boldly exposed surface and the pit specimens was a few millivolts. For the nonreactive wall pits, the potential difference was on the order of 70 mV. The current was observed to decrease for smaller pit diameter/depth ratios (deeper pits) for both reactive wall and nonreactive wall pits. The corrosion current increased by a factor of 8 with the presence of a mill scale on the boldly exposed surface. In this case, the open circuit potential of the boldly exposed surface shifts by +100 mV resulting in a larger driving force for pitting. In all cases, nonreactive wall geometries tended to overestimate the pit propagation rate.

An empirical relationship of pit propagation rate for carbon steel in 0.1 M HCO_3 and 1,000 ppm Cl^{-} was determined to be $P_{max}=8.35t^{0.46}$ where P is in millimeters and t is in years (Marsh et al., 1985). For a 1,000-yr lifetime, the maximum pit depth would be 200 mm. The question arises whether or not pits grown to these depths would continue to propagate. The IR drop for such large pits may prohibit their further propagation in favor of the initiation of new pits. A similar relationship, $P_{max}=0.746t^{0.37}$, has been reported for wrought steels in field service (Accary, 1985).

A long-term study (Marsh et al., 1988) of localized corrosion of Carbon 20 steel (0.173% C, 0.06% S, 0.75% Mn, 0.02% S, 0.02% P) under potentiostatic control in 0.1 M $NaHCO_3$ + 1,000 ppm Cl^{-} at 90 °C for periods up to 10,000 hr found that the pit propagation rate followed an unlimited exponential distribution function of the form:

$$x = x_0 - \frac{1}{b} \ln \left[\frac{P_A(x)a}{N \cdot A} \right] \qquad (2\text{-}12)$$

In the above equation, x is the pit depth, x_0 is the beginning of the measured size distribution and not necessarily the minimum pit depth, and b is a scale parameter characterizing the spread of the distribution. N is the number of pits measured on a sample of area, a. $P_A(x)$ is the probability of a pit exceeding a depth of x on a waste container of area A. The experimentally measured pit density, in terms of number of pits per unit area, given as N/a, was not observed to vary outside of an order of magnitude within the range of measurements taken. The value of x_0 was observed to follow the relationship:

$$x_0 = 9.5 \times 10^{-5} t \qquad (2\text{-}13)$$

where t is time in hours.

The value of b was determined to vary with time according to the expression:

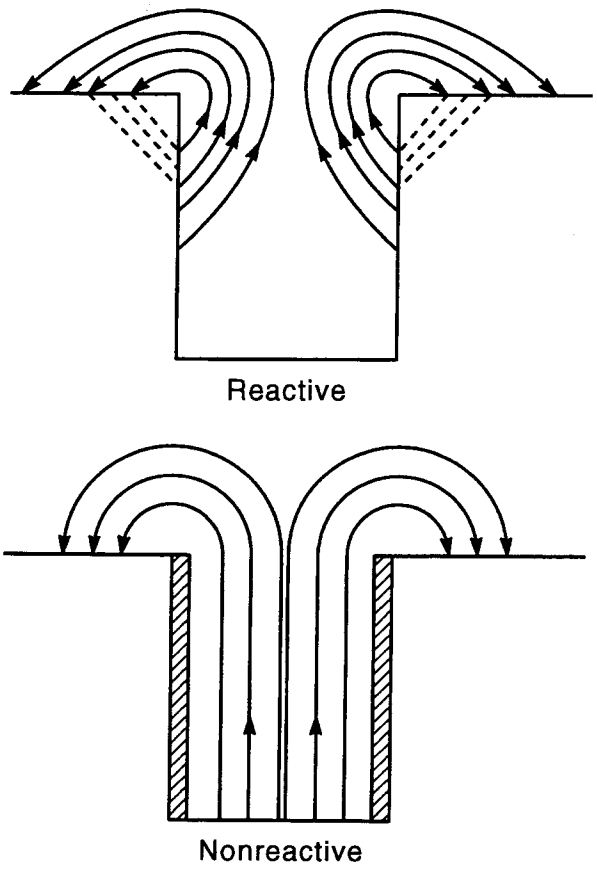

Figure 2-9. Schematic diagram of current flow for reactive and nonreactive pit walls (Beavers et al., 1987a)

$$b = 77.6t^{-0.38} \tag{2-14}$$

With increasing time, the value of b decreases. This, in turn, increases the breadth of the pit distribution, which was observed during the investigation. It is interesting that x_0, which effectively is an uneven general corrosion front, does not decrease with time. This behavior is attributed to the inability of the material to maintain a protective passive film due to the acidic conditions created by the presence of a large number of pits.

Using a probability of 10^{-4}, the corrosion allowance for the waste container may be calculated to be 160 mm assuming that the conditions for pitting corrosion are possible for a period of 125 yr. The general corrosion front, taken as x_0, can be calculated to advance 104 mm in the same time period. It is uncertain if such high propagation rates could be maintained without the use of potentiostatic control. Thus, the authors suggest the calculations show a worst case scenario for this time frame.

Current and pH distribution as a function of time for pits on iron in dilute chloride and sulfate solutions using a scanning vibrating electrode indicate that the pits are initiated at very discrete sites (Isaacs, 1987). The distribution of current density for iron pitting under these conditions as a function of time is shown in Figure 2-10. Initially, the anodic areas are very small and a large area acting as a

cathode exists. After 2 hr, both the number of anodic sites and the current density increase. With extended times, the area of the anodic sites become very large and the area of cathodic sites is reduced. At this point, the current density of the large anodic area is very low, and that of the smaller cathodic area is much higher. Repassivation of the pits is not observed but, alternatively, the pits are observed to spread laterally which significantly decreases the pit propagation rate. Measurements of local pH values with a 0.2-mm antimony probe indicated that the solution over anodic regions had pH values <6 and cathodic areas had pH values >10.

The distribution of pit depths was determined to be a function of both temperature and specimen orientation in dilute chloride and sulfate solutions at pH 8.0 following autoclave exposure for 48 hr at 100 and 200 °C (Bhakta and Solomon, 1987). Plots of pit number density versus pit depth are shown in Figures 2-11 and 2-12. The deepest pits, determined by sectioning, were found on vertical faces at 100 °C. At 200 °C, the pit depth and the pit number density decrease for all surface orientations. The presence of 200 ppm dissolved O_2 resulted in deeper pits.

2.3 STRESS CORROSION CRACKING AND HYDROGEN-ASSISTED CRACKING

2.3.1 Stress Corrosion Cracking

Stress corrosion cracking (SCC) of low- and medium-strength (<690 MPa) ferritic steels occurs in a variety of environments, as reviewed among others by Parkins (1977), Ford (1983), and Kowaka (1990). For alloys that are not normally considered passive, such as carbon and low-alloy steels, SCC occurs in environments which lead to the formation of passive films. This is illustrated in Figure 2-13, in which the potential pH ranges for SCC of carbon steels in acidic and alkaline nitrate (NO_3^-), acidic phosphate ($H_2PO_4^-/HPO_4^{2-}$), bicarbonate/carbonate (HCO_3^-/CO_3^{2-}), and caustic (OH^-) solutions are superimposed on a Pourbaix diagram for the Fe/H_2O system at 25 °C. Severe susceptibility to cracking is encountered when a thermodynamically stable or metastable protective film (magnetite, ferrous phosphate, or ferrous carbonate) is formed, but if ruptured, stable soluble species (Fe^{2+}, $HFeO_2^-$) can be generated. Figure 2-13 includes environments associated with species usually present in groundwaters, with the exception of phosphates. No attempt has been made to incorporate anion concentrations and temperature as variables in the potential-pH plot. It should be noted, however, that SCC of low- and medium-strength ferritic steels occurs in relatively concentrated solutions (>1 M) and at temperatures ranging from 50 °C to the boiling point of the solutions. Figure 2-13 was originally presented by Ford (1983), but modified here to include the range of cracking in alkaline nitrate solutions that was first reported by Parkins and Usher (1962), confirmed under anodic polarization by Hoar and Galvele (1970) and later observed in storage tanks of radioactive waste from defense reprocessed spent fuel (Donovan, 1977; Ondrejcin, 1979; Ondrejcin et al., 1979).

Crack propagation rates have been measured and correlated with measurements of current density on bare surfaces produced in the same solutions and at the same potentials by fast straining, scratching, or fast sweep rate polarization to demonstrate that SCC is promoted by anodic dissolution in all the environments described above. As compiled by Parkins (1980) and shown in Figure 2-14, crack propagation rates can range from 10^{-6} mm/s for phosphate solutions to 2.0×10^{-3} mm/s for acidic nitrate solutions. The line indicates the faradaic relationship between current density and crack velocity. The trend in crack propagation rates for the various environments is in semiquantitative agreement with the cracking severity which increases in the sequence phosphate < carbonate < hydroxide < nitrate (Parkins et al., 1981).

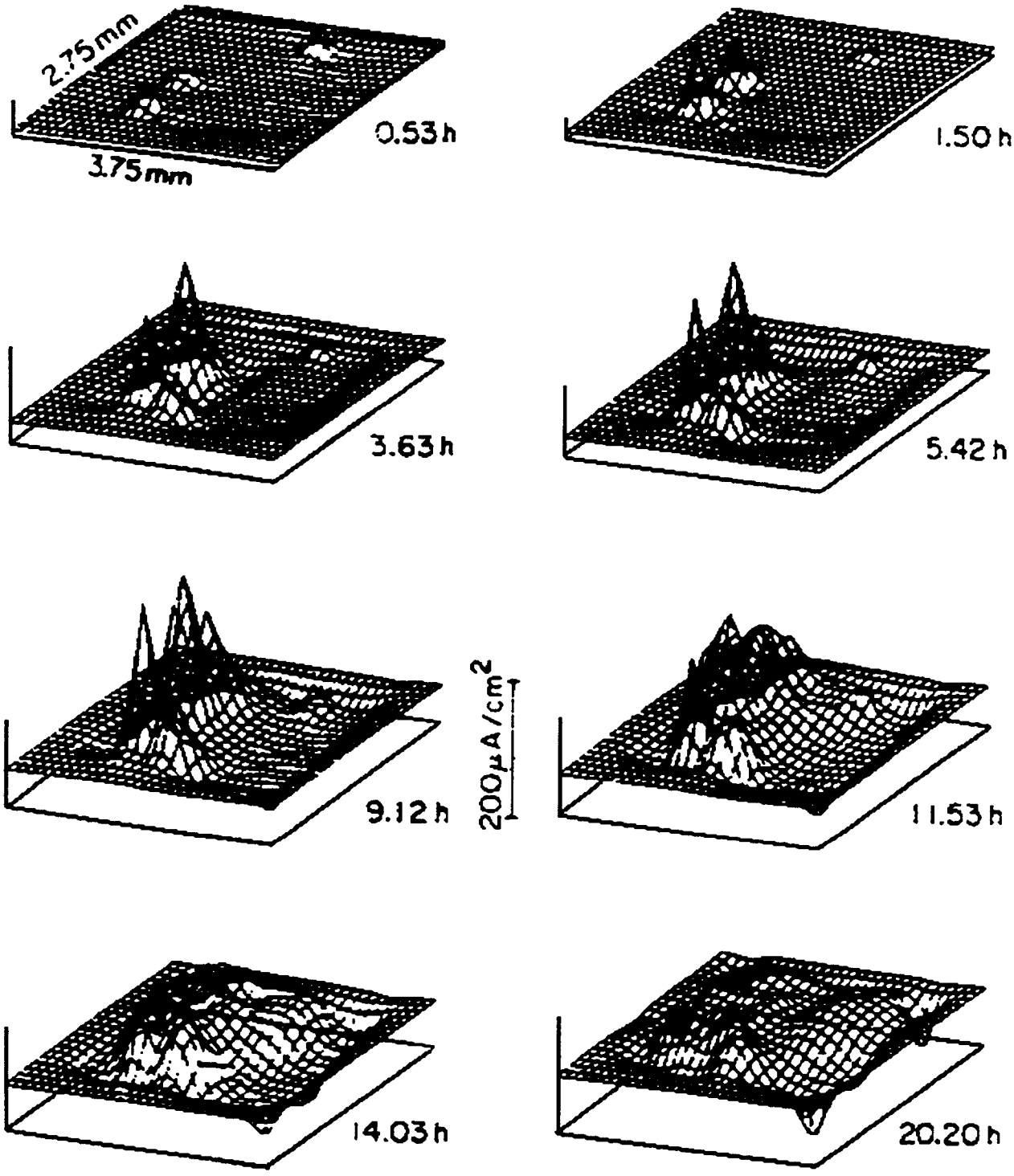

Figure 2-10. Current density distribution with time for iron undergoing pitting corrosion in a 1 mM NaCl + 1-mM Na_2SO_4 solution (Isaacs, 1987)

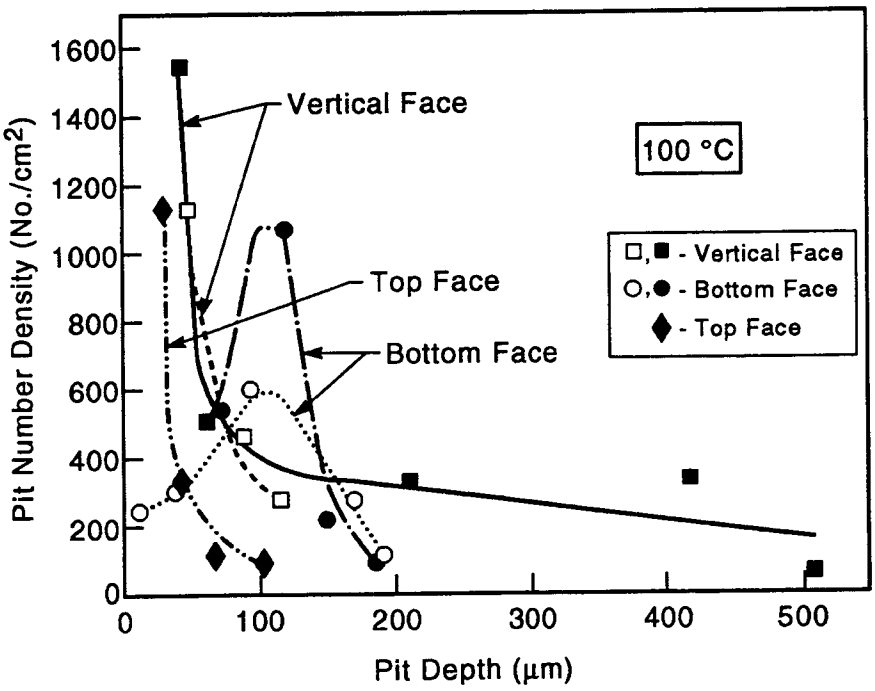

Figure 2-11. Pit number density and pit depth on low carbon steel at 100 °C in 0.006 N NaCl + 0.009 M Na_2SO_4. Open symbols represent solution deaerated with Ar/5% H_2. Filled symbols for solutions deaerated with argon containing 200 ppm O_2 as an impurity. (Bhakta and Solomon, 1987)

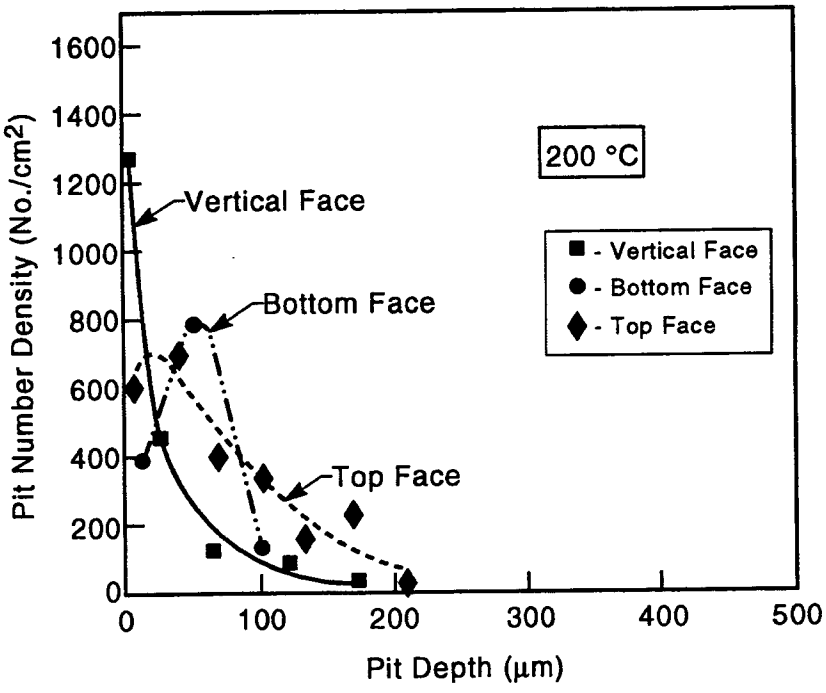

Figure 2-12. Pit number density versus pit depth at 200 °C. Solution deaerated with Ar/5% H_2. (Bhakta and Solomon, 1987)

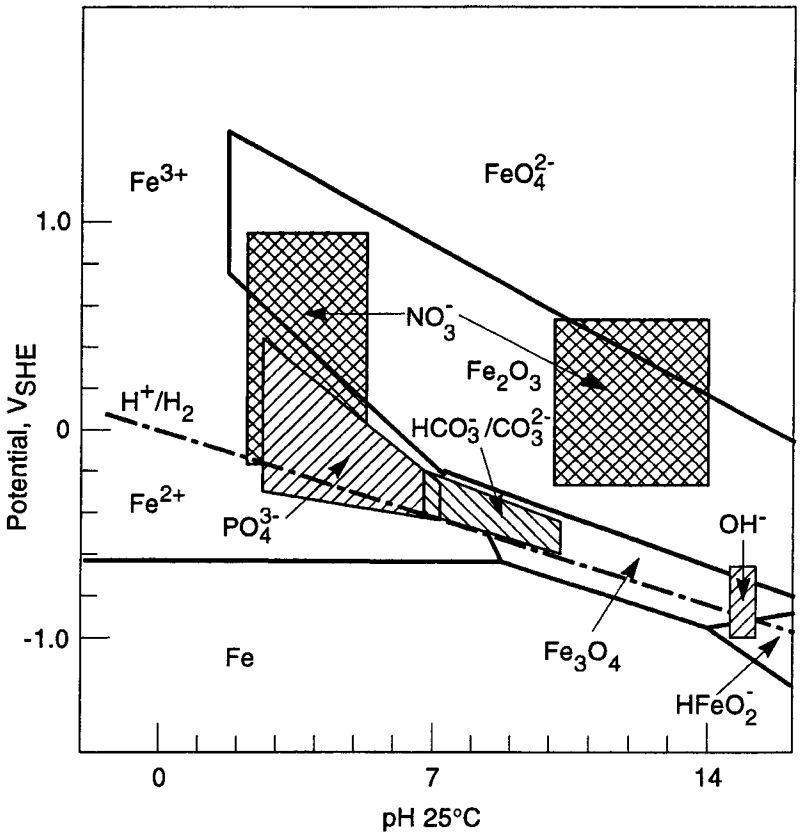

Figure 2-13. Relationship between pH-potential ranges for SCC of carbon steel in various environments and the stability regions for solid and dissolved species on the Pourbaix diagram for iron in water at 25 °C. Adopted and modified from Ford (1983).

In the environments considered in Figure 2-13, SCC is intergranular with the exception of phosphate solutions in which transgranular cracking has been observed (Parkins et al., 1978), although the predominance of intergranular cracking was reported by Flis (1979). Parkins et al. (1978) used a 0.23 percent carbon steel, whereas Flis (1979) tested Armco iron (0.011-percent carbon), which may be the reason for the difference in crack morphology.

A data point for the SCC of a ferritic steel containing nickel as a single alloying element (6-percent Ni) in $MgCl_2$ solution is included in Figure 2-14 for comparison. Ferritic steels with the single addition of nickel are susceptible to transgranular cracking in chloride solutions when the nickel content is above 1 percent Ni (Poulson and Parkins, 1973). It should be emphasized, however, that ferritic steels of strength lower than 690 MPa are not usually susceptible to cracking in chloride-containing solutions. On the contrary, high-strength steels are extremely susceptible to environmentally assisted cracking in chloride solutions (Kowaka, 1990; Ciaraldi, 1992), but the susceptibility is related to hydrogen embrittlement. The same embrittlement process is the cause of cracking in the presence of H_2S, as widely reported for failures in sour gas wells. Cracking also occurs in moist mixtures of CO and CO_2 (Figure 2-14), but CO is only found in coal combustion process and similar industrial applications in which incomplete oxidation of carbon or hydrocarbons occur.

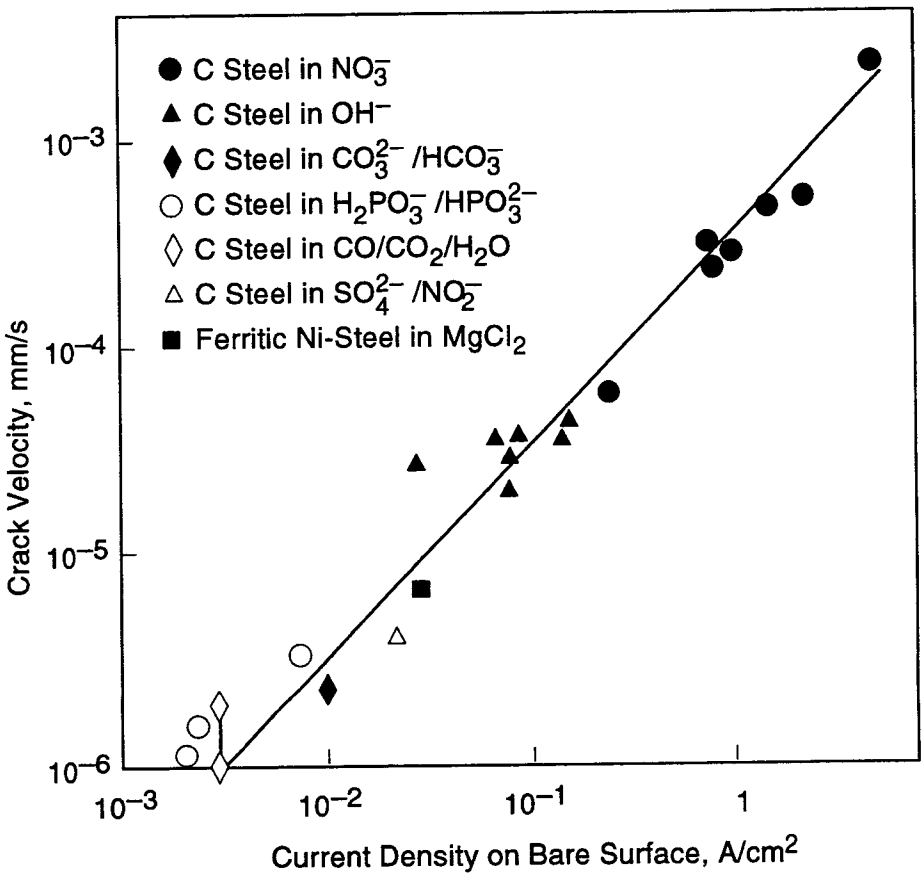

Figure 2-14. Observed crack velocities and current densities associated with bare surfaces for carbon steel in various environments. Adopted and modified from Parkins (1980).

Of all the species involved in the SCC of carbon and low-alloy steels, as summarized before, carbonate/bicarbonate anions may be present in a tuff repository environment at a sufficiently high concentration to promote cracking within the appropriate pH range. It is interesting to note that in the case of carbonate cracking of pipeline steel, the environment that promoted cracking was formed by dissolution of CO_2 present in the soil in the alkaline solutions formed on the pipeline surface as a result of cathodic protection (Payer et al., 1979).

The nitrate concentration in the groundwater is similar to that of chloride, but evaporation processes may lead to high concentrations. However, it appears that high pHs are required to induce cracking in nitrate solutions. Although the formation of nitrate can be considered possible in humid air in the presence of γ-radiation (Reed and van Konynenburg, 1991), the design of the waste package with a carbon steel overpack will presumably provide enough shielding to suppress the formation of oxidized nitrogen species at the outer surface. In principle, the risk of caustic cracking can be precluded because pH values greater than 9.5, or at the most 10.0, are not expected in the near-field environment. The concentration of phosphate is negligible in the groundwater, and, therefore, even in the presence of evaporation processes that may raise the concentration, it is difficult to anticipate concentrations in the molar range as required for cracking to occur (Flis, 1979).

The cracking of carbon steels in carbonate/bicarbonate solutions has been extensively investigated. As shown in Figure 2-15, SCC occurs in a narrow potential range of less than 200 mV in a 1N Na_2CO_3 + 1N $NaHCO_3$ solution at 90 °C, as indicated by the percentage in the reduction in area at fracture (Sutcliffe et al., 1972). The potential range for cracking corresponds to that at which a current peak is observed in the fast sweep rate polarization curve and a substantial current decay, corresponding to the beginning of passivation, in the slow sweep rate curve. It was noted that SCC also occurs at the same temperature in solutions with different ratios and concentrations of CO_3^{2-} and HCO_3^-, down to a total carbonate (CO_3^{2-} + HCO^-_3) concentration of 0.25 N, covering the pH range indicated in Figure 2-13. However, no cracking was observed in solutions containing Na_2CO_3 alone in which the pH is well above 9.5, suggesting that cracking is inhibited at high pHs. Caustic cracking takes place in highly concentrated hydroxide solutions in which the pH is well above 14 at temperatures higher than 70 °C.

The effect of temperature on the SCC in carbonate/bicarbonate solutions is shown in Figure 2-16 (Sutcliffe et al., 1972). The percentage of reduction in area at fracture increases and the potential range for cracking decreases with decreasing temperature, indicating the SCC becomes less severe at lower temperatures. Arrhenius' plot of crack velocities as a function of the inverse of absolute temperature gives an apparent activation energy of about 46 kJ/mole, which is equivalent to that obtained from the current density on bare surfaces (Parkins, 1975a). SCC in carbonate/bicarbonate solutions is inhibited in different degrees by several anionic species. The inhibiting power increases in the following order: Na_2SiO_3 < NaH_2PO_4 < Na_2CrO_4 (Parkins, 1975b). It is unfortunate that silicates, which are abundant at the potential repository site, are not very efficient inhibitors for the cracking in carbonate/bicarbonate solutions.

In most of the experimental studies conducted in the environments described above, and in particular in carbonate/bicarbonate solutions, steels with carbon contents ranging from 0.04–0.30 percent have been used, representing a wide variety of product forms, including cold- and hot-rolled plates and round bars, tubular products, and in minor proportion steel castings. In general, increases in carbon content within that range have a beneficial effect on the resistance to SCC for carbon steels in the as-rolled or annealed condition, although pure iron is extremely resistant to cracking, which leads to a maximum in susceptibility around 0.03 percent carbon. This trend is affected by heat treatment (Parkins et al., 1973). Very low carbon steels are made more resistant by quenching, while in higher carbon steels (>0.1 percent carbon) the opposite effect is observed as compared to the behavior of annealed material. Subsequent tempering at sufficiently high temperatures (>500 °C) increases the resistance to SCC of higher carbon steels but decreases the resistance of steels with very low carbon content (~ 0.05 percent carbon). Prolonged tempering times result in the maximum resistance to cracking being moved to lower temperatures. In the quenched and tempered steels the crack path is intergranular but following the prior austenite grain boundaries. High resistance to cracking is associated with lower crack velocities and a tendency for multiple branching to develop along ferrite lath boundaries (Parkins et al., 1973).

Alloying elements also have an important effect on the SCC susceptibility in carbonate/bicarbonate solutions. This is clearly illustrated in Figure 2-17. The addition of various transition metals has a beneficial effect that increases in the order Ni < Mo < Cr < Ti, as evaluated by the increase in the time to failure ratio in 1N Na_2CO_3 + 1N $NaHCO_3$ solution at 75 °C within the potential range of maximum susceptibility for the plain carbon steel (0.26 percent carbon) (Parkins et al., 1981). The effect of alloying elements was quantitatively expressed using a multiple regression equation by defining the stress corrosion index (SCI) as an integrated area in the time-to-failure ratio versus potential plot (Figure 2-17). The index was normalized by adopting as a unit an area defined by 20 mV for the potential range and 0.05 for the time-to-failure ratio. The time-to-failure ratio is the quotient

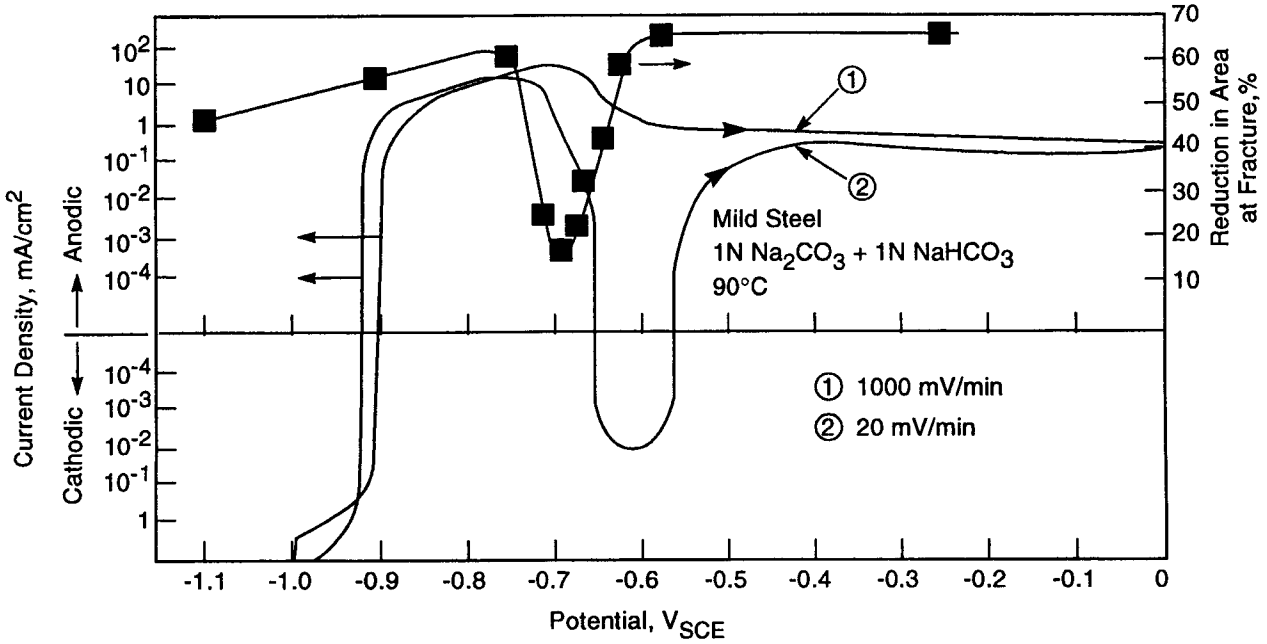

Figure 2-15. Polarization curves at two sweep rates and slow strain rate test results for mild steel in 1N Na_2CO_3 + 1N $NaHCO_3$ solution at 90 °C (Sutcliffe et al., 1972)

between the time to failure in solution and that in an inert environment (e.g., oil). The expression for the SCC in carbonate solutions is:

$$SCI = 41 - 17.3\ (\%Ti) - 7.8\ (\%Mo) - 5.6\ (\%Cr) - 4.6\ (\%Ni) \qquad (2\text{-}15)$$

in which the effect of minor alloying elements, such as Mn, Al, and Si, was removed from the equation because the *t* ratio (coefficient divided by the standard deviation of the coefficient) was <2, indicating that their influence is marginal. Although the effect of carbon is not included in this equation, Parkins et al. (1981) indicated that cracking resistance increases with increasing carbon content, at least above 0.03-percent carbon.

Residual stresses resulting from fabrication processes, in particular welding, are among the predominant mechanical factors to be considered for assessing the possible incidence of SCC on the performance of HLW containers. Although no studies on the beneficial effect of stress relief has been reported in the open literature for the case of SCC in carbonate/bicarbonate solutions, it is likely that post-weld heat treatments are beneficial for preventing SCC in these solutions as in nitrate and caustic solutions (Parkins, 1985). Although temperatures as low as 400 °C have an effect through partial stress relief, optimum resistance to SCC can only be restored by heating around 650 °C, a temperature at which full stress relief can be attained (Parkins, 1985). While full stress relief treatment of a large container or

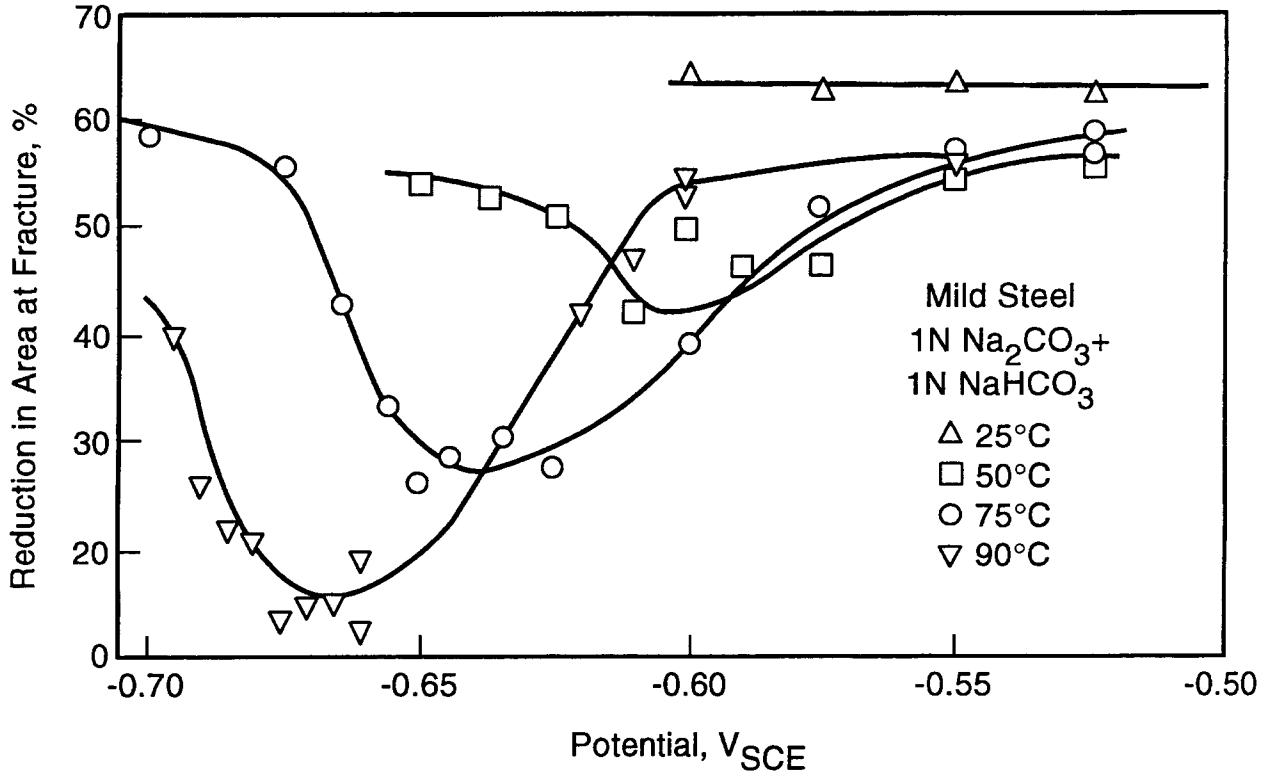

Figure 2-16. Effect of temperature on the SCC of mild steel in slow strain rate tests at various potentials in 1N Na_2CO_3 + 1N $NaHCO_3$ solution (Sutcliffe et al., 1972)

overpack should not be difficult since it is customarily applied to large pressure vessels, heat treatment after closure requires additional consideration in the case of HLW containers. For example, stress relieving of steel at 650 °C may cause severe sensitization of austenitic SS components. Probably, partial stress relief will be used or application of local heating in the closure (welded) area. In the last case, unfavorable redistribution of residual stresses may become a matter of concern.

At the beginning of the 1980s, transgranular cracking of carbon steel in high-temperature (150–280 °C) high-purity water in the presence of dissolved oxygen concentrations of about 0.15 ppm was first observed in laboratory experiments (Weinstein, 1982; Mizuno et al., 1984). Research actively continued in the following years in this apparently innocuous environment as a result of the implications of this finding on the integrity of nuclear pressure vessels. Work conducted in that period revealed that pressure vessel steels were susceptible to cracking in oxygenated water at elevated temperatures (Choi et al., 1982). Transgranular SCC (TGSCC) of ASTM A508-2 steel was observed in pure water containing 1- or 8-ppm oxygen in the temperature range extended from 100–288 °C. However, TGSCC only occurred at 200 °C in the presence of 0.1-ppm oxygen. The susceptibility to SCC increased with increasing oxygen content, but exhibited a maximum as a function of temperature at 250 °C. In the temperature range of 100–150 °C, transgranular cracks initiated from corrosion pits formed in areas adjacent to MnS inclusions.

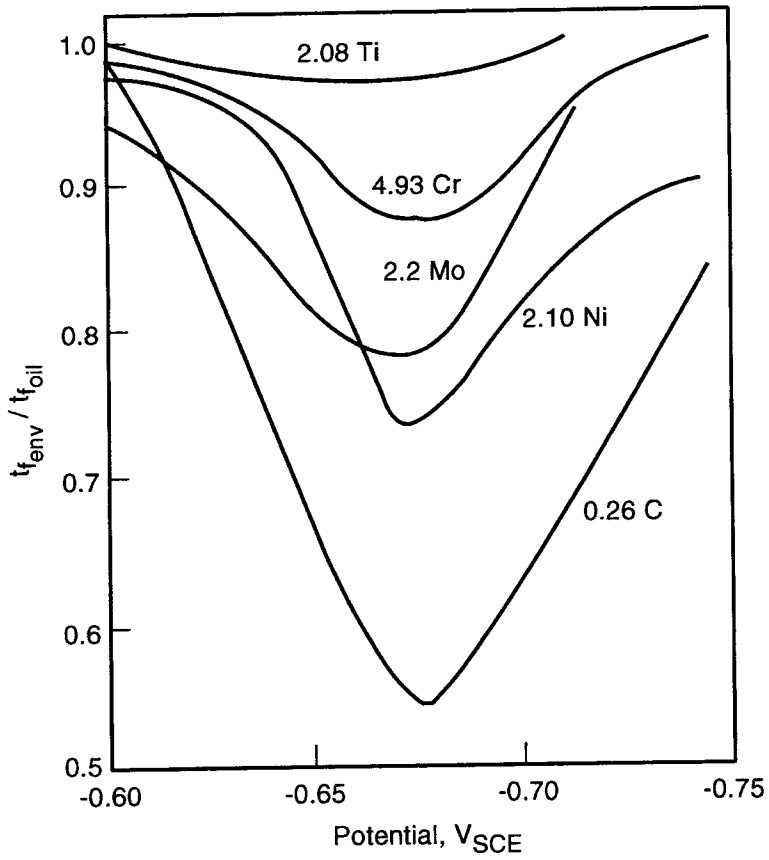

Figure 2-17. Effects of various alloying additions on the SCC of a ferritic steel in 1N Na_2CO_3 + 1N $NaHCO_3$ solution at 75 °C and various potentials (Parkins et al., 1981)

The results described previously as well as many other investigations were summarized by Lenz and Wieling (1986) in the plot shown in Figure 2-18. The range of TGSCC is defined in the three-dimensional (3D) plot in terms of temperature, oxygen concentration, and strain rate. It is evident that TGSCC occurs at very low oxygen concentrations at 250 °C, which is the isotherm corresponding to the highest susceptibility. The susceptibility to cracking decreases abruptly at temperatures close to 100 °C, even at very low strain rates. The role of strain rate is emphasized in this plot because medium-strength, low-alloy steels used for pressure vessels and piping in high temperature water systems seem to be susceptible to TGSCC when tested at low extension rates, but not under constant loading conditions. Hickling and Blind (1986) have reviewed several cases of field failures in which these conditions were considered to be relevant. Cracks located in the HAZ of fillet welds or a nozzle weld were detected in feedwater tanks containing water with approximately 1-ppm oxygen at 180 °C and 10 bar pressure. Other failure cases were observed in thin-walled piping, mostly in the HAZ of welds.

Extensive investigations on the SCC of pressure vessel steels have been conducted and summarized by Speidel and Magdowski (1988). They conducted fracture mechanics tests using precracked compact tension (CT) specimens and double cantilever beam (DCB) specimens of ASTM A533 Gr B steel (yield strength 500 MPa) at temperatures ranging from 100–288 °C. TGSCC was observed in water containing 8 ppm oxygen at 288 °C with crack velocities in the range of 10^{-8}–10^{-7} m/s for the plateau region of the crack velocity versus stress intensity curve. A threshold stress intensity of 20–30 MPa·$m^{1/2}$

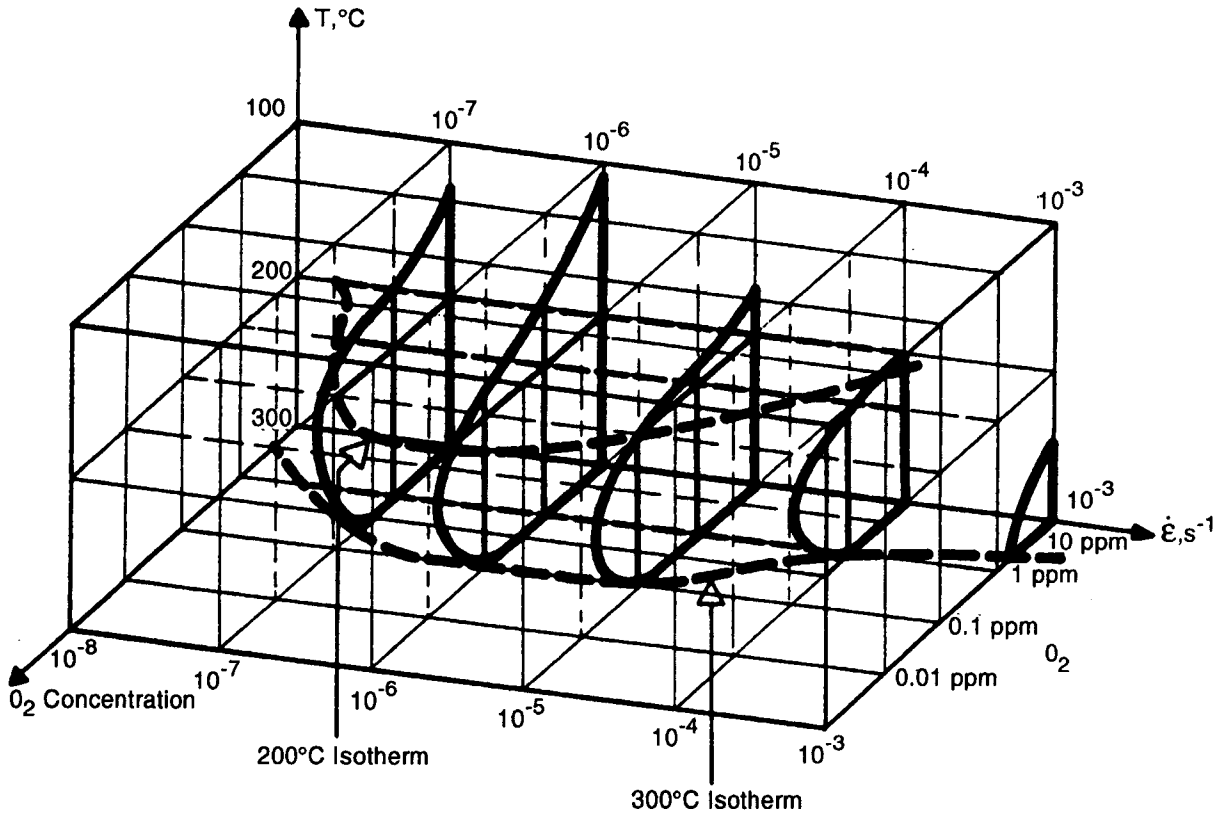

Figure 2-18. Domain of SCC susceptibility of low alloy steels in high temperature water in terms of temperature, oxygen concentration, and strain rate (Lenz and Wieling, 1986)

was determined at the same temperature. The crack velocity decreased to 10^{-11} m/s when the temperature was decreased to 100 °C, which is close to the temperature expected at atmospheric pressure under repository conditions. High pressures, unlikely to be found under repository conditions, are required at temperature above 150 °C to maintain a liquid phase. Magdowski and Speidel (1988) have conducted a similar study using steam turbine rotor steels in which the yield strength ranged from 600–1,200 MPa. For these materials, in which cracking is intergranular, they have demonstrated that crack propagation rate increased with increasing yield strength. Also, cracking was observed at 100 °C even at very low oxygen concentrations. These two observations tend to suggest that for medium strength steels (yield strength below 680 MPa), increasing resistance to SCC should be expected with decreasing strength. However, insufficient data exist at temperatures around 100 °C to evaluate the behavior of pressure vessel steels as a function of other environmental variables, such as oxygen concentration or potential. On the other hand, slow strain rate testing of pressure vessel steels conducted at 250–288 °C have demonstrated that a critical potential exist below which no TGSCC occurred (Hurst et al., 1986). No such data exist at lower temperatures (< 150 °C), probably due to the fact that it is difficult to initiate cracking under such temperature conditions.

McCright and Weiss (1985) conducted a limited number of tests using bent beam specimens (four-point loading) of nodular cast iron, 9Cr-1Mo steel, and AISI 1020 steel fabricated from welded plates. Nine specimens of each material were exposed for 9,000 hr to J-13 well water at 90 °C. None

of the AISI 1020 specimens failed, whereas failure of six 9Cr-1Mo steel specimens and of one nodular cast iron specimen occurred. Failure was related to intergranular cracking in the weld area and was attributed to hydrogen embrittlement as a result of the presence of martensite.

Pitman (1987) evaluated the susceptibility to SCC of ASTM A216 Grade WCA, a cast mild steel, in brine environments containing 5.4 M of chloride anions at temperatures ranging from 90 to 200 °C. No cracks were found in U-bend tests conducted at 90, 150, and 200 °C for 3 months, including tests conducted at 150 °C with welded specimens. Welded and as-cast modified wedge-opening-loading (WOL) specimens did not exhibit crack growth during a 6-month-period exposure in brine at 150 °C. Although decreases in elongation and reduction in area were observed with respect to those in air in slow strain rate tests conducted in brine at 150 °C, no SCC was reported. No cracking was observed in slow strain rate tests conducted at 150 °C under irradiation (1×10^3 rad/hr). The results of these tests, even though limited to open circuit conditions, seem to confirm the resistance of carbon steels to cracking in concentrated chloride solutions.

There is lack of relevant data for the materials of interest in the temperature range around 100 °C. Although the cracking of pipeline steels on the presence of carbonate/bicarbonate solutions is well documented, there are no data for cast steels. The same argument is valid in the case of the cracking in pure water, with the additional complication that in this case not even a good phenomenological characterization of the cracking of pressure vessel steels exist at 100 °C. It appears, however, that in both types of environments the presence of welds and the associated HAZ is a matter of additional concern. The appropriate closure methods should be thoroughly evaluated to avoid increasing risk of SCC under the environmental conditions present in the repository.

2.3.2 Hydrogen-Assisted Cracking Phenomena

2.3.2.1 Terminology

The literature on the hydrogen embrittlement of iron-base alloys is vast and the reader is referred to a number of books and proceedings of conferences devoted to this subject (Staehle et al., 1977; Interrante and Pressouyre, 1982; Oriani et al., 1985; Moody and Thompson, 1990; Gangloff and Ives, 1990). There does not seem to be a single, widely accepted terminology for the various types of hydrogen-assisted cracking processes. The following definitions are adopted for various types of hydrogen-assisted cracking phenomena (ASM International, 1987; NACE International, 1993):

- **Hydrogen Damage**: A general term for the embrittlement, cracking, blistering, and hydride formation that can occur when hydrogen is present in some metals.

- **Hydrogen Embrittlement**: A process resulting in a decrease in toughness or ductility due to the presence of hydrogen. *Internal hydrogen embrittlement* occurs due to the entry of hydrogen from the molten metal which then becomes supersaturated upon solidification. *Environmental hydrogen embrittlement* results from hydrogen absorbed in solid metal either from gaseous sources or electrochemical reactions. The term, as currently accepted, encompasses hydrogen-induced cracking (HIC), hydrogen blistering, hydrogen-assisted cracking, and hydrogen-stress cracking (HSC).

- **Hydrogen-Induced Cracking**: According to NACE and ASM guidelines (ASM, 1987; NACE, 1993), this term is no longer accepted as a standard usage. However, this term has been in common usage especially in the oil and gas industry. As it was used originally, it referred to a form of hydrogen embrittlement in which stepwise cracking was caused by the presence of internal hydrogen.

- **Hydrogen Blistering**: This term is no longer accepted in standard usage. It referred to another form of hydrogen embrittlement in which blisters formed below the surface due to accumulation of molecular hydrogen causing excessive internal pressure.

- **Hydrogen Stress Cracking**: This term refers to hydrogen embrittlement that occurs due to cathodically generated hydrogen and the presence of tensile stresses leading to subcritical crack growth.

- **Hydrogen Attack**: This term has not been included in either the ASM or the NACE documents. However, it will be used as such in this report because of its wide usage for a specific phenomenon. This term refers to cracking due to the reaction of hydrogen that enters from the environment with the carbon from the second phase particles in steel to form high-pressure methane bubbles at defect sites in the metal.

- **Hydriding**: This is another term not included in the ASM and NACE documents. It commonly refers to the reaction of hydrogen with the parent metal, such as zirconium and titanium, to form brittle hydrides.

2.3.2.2 Hydrogen Embrittlement

There is complete agreement in the literature that higher temperatures (100 °C or above) lead to a lower tendency to cracking by this mechanism. While the microscopic/atomistic mechanism for the embrittlement phenomenon may still be under debate (Birnbaum, 1990), the lessening of embrittlement with temperature is believed to be due to a decrease in accumulation of hydrogen at defect sites and sites of high triaxial stresses. Based on equilibrium segregation theory (McLean, 1958), the concentration of hydrogen at a defect site can be estimated to be:

$$C_D = C_0 \cdot e^{\left(\frac{E_b}{RT}\right)} \tag{2-16}$$

where C_D is the concentration at the defect site, C_0 is the concentration in the lattice, and E_b is the binding energy of hydrogen to the defect. It must be noted that Eq. (2-6) assumes that the concentrations are $<<1$. Since the binding energy is a positive term, Eq. (2-6) indicates a decrease in concentration of hydrogen at higher temperatures. This does not mean, however, that hydrogen embrittlement can be disregarded as a failure mode for carbon steels. Recent study by Anzai et al. (1992) showed that hydrogen-induced crack growth of A533-B steel can occur at temperatures as high as 165 °C, provided sufficient hydrogen exists at the crack tip. Their results are shown in Figure 2-19. The data in this figure were obtained by exposing specimens to gaseous hydrogen at various pressures and conducting constant extension rate tests. The crack tip hydrogen concentration was calculated from the hydrogen partial pressure in the gas by using the following equation:

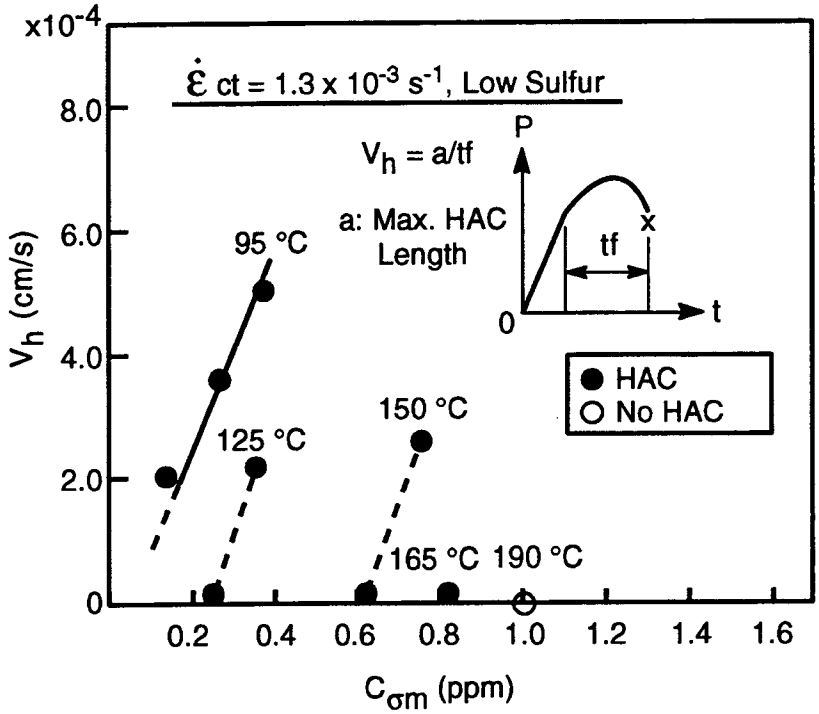

Figure 2-19. Effect of calculated crack tip hydrogen concentration on gaseous hydrogen induced crack growth in A533–B steel at various temperatures (Anzai et al., 1992). V_h = crack velocity; a: max. crack length; t_f = time to failure; $\dot{\epsilon}$ = strain rate; $C_{\sigma m}$ = calculated crack tip hydrogen concentration.

$$C_{\sigma m} = K_0 p^{\frac{1}{2}} e^{\left[\frac{-\Delta H_c + \frac{(1+\pi)\sigma_y V}{\sqrt{3}}}{RT}\right]} \tag{2-17}$$

where $C_{\sigma m}$ is the crack-tip concentration, K_0 is the Sievert's law constant for hydrogen, p is the hydrogen partial pressure, ΔH_c is the partial molar enthalpy, σ_y is the yield strength of the steel, V is the partial molar volume of atomic hydrogen, R is the gas constant, and T is the absolute temperature. Somewhat similar response of hydrogen embrittlement to temperature and hydrogen fugacity was indicated for high-strength steels of the 4340 and 4130 types by Wei and Gao (1985), who examined a much wider temperature range. Hence, the possibility of hydrogen embrittlement due to atomic hydrogen depends on the anticipated hydrogen fugacity at the overpack surface in the repository. If one assumes that the radiation shielding due to the 3-in.-thick MPC in combination with the 10-in.-thick steel is effective, the hydrogen fugacity depends mainly on the corrosion rate. In the tests done for hydrogen gas generation in steel containers in the WIPP site (Telander and Westerman, 1993), the partial pressure of hydrogen gas generated due to the corrosion process in anoxic brine at 30 °C was measured to be about 80 psig (0.55 MPa) after 24 months. Telander and Westerman did not measure the hydrogen absorbed in the steel. Ahn and Soo (1984) also measured hydrogen in the vapor space of an autoclave where cast iron

of type ASTM A216-WCA was tested in basaltic groundwater at 150 °C; they conducted corrosion tests under nonirradiated and γ-irradiated (1.36×10^6 rad/hr) conditions and noted that mole percent of hydrogen in the extracted gases from the autoclave increased with test time. The concentration of hydrogen in the gas was also higher for the irradiated condition, perhaps indicating the effect of radiolysis. However, due to problems with the pressure transducer, the total pressure measurements are unreliable and the fugacity of hydrogen cannot be estimated accurately. Ahn and Soo (1984) did not measure the absorbed hydrogen in the metal samples. Hence, the current experimental results do not permit an estimation of the hydrogen concentration likely to be present in steel overpacks due to environmental effects under the anticipated Yucca Mountain repository conditions.

Hydrogen can also enter from welding processes and cause either blistering due to molecular hydrogen formation or cracking from atomic hydrogen. The atomic hydrogen embrittlement due to weld generated hydrogen, also called delayed hydrogen cracking because of its tendency to occur a certain time period after welding, will be briefly reviewed in this section. This review is excerpted from a more extensive review published by Yurioka and Suzuki (1990). Typical weld metal hydrogen content for various types of welds is shown in Table 2-7 (Yurioka and Suzuki, 1990). It can be seen from Table 2-7 that the hydrogen generated from the gas metal arc welding process is about 1.6 mg/1,000 g of deposited metal, which is quite low. However, submerged arc welding and shielded metal arc welding both give significantly higher hydrogen concentration in the weld metal. It has been shown that the hydrogen in the metal or generated during the welding process segregates toward the weld and is higher under the last pass in the weld (Yurioka and Suzuki, 1990). Preheating the base plate reduces the extent of segregation of hydrogen. The hydrogen embrittlement tendency of a weldment is not only determined by the welding process and filler metal, but also by preheating of the base metals, the type of restraint on the weldment, the post-weld heat treatment, and the base metal composition. Preheating temperature, in addition to its effect on hydrogen segregation, determines the cooling rate after welding and the residual stresses generated. The effect of weld hydrogen content on the preheat necessary to prevent cracking for a medium-strength steel is shown in Figure 2-20. The preheat necessary to prevent cracking for a variety of C-Mn steels has also been evaluated by Hart and Jones (1982). The decay heat of the spent fuel can be used to preheat the steel overpacks before closure welding either at the plant site or at subsequent operations. The effect of post-weld heat treating temperature on hydrogen cracking susceptibility of a variety of steels is shown in Figure 2-21 (Yurioka and Suzuki, 1990). Again, it can be seen that for the A533-B steel, the decay heat can be sufficiently high to prevent hydrogen cracking.

From the brief review of the hydrogen embrittlement of the steel weldments, this mode of failure does not seem to be an important one.

2.3.2.3 Hydrogen Attack

Hydrogen attack occurs when hydrogen entering the metal reacts with carbon in the carbide to form methane gas at internal defects (e.g., at grain boundaries) resulting in crack nucleation due to internal pressure. Steels exposed to high pressure hydrogen in the temperature range of 300–600 °C retain their mechanical properties for days or even months and then suffer rapid deterioration of ductility. After the onset of this embrittlement, grain boundary methane bubbles, which coalesce into cavities, are noted. If the steel continues to operate under these conditions, the grain boundary cavities grow resulting in cracking or loss of strength due to complete decarburization. It must be noted that the cracking process occurs due to internal pressurization, and as such does not require external loading. However, external tensile stresses have been found to aid in the crack nucleation process. This cracking phenomenon was studied originally with respect to cracking of components in various hydrogenation processes (Nelson,

Table 2-7. Typical weld metal hydrogen content for various welding processes (Yurioka and Suzuki, 1990)

Process	Weld Filler	Hydrogen Content ml/100 g			
		D*	R*	M*	U*
Shielded Metal Arc Weld(SMAW)	Basic, lime coated (dried at 70 °C)	9.7	0.9	Hg	FM
	Rutile (from stock)	24.8	6.4	Hg	FM
	Acid (from stock)	18.9	7.4	Hg	FM
	Low H, E9018-M filler (dried at 300 °C)	6.6	—	Hg	DM
	Cellulosic, E8010-G (as-received)	54.0	—	Hg	DM
Submerged Arc Weld (SAW)	Fused (4 days after dried)	4.5	—	GC	DM
	Agglomerated (4 days after dried)	7.0	—	GC	DM
Gas Metal Arc Weld (GMAW)	Ar-20% CO_2 (1.6 mm dia., 28V)	1.8	—	GC	DM

* — D = Diffusible Hydrogen
R = Residual Hydrogen (by vacuum extraction at 650 °C)
M = Method of Measurement: Hg: Mercury displacement
Gc: Gas chromatography
U = Location
DM = per deposited weld metal
FM = per fused weld metal

1 ml/100 g assuming standard pressure and temperature = 8.9×10^{-4} g of H/1,000 g of metal

1949, 1965), and regions of cracking in terms of pressure and temperature were delineated in Figure 2-22. The Nelson curves are used in American Petroleum Institute (API) standards for steels involved in high pressure hydrogen service in the temperature range of 300–600 °C.

The process of methane bubble nucleation preceding cavity growth has been modeled as involving the following steps (Vitovec, 1982):

H_2 (gas) → 2H (adsorbed on surface)
H (adsorbed) → H (dissolved in metal)
H (dissolved) → Diffusion to reaction site

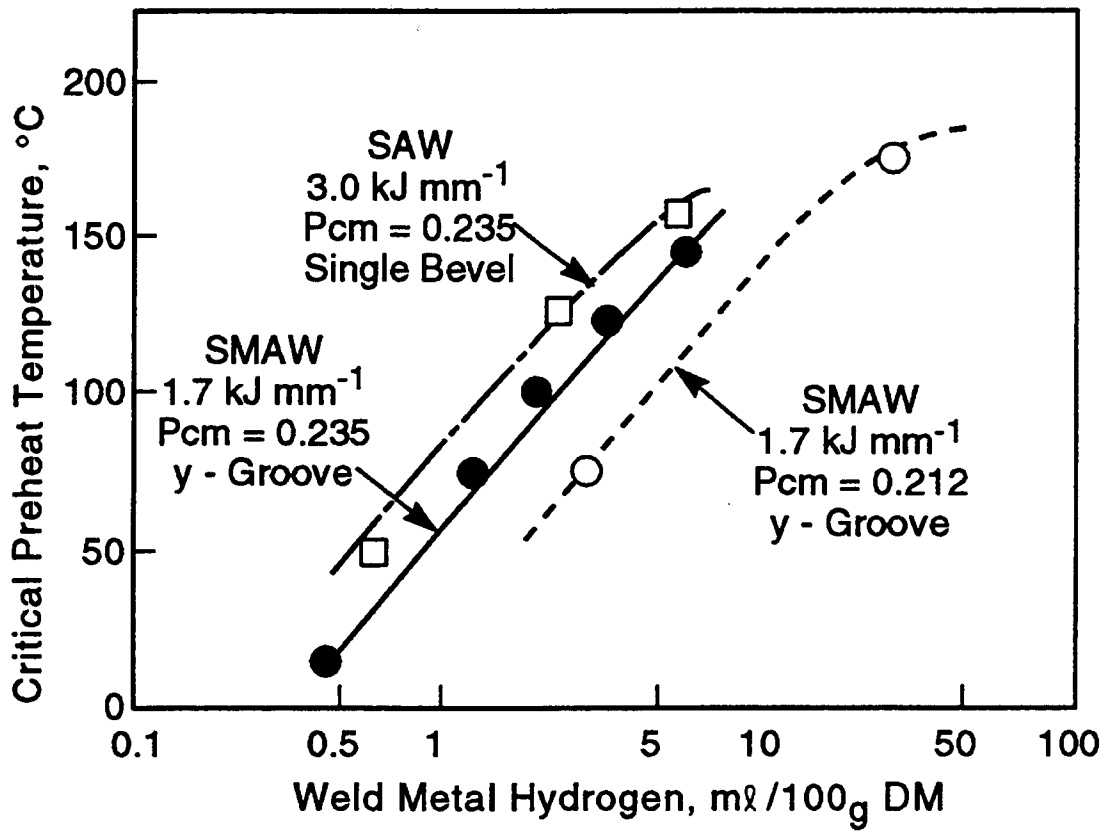

Figure 2-20. Preheat temperature necessary to prevent cracking in 460 MPa yield strength steels versus diffusible hydrogen content (Yurioka and Suzuki, 1990)

Me_xC (metal carbide)	→	$x \cdot Me + C$ (dissolved)
C (dissolved)	→	Diffusion to reaction site
2H (dissolved)	→	H_2 (desorbed at reaction site)
C (dissolved)	→	C (adsorbed at reaction site)
C (adsorbed) $+2H_2$	→	CH_4

Generally, the adsorption and transport of hydrogen to reaction site is not considered to be rate limiting at the temperatures (above 300 °C) and pressures (several MPa) involved. However, the source of surface hydrogen may be an important rate limiting process in the repository environment. At high temperatures and low pressures of hydrogen, the methane is essentially in equilibrium with the carbide and hence bubble nucleation is essentially limited by the supply of hydrogen (external hydrogen fugacity) (Shewmon, 1976). This is indicated by the vertical part of the Nelson curve (Figure 2-22). At low temperatures and high hydrogen pressures, the nucleation of bubbles is governed by the diffusion of carbon from the carbide to the reaction site. This is then indicated by the horizontal part of the Nelson curve. While the Nelson curve was generated for plain-carbon steels of older vintages, more modern, alloyed steels have been shown to have better resistance mainly due to more stable carbides and refined grain size (Sundararajan and Shewmon, 1980; Vitovec, 1982; Masaoka et al., 1982). This is indicated in Figure 2-22, for various additions of Cr and Mo. However, large grain sizes present in the HAZ of

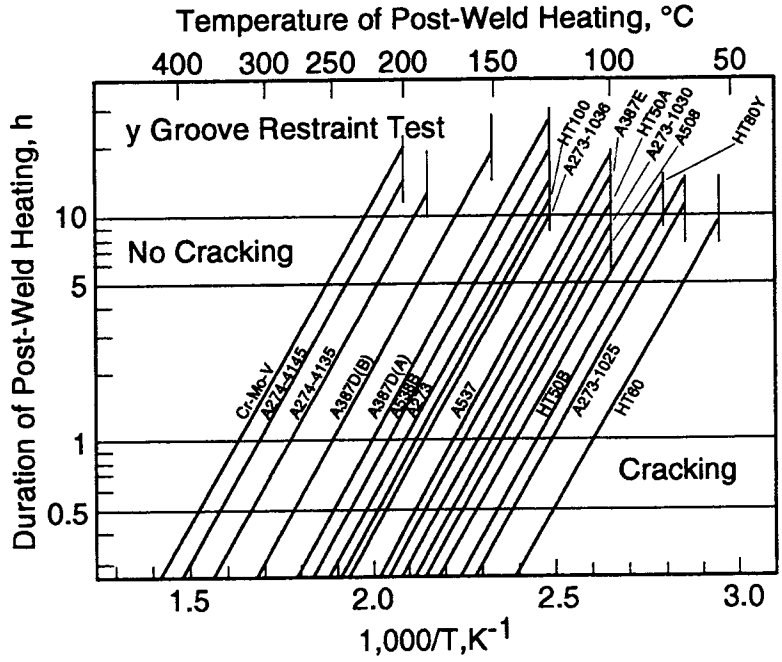

Figure 2-21. Post-weld heat treatment conditions to avoid hydrogen embrittlement of various grades of steel weldments (Yurioka and Suzuki, 1990)

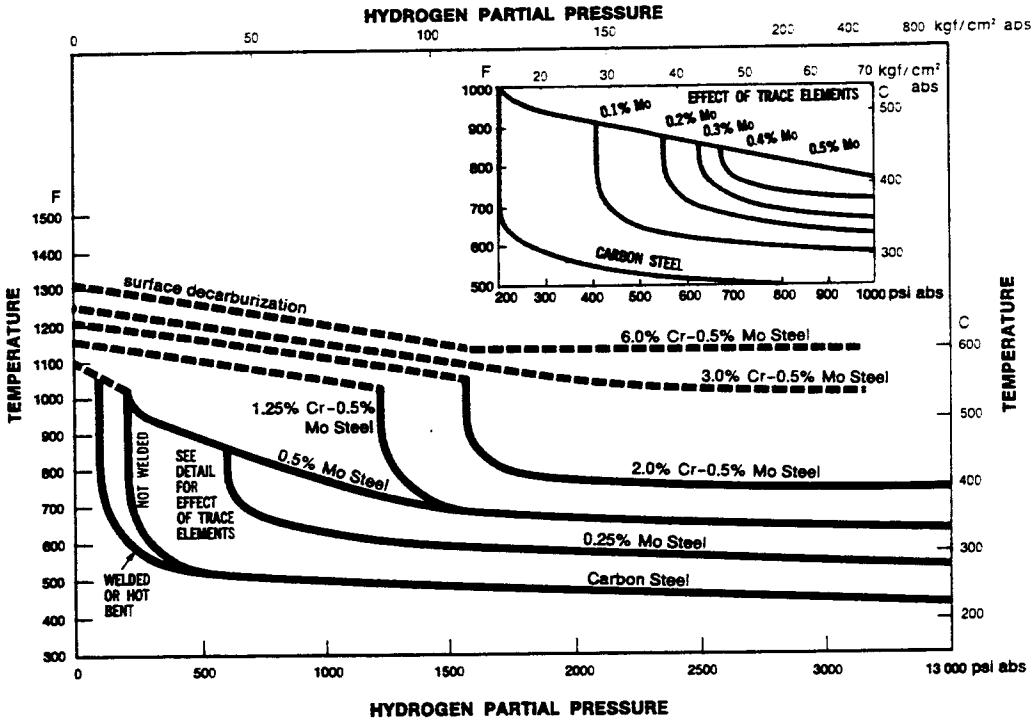

Figure 2-22. Typical pressure-temperature diagram for hydrogen attack of carbon steels (Nelson, 1966)

weldments can increase the severity of hydrogen attack (Masaoka et al., 1982). The incubation time for bubble formation has been related to temperature and pressure by:

$$t_i = kp_{H_2} e^{-\left(\frac{Q}{RT}\right)} \tag{2-18}$$

where p is the hydrogen pressure and Q is an activation energy usually derived empirically.

For the repository environmental considerations, hydrogen pressure is expected mainly from corrosion reactions since radiolysis will be minimal due to shielding of γ radiation. While the current data on hydrogen attack of low-alloy steel may indicate lack of concern with respect to hydrogen attack (region below the Nelson curve), hydrogen attack cannot be ruled out as a possibility for several reasons: (i) much longer time frames are involved (Nelson curves were concerned with only time frames of the order of a decade), (ii) the presence of large grains due to welding may increase the susceptibility to hydrogen attack, and (iii) the ductile iron is considered as a possible disposal overpack. Ductile iron has much higher carbon content and the presence of silicon may increase the activity of carbon, which is an important factor in the low-temperature region. However, no data on hydrogen attack of ductile iron is available.

2.4 MICROBIALLY INFLUENCED CORROSION

The potential for microbially influenced corrosion (MIC) of the candidate and alternate container materials for the proposed Yucca Mountain repository site was examined in detail in a previous report (Geesey, 1993). The environmental conditions expected outside the waste packages, in terms of the geology, hydrology, water chemistry, radiation, temperature, and moisture content were described and followed by a detailed discussion on the characteristics of microbial life in subsurface environments. The ubiquitous nature of many microorganisms was noted, indicating that some of them have survived, and even grown, under extreme temperature conditions or under the high radiation fields encountered in the core of nuclear power reactors. Microorganisms tend to form biofilms on many types of substrates as a complex assemblage of distinct microbial species attached to the substrate through a matrix of extracellular polymeric substances. The importance of microbial biofilms was emphasized in terms of heterogeneous cell distribution and metabolism-driven chemical gradients at or near metal/solution interfaces which may lead to the occurrence of localized corrosion. The influence of biofilm formation in the modification of the corrosion potential established at a metal/solution interface was noted. This variation may lead to the initiation of localized corrosion if the corrosion potential evolves to values above a certain critical potential for that corrosion process.

Although bacteria, as a group of living microorganisms, can function over a wide range of water activity, pH, salinity, temperature, and oxygen concentrations, it was noted that a given species is limited to a substantially narrower range of these parameters for growth. A variety of aerobic and anaerobic microorganisms known to be implicated in MIC were discussed emphasizing the type of metabolic products that their activity generates, as well as their nutrient requirements. By examining the energy requirements to maintain microbial growth under repository conditions, it was concluded in the case of a Swiss repository, that the main energy-producing reaction would be the corrosion of the steel container and that the amount of energy available would be a greater limiting factor than the nutrient availability.

MIC manifests itself primarily as localized corrosion in the form of pitting corrosion. It was emphasized that, during biofilm development, discrete microcolonies of distinct bacteria are found as a heterogeneous and patchy distribution on the metal surface, occluding some areas and leaving others fully exposed to the bulk aqueous phase. This uneven accessibility of the reducible species present in solution to the metal surface (i.e., oxygen under aerobic conditions) leads to the formation of electrochemical cells characterized by the physical separation of cathodic and anodic areas. The depletion of the cathodic reactant (i.e., oxygen) in the occluded area under the biofilm enhances the anodic dissolution of this area, promoting acidification as a result of the hydrolysis of the metal cations, increasing the concentration of aggressive anions (i.e., chloride) and fostering the oxidative dissolution of detrimental species from the metal (i.e., sulfur species from MnS inclusions). In turn, these physicochemical processes tend to increase even more the rate of localized anodic dissolution. The localized environments in these occluded areas are far more complex in the case of MIC than those present under abiotic conditions in crevices or beneath deposits. This complexity is the result of the multiple biochemical reactions associated with the generation of metabolic products through bacterial activities. For these reasons, it is emphasized that inclusion of appropriate controls to account for all other abiotic corrosion reactions is a necessary requirement for the experimental demonstration of microbial involvement in a given corrosion process.

An extensive literature exists on MIC of steels in soil under aerobic and anaerobic conditions. The roles of anaerobic sulfate reducing bacteria (SRB), aerobic sulfur-oxidizing bacteria, and iron-oxidizing and iron-reducing bacteria in the corrosion of mild steel were discussed with special consideration of environmental factors, such as, salinity, temperature, pH, and water potential, as well as mechanistic interpretation of the different steps in the electrochemical corrosion process. Under anaerobic conditions, corrosion of carbon steel in most of the cases is mediated by SRB. The potential for stress corrosion cracking and hydrogen embrittlement of steels in the presence of certain microorganisms that generate molecular hydrogen as a by-product of their metabolism was also evaluated. The section on steels was completed with a review of some publications dealing with studies conducted in Switzerland and the United Kingdom on microbial corrosion of steel containers.

Because the alternate designs involve thick overpacks, radiation is less likely to be a disruptive force for microbial growth. Hence, the effect of temperature on the type and extent of microbiological activity must be the focus of future research. The presence of carbon steel overpack which may supply the energy as a result of corrosion processes and the nutrient supply from repository operations make MIC a potentially important failure mode that needs future research.

3 STAINLESS STEELS AND NICKEL-BASED ALLOYS

Previous Center for Nuclear Waste Regulatory Analyses (CNWRA) reports reviewed various failure processes in this class of alloys. The pitting and crevice corrosion behavior of these alloys was reviewed by Cragnolino and Sridhar (1991). However, this review was limited to the SCP candidate alloys and to the relatively low chloride environment then thought to represent the near-field environment. The SCC behavior of SCP design candidate alloys was reviewed by Cragnolino and Sridhar (1992). This again was essentially confined to relatively low chloride environments. The hydrogen embrittlement susceptibility of these alloys was reviewed briefly by Sridhar et al. (1991). The microbially influenced corrosion of these alloys has been reviewed by Geesey (1993). The objectives of this chapter are: (i) to review those aspects of the behavior of this class of alloys not reviewed before, and (ii) to extend, where necessary, the scope of previous reviews.

3.1 THERMAL STABILITY

Since the MPCs and overpacks are expected to be dry during storage and the initial disposal period, the effect of long-term aging on mechanical properties, at temperatures in the range of 200–350 °C, is examined first. The maximum allowable fuel cladding temperature is 350 °C. The effect of aging on corrosion and environmental cracking is examined in the next section.

3.1.1 Thermal Stability of Multipurpose Canister Materials

3.1.1.1 Wrought Materials

As mentioned in Chapter 1, the MPC has become an important component of the DOE overall waste management system. These MPCs are anticipated to be transported to the MRS site where they will be stored under dry conditions until a disposal facility becomes available. The effect of thermal exposures during storage on the mechanical properties of the MPC is considered first. Further thermal exposure during disposal is also evaluated as well as additional effects due to corrosion during the disposal period.

Under the currently proposed design, the main candidate material for the MPCs is type 316L SS (U.S. Department of Energy, 1993a,b). A proposed alternate MPC material is alloy 825 (Table 1-2). The MPCs will be sealed by circumferential welding, although the details of the welding processes have not been specified. The thermal stability of wrought type 316L SS has been reviewed by Gordon (1977) and Bullen and Gdowski (1988). It has been shown (Weiss and Stickler, 1972) that aging of type 316 and 316L SS in the temperature range of about 500–950 °C resulted in the precipitation of $M_{23}C_6$ (M=Cr,Fe,Mo) carbides and the intermetallic phases, χ, σ, and η (also known as Laves phase). Electrolytic phase extraction in a methanol + HCl mixture and subsequent chemical analysis revealed that the χ and σ phases were enriched in Cr and Mo whereas the η phase was enriched in Mo. These authors also showed that the presence of higher carbon in the alloy (type 316 versus type 316L SS) retarded the formation of the intermetallic phase but accelerated the formation of the carbide. They indicated that aging at 650 °C resulted in considerable loss of impact toughness of wrought type 316L SS. The loss of impact toughness followed the precipitation of $M_{23}C_6$ carbide.

Cold-working prior to aging accelerated the precipitation of carbides and intermetallic phases in type 316 SS (Weiss and Stickler, 1972). Advani et al. (1991) also found that cold-working prior to aging increased the kinetics of precipitation in type 316 SS. They did not measure the effect of

Table 3-1. Calculated diffusion coefficients of chromium from sensitization kinetics as a function of applied strain for type 316 SS (Advani et al., 1991)

Strain Percent	Calculated Chromium Diffusivity, cm^2/s
0	50 exp (−76,000/RT)
2	20 exp (−74,000/RT)
6	0.3 exp (−65,000/RT)
10	0.3 exp (−64,000/RT)
16	0.1 exp (−62,000/RT)
Diffusivity of Cr (Literature): 0.08 exp (−58,711/RT) — Stawström and Hillert (1969) for 18-8 type SS 1.6 exp (−66,2697/RT) — Pruthi et al. (1977) for alloy 600 0.27 exp (−58,711/RT) — Williams and Faulkner, (1987) for type 310 SS	

precipitation on mechanical properties, but quantified it in terms of a degree of sensitization (DOS) using an electrokinetic potential reactivation (EPR) technique. The effect of cold-work and aging time on EPR DOS is shown in Figure 3-1. Advani et al. (1991) found that the sensitization in this material arose essentially from the precipitation $M_{23}C_6$ which is consistent with the observation of Weiss and Stickler (1972) that high carbon alloys show slower precipitation of intermetallic phases. Assuming that the sensitization kinetics is determined by chromium diffusion, these authors calculated the activation energy for Cr diffusion as a function of prior cold-work (plastic strain). This is shown in Table 3-1. The diffusivity of chromium in austenite reported in the literature is also shown in Table 3-1. It can be seen that cold-work reduces the pre-exponential term and the activation energy. However, the diffusivity value reported in the literature corresponds more closely to that calculated for the cold-worked alloy.

The effect of aging on the mechanical properties of wrought alloy 825 has not been reported to any useful extent in the literature. A somewhat similar material, alloy 800 (31 percent Ni compared to 42 percent Ni in alloy 825, no molybdenum or copper as compared to 3 percent Mo and 2 percent Cu in alloy 825), has been examined by Matthews (1976). He has shown that aging at 650 °C for 8,000 hr resulted in a 30 percent reduction in tensile elongation and 60 percent reduction in Charpy V-notch toughness. It is anticipated (Cragnolino and Sridhar, 1993), based on d-band energy calculations, that the presence of Mo in alloy 825 would increase the susceptibility to the precipitation of σ phase. Hence, further examination of low-temperature aging on the fracture toughness of alloy 825 is needed.

3.1.1.2 Weld Metal

Of greater importance to the structural integrity of the MPC is the fracture toughness of the circumferential welds. It is well known that in welding austenitic alloys such as types 304L and 316L SS, a certain amount of ferrite is needed in the weld fusion zone in order to prevent hot cracking (Brooks and Thompson, 1991). Additionally, a primary ferrite solidification mode also minimizes hot-cracking susceptibility (Brooks and Thompson, 1991). The amount of ferrite in the weld fusion zone and the

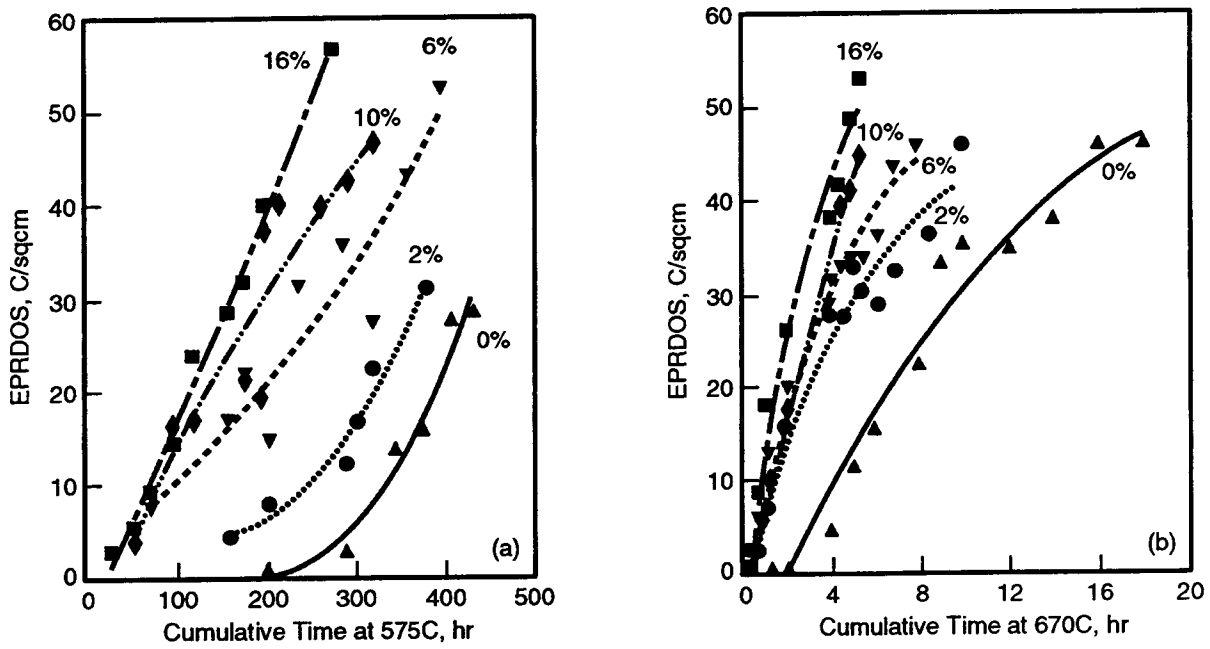

Figure 3-1. Effect of cold-work on the kinetics of aging (sensitization) of wrought type 316 SS at 575 and 670 °C (Advani et al., 1991)

solidification mode are primarily controlled by the ratio of ferrite stabilizing elements (chromium equivalence) to the austenite stabilizing elements (nickel equivalence). The terms chromium equivalence and nickel equivalence arose from a consideration of the Fe-Cr-Ni ternary phase diagram where Cr stabilizes the body centered cubic (bcc) ferrite phase whereas nickel stabilizes the face centered cubic (fcc) austenite phase. For multicomponent systems undergoing nonequilibrium solidification, it is not possible to develop phase diagrams and many empirical regression relationships have been established (Figure 3-2 and Table 3-2) that delineate the regions of stability (at room temperature) of ferrite, austenite, and martensite in terms of a plot of chromium equivalents versus nickel equivalents. Typically, the ferrite content of AISI 300 series weld metal ranges from 3–9 percent. This ferrite can transform to a variety of carbides and intermetallic phases upon subsequent exposure to service temperatures (Smith and Farrar, 1993). It is important to note that, as a general rule, the kinetics of these deleterious phase transformations in the ferrite phase is more rapid than in the austenite phase because of greater diffusivity of substitutional elements in the more open ferrite lattice. The formation of deleterious phases is further exacerbated because, during the solidification of the weld, alloying elements such as Cr and Mo, which are responsible for the carbide and intermetallic precipitates, segregate to the ferrite. The mechanical integrity of the MPC may be determined by the changes in the fracture toughness of the weakest link that is the circumferential weld. Hence, the kinetics of phase transformation of the weld need careful examination.

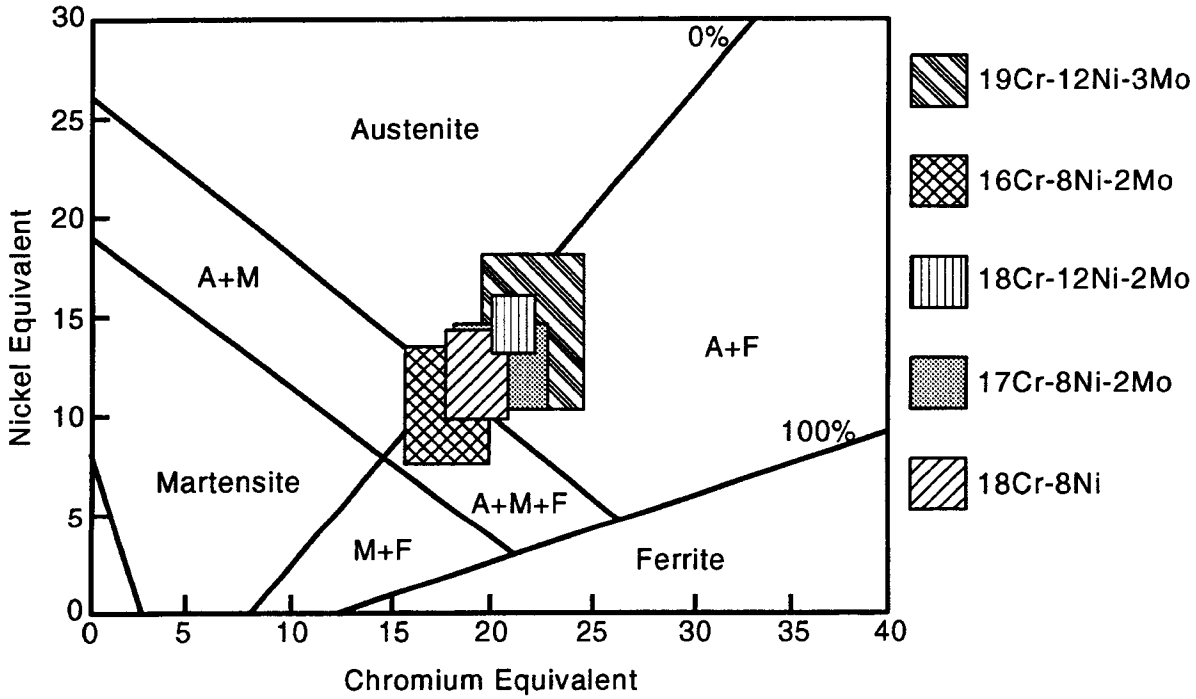

Figure 3-2. Typical compositional ranges of weld metal for AISI 300 series SS plotted on a Schaeffler diagram. The calculation of chromium and nickel equivalents is shown in Table 3-2.

The phase transformations of the ferrite phase of the austenitic SS weld have been reviewed by Smith and Farrar (1993). In essence, the type of phases that form upon aging at temperatures ranging from 500–900 °C are no different from that outlined for the austenitic wrought metal in the previous section. These include the $M_{23}C_6$ type carbide and the intermetallic phases, χ, σ, and η (also known as Laves phases). Gill et al. (1989) have examined the kinetics of precipitation in the temperature range of 500–900 °C and tensile property change in type 316L bead-on-plate weld and found that the σ phase formed the predominant constituent of the precipitates and grew at the expense of $M_{23}C_6$. As in the case of the wrought material, the propensity of the weld metal to forming these phases can be limited by judicious selection of weld metal composition. For example, restricting the molybdenum and silicon and increasing the carbon content of the weld consumable have been shown to retard σ-phase precipitation (Smith and Farrar, 1993).

It has been shown that carbide precipitation has significantly less effect on mechanical properties of the weld than intermetallic precipitation (Smith and Farrar, 1993). Attempts have been made to predict the effect of aging on the mechanical property of type 316 SS welds in terms of a Larson-Miller type parameter as shown in Figure 3-3 (Smith and Farrar, 1993).This is based on aging experiments in the range of 500–900 °C. The data shown in Figure 3-3 indicate, for example, that for a 50 percent reduction in fracture toughness, the weld metal has to be exposed to 300 °C for 8.2×10^{15} yr. The plot of the change in mechanical property as a function of Larson-Miller parameter has no mechanistic justification,

Table 3-2. Chromium and nickel equivalents used in various approaches to predict weld metal ferrite content. Extracted from Smith and Farrar (1993).

Approach	Source	Equivalent	Relationship (weight percent)
Schaeffler	Weld Metal	Cr_{eq}	%Cr + %Mo + 1.5%Si + 0.5%Nb
		Ni_{eq}	%Ni + 0.5%Mn + 30%C
DeLong et al.	Weld Metal	Cr_{eq}	%Cr + %Mo + 1.5%Si + 0.5%Nb
		Ni_{eq}	%Ni + 0.5%Mn + 30%C + 30%N
Guiraldenq	Casting	Cr_{eq}	%Cr + 2%Mo + 1.5%Si + %Nb + 4%Ti
		Ni_{eq}	%Ni + 30%C + 30%N
Hull	Casting	Cr_{eq}	%Cr + 1.21%Mo + 0.48%Si + 0.14%Nb + 2.2%Ti + 2.27%V + 2.48%Al + 0.72%W + 0.21%Ta
		Ni_{eq}	%Ni + 0.11%Mn − 0.0086(%Mn)^2 +24.5%C + 18.4%N + 0.44%Cu + 0.41%Co

unlike the case of creep rate for which it was originally devised (Larson and Miller, 1952). For example, the Larson-Miller parameter under ideal circumstances must be equal to the activation energy divided by gas constant. This is certainly not the case for the data in Figure 3-3 where the activation energy is expected to be that for Cr diffusion. Another factor that argues against the use of Larson-Miller parameter is the dependence of fracture toughness on specific weld filler metal compositions and ferrite content. For example, in cast SS such as CF-8M (cast equivalent to the wrought type 316 SS) which contains much higher volume fractions of ferrite, much faster reduction in toughness to values below the acceptable limit has been predicted (Jaske and Shah, 1989).

It is interesting to note that aging at temperatures below 500 °C for type 316/316L SS welds has not been investigated. In contrast, the SS castings of equivalent compositions, CF-3M and CF-8M, have been examined after aging in the temperature regime of 280–400 °C (Jaske and Shah, 1989; Chung and Chopra, 1989; Chung, 1992). In these alloys, α', a high-chromium phase formed by the spinodal decomposition of the ferrite, is the main cause for lowered toughness. The spinodal decomposition occurs by the segregation of Cr in zones spaced about 8 atoms apart and is affected by the precipitation of a Ni- and Si-rich phase termed the G-phase (Chung and Chopra, 1989). The activation energy of toughness reduction after aging at these temperatures has been found to vary from 18 to 55 kcal/mole. It has been speculated that this is due to the effect of temperature dependent activation energy dictated by G-phase kinetics (Chung and Chopra, 1989). It is important to note that the spinodal decomposition does not occur at temperatures higher than about 400 °C, as shown in Figure 3-4. Jaske and Shah (1989) have used a time-temperature parameter which they also termed P, but which is different from the Larson-Miller parameter, to predict toughness decrease in this temperature regime. Because the CF-8M type castings contain higher ferrite volume fraction than type 316L welds, they are more likely to suffer from α' precipitation.

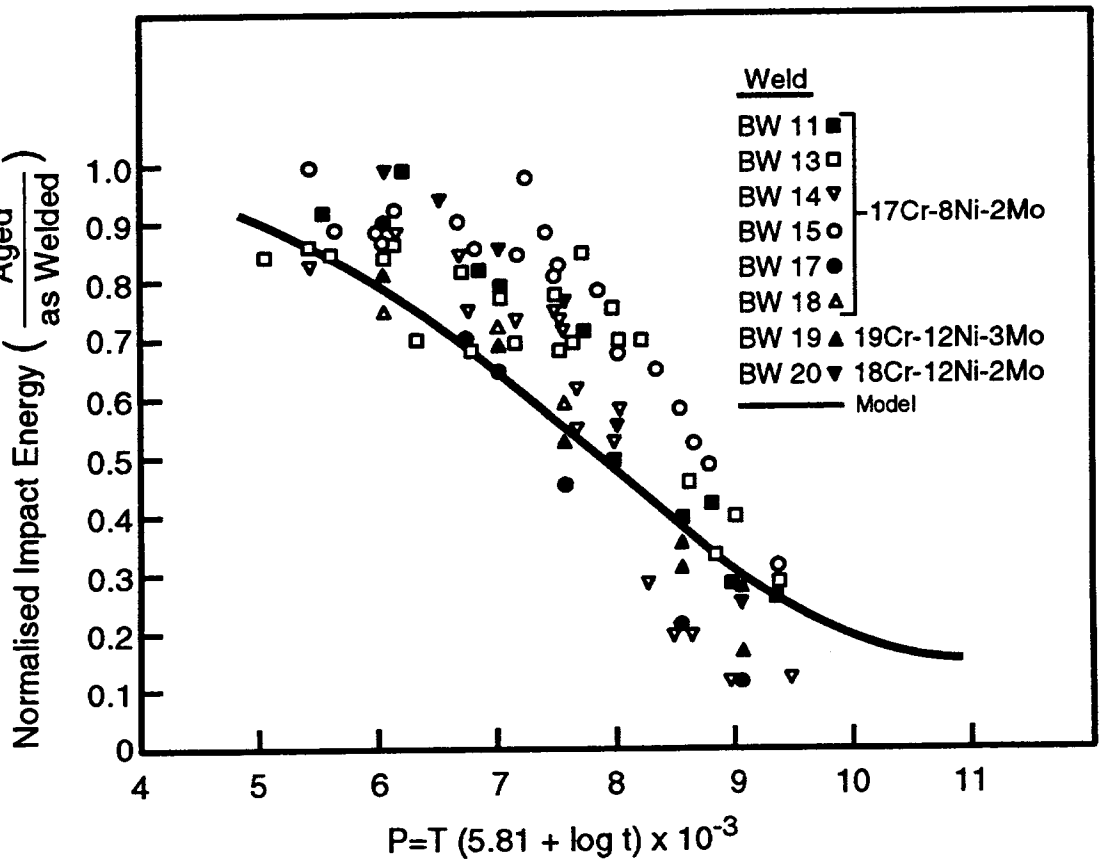

Figure 3-3. Effect of aging at different temperatures and time on the impact energy of type 316 SS welds shown in terms of a normalized impact energy versus Larson-Miller parameter for different weld filler metal composition (Smith and Farrar, 1993)

The effect of aging on the weld metal toughness of the alloy 825 weldments is not known. Because significant segregation of Cr and Mo do occur to the interdendritic spaces of the weld metal, it may be expected that the weld metal may be more prone to the precipitation of σ phase. More information is needed in this area. The effect of plastic strain on the weld metal transformation kinetics is expected to be the same as in the case of the wrought materials, but has not been studied in any of the alloy systems previously discussed.

Finally it must be emphasized that all the discussion in this and previous sections pertained to mechanical property data at room temperature and not at the anticipated repository temperatures. There are virtually no toughness data at temperatures in the range of 100–300 °C. The ferrite phase may have a ductile-brittle transition in this temperature range if a significant amount of α' phase precipitates. However, even with the presence of a α' phase. DBTT may occur at a much lower temperature, in which case, brittle fracture may not occur at repository temperatures. In addition to impact toughness data, other toughness measures, such as critical stress intensity factor (K_{Ic}) or J-integral (J_{Ic}), are necessary for design purposes.

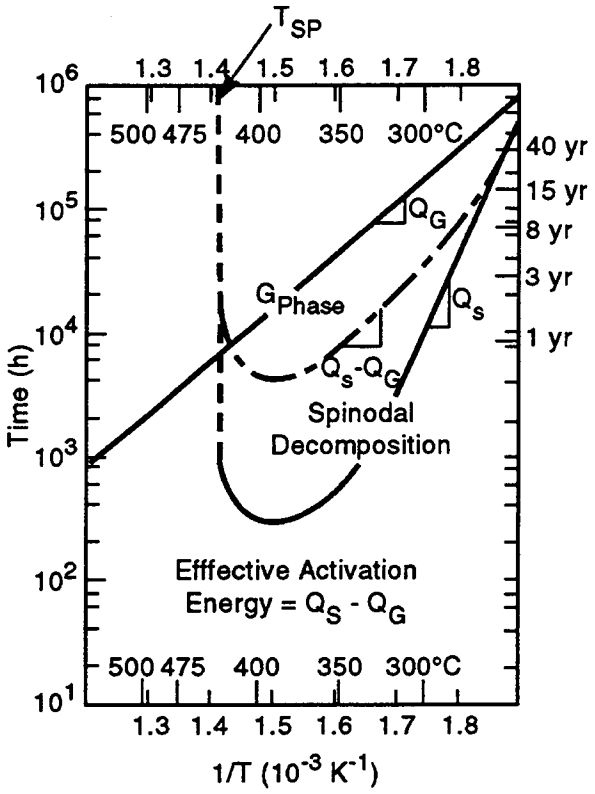

Figure 3-4. Activation energy for the formation of α' phase for CF-3, CF-8M type castings at different temperatures (Chung and Chopra, 1989)

3.1.2 Thermal Stability of Disposal Overpack (Container) Materials

3.1.2.1 Wrought Materials

The carbon steel overpacks are examined in Chapter 2. A potential alternative is the use of robust waste packages (Doering, 1993) where a corrosion resistant inner liner is surrounded by a thick carbon steel outer liner, both together surrounding an MPC. As shown in Table 1-2, alloys 825 and C-4 are being considered as candidate Ni-base alloys for the inner liner. Alloy 825 has already been mentioned in the previous section. Alloy C-4 (Table 1-2) is a Ni-Cr-Mo alloy in the C-family of alloys that was designed specifically for thermal stability towards μ-phase precipitation (Hodge and Kirchner, 1976). Alloys in this class, which include alloy C-22 being used in the IWPE project as a CNWRA reference material, are prone to the formation of M_6C type carbide and intermetallic phases such as μ, σ, P, and Laves (Raghavan et al., 1982). The resistance of alloy C-4 to μ-phase and M_6C-type carbide formation is provided by a reduction of tungsten content, control of iron, reduction of carbon, and addition of the stabilizing element titanium (Hodge and Kirchner, 1976). However, the reduction of tungsten entails a penalty in localized corrosion resistance. Newer alloys such as alloy 59 (Heubner and Köhler, 1992) seek to remedy this deficiency by reducing the tungsten and iron contents and increasing the chromium content.

All the alloys in the Ni-Cr-Mo alloy class suffer from an ordering transformation which occurs in the temperature range of 200–550 °C. The ordering transformation in this system has been studied in

great detail by Tawancy (1981), Raghavan et al. (1981), and Hodge and Ahluwalia (1993). The ordering in this temperature regime involves an initial short-range ordering followed by a long-range ordering. The long-range ordering in these alloys follows the same type of crystallographic modifications found in pure Ni_2Cr^- (Klein et al., 1970) and involves formation of an orthorhombic crystal structure from the (420) or the (220) planes of the parent fcc phase. Long-range ordering does not seem to occur in alloys that contain >10 percent iron as an alloying element (Kargol and Ladna, 1982). It has been shown (Klein et al., 1970) that six orientations of this orthorhombic structure with respect to the parent fcc lattice are possible. Because of the definite orientation requirements, a twinning type deformation mode is preferred over dislocation slip. This increases the work hardening rate and contributes to increased susceptibility to SCC and hydrogen embrittlement. The kinetics of ordering in alloy C-276 is increased by prior cold-working (Sridhar et al., 1980) and alloy C-4 appears to order as much as alloy C-276 (Tawancy et al. 1983). The effect of aging at lower temperatures for longer time periods on the mechanical properties of alloy C-4 has been reported by Hodge and Ahluwalia (1993) and shown in Figure 3-5. It is not clear whether the embrittlement observed due to aging at 538 °C is due to precipitation of M_6C-type carbide or A_2B-type long-range ordering. The microstructural changes under these aging conditions are reported in Figure 3-6 (Hodge and Ahluwalia, 1993). The solid lines indicate approximate time-temperature condition under which long-range ordering (A_2B phase) and M_6C-type carbide occur. Based on these data, Hodge and Ahluwalia concluded that long-range ordering in alloy C-4 or related alloys is not likely under repository thermal conditions for the required containment periods (300–1,000 yr).

Several caveats must be offered for the above conclusion regarding the possibility of long-range ordering under repository thermal conditions. Cold-work prior to aging can increase the kinetics of aging markedly. This is illustrated in Figure 3-7 for alloy C-276 under various cold-rolled conditions (Sridhar et al., 1980). Local areas of cold-work on the containers may occur, for example, due to rock impingement, mechanical damage during handling, or on areas where surface defects such as weld spatter have been mechanically ground. Cold-working in the form of residual strains can also occur from the cylinder rolling operation. The aging kinetics can also be altered in the weld where there are regions of higher Cr and Mo. Data reported by Matthews (1976) suggest that aging for 8,000 hr at 649 °C did not result in a significant drop in tensile ductility of weldment of alloy C-4. Unfortunately, the data are too sparse to make any conclusion with confidence. The temperature is also too high for long-range ordering to occur.

Exposure to temperatures in the range of 200–500 °C not only results in long-range ordering in the Ni-Cr-Mo alloys but also grain boundary segregation of metalloid elements such as phosphorus (Berkowitz and Kane, 1980). As an additional complication, there appears to be coupling between the phosphorus content and ordering in the Ni_2Cr alloy system (Lehman and Kosel, 1985) as higher P content results in a faster ordering reaction. However, the effect of grain boundary segregation on mechanical property, exclusive of environmental effects, has not been studied in any detail.

3.1.2.2 Weldment

Unlike the case of austenitic SS, the Ni-base alloys solidify as fully austenitic welds. However, because of the high alloy content in the Ni-Cr-Mo type alloys and the rapid weld thermal cycles, significant segregation of Cr and Mo occurs in the weld, attended by solid state transformation to intermetallic phases. The welding metallurgy of alloys C-4, C-22, and C-276 has been studied by Cieslak et al. (1986a,b) and Flasche and Ahluwalia (1993). Alloy C-4 was found to be the least likely of the three C-type alloys to form intermetallic phases. The transformation sequences for the three alloys in their autogenous welds are shown in Eq. (3-1). In all the alloys, Cieslak et al. (1986a,b) found a significant

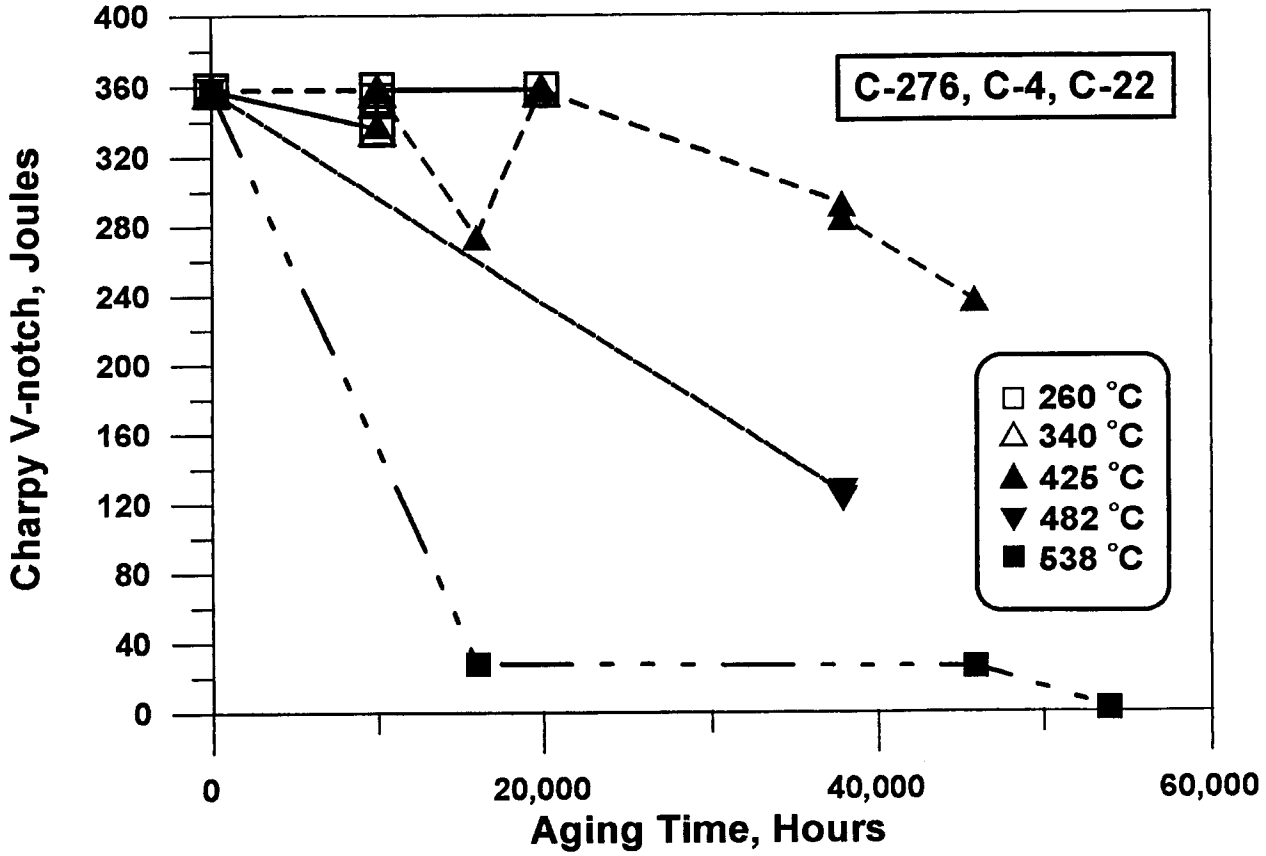

Figure 3-5. Changes in the room temperature Charpy V-notch impact properties as a result of aging for various time periods and temperatures. Drawn from data of Hodge and Ahluwalia (1993).

segregation of alloying elements between the dendrite center (DC) and interdendritic (ID) areas (Figure 3-8). As expected, the segregation of Mo was more than that of Cr because of its greater atomic size and slower diffusivity. While the segregation has been shown to have significant effect on corrosion, the effect on mechanical properties is unknown. Further studies of the effect of low-temperature aging of weldments are needed for these materials.

$$\begin{array}{c} \underline{C\text{-}4} \\ L \rightarrow L+\gamma \rightarrow L+\gamma+TiC \rightarrow \gamma+TiC \\ \\ \underline{C\text{-}276} \\ L \rightarrow L+\gamma \rightarrow L+\gamma+P \rightarrow \gamma+P \rightarrow \gamma+P+\mu \\ \underline{C\text{-}22} \\ L \rightarrow L+\gamma \rightarrow L+\gamma+\sigma \rightarrow \gamma+\sigma \rightarrow \gamma+\sigma+P \rightarrow \gamma+\sigma+P+\mu \end{array} \qquad (3\text{-}1)$$

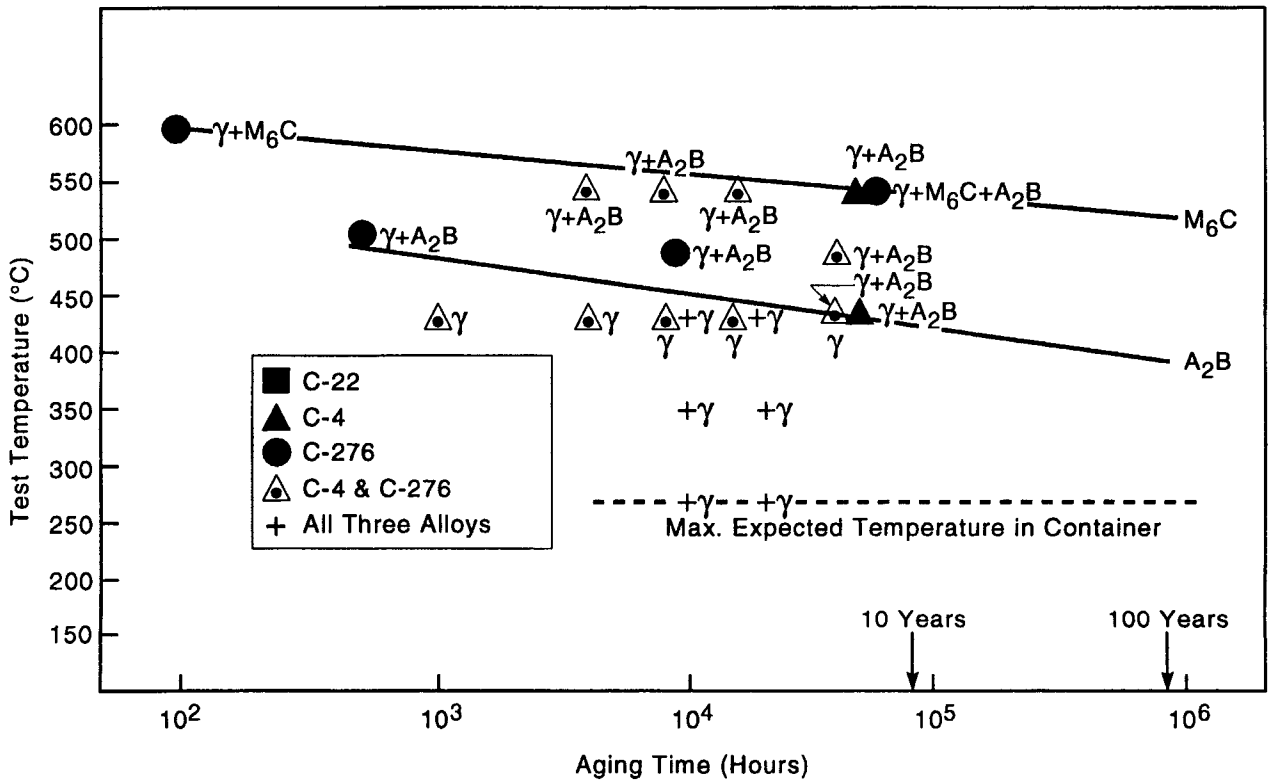

Figure 3-6. Effect of aging at various temperatures and time periods on the microstructures of alloys C-4, C-276, and C-22. Data for all three alloys are combined (Hodge and Ahluwalia, 1993).

3.2 ENVIRONMENTAL EFFECTS

3.2.1 Localized Corrosion

Many aspects of the localized corrosion (pitting and crevice corrosion) of SCP candidate alloys and alternate alloys were reviewed in previous reports (Cragnolino and Sridhar, 1991; Sridhar et al., 1993b). The experimental studies on localized corrosion in the IWPE project have focused on the applicability of repassivation potential to long-term prediction of the occurrence of localized corrosion. The results generated thus far, essentially on type 316L SS and alloy 825, confirm other literature findings that repassivation potential is a conservative parameter for predicting their susceptibility to localized corrosion in the long term (Sridhar and Cragnolino, 1993). However, comparison of short-term laboratory data to field experience with these alloys has not been attempted, the main hindrance being the lack of corrosion potential data in many field tests or in-service components. A limited attempt is made here to compare the performance of alloys in those field tests where some information was available or the corrosion potential can be estimated. With respect to alternate austenitic materials (the C-type alloys) for the overpacks, the following issues are addressed: (i) the types of available laboratory data on localized corrosion, (ii) the applicability of repassivation potential concept and test technique to these types of alloys, and (iii) the comparison of laboratory test data to field experience.

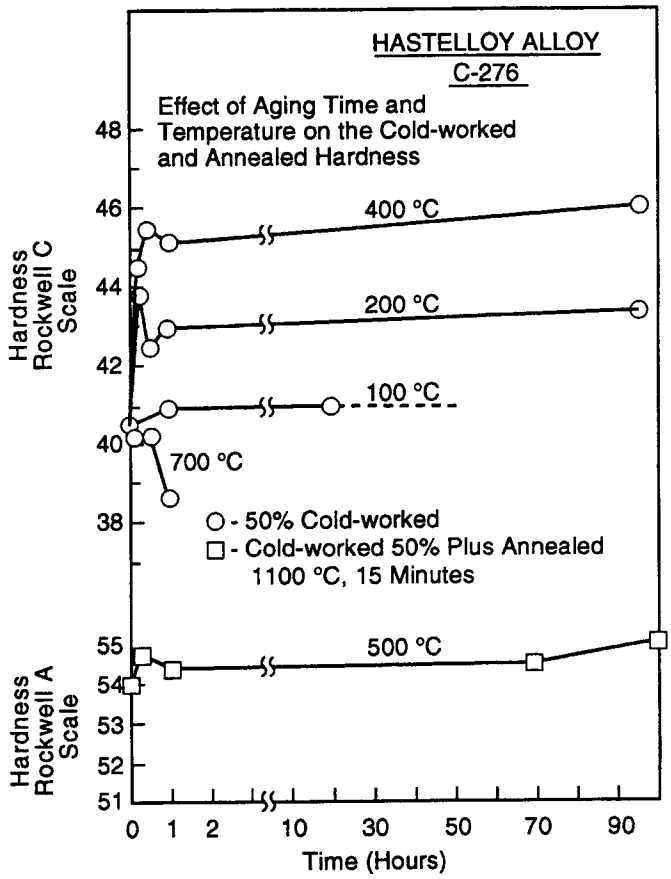

Figure 3-7. Effect of short aging time on room temperature hardness of cold-rolled and solution annealed alloy C-276 (Sridhar et al., 1980)

In long-term tests conducted at the CNWRA under potentiostatic conditions, alloy 825 has exhibited crevice corrosion if maintained 100 mv above the repassivation potential measured in short-term tests. When maintained at a potential 100 mv below the repassivation potential, no localized corrosion has been observed in about 6 months. This is shown in Figure 3-9. These specimens were removed from the solution once a month and observed visually at 70×. The mill-finished surfaces, which are depleted in Cr (Dunn et al., 1993), show a high corrosion rate initially, but then passivate once the Cr-depleted layer is dissolved. After about 5 months, the specimen at 200 mV_{SCE} showed crevice corrosion at the specimen-holder interface, while no visual evidence of localized corrosion has been observed to-date on the specimen held at 0 mV_{SCE}.

Bernhardsson and Mellström (1983) reported failure due to pitting of alloy 825 compressor coolers on a gas lift platform. The environment was chlorinated seawater at 42 °C and failure took place after 4 months (minimum penetration rate estimated to be about 5 mm/yr). The repassivation potential for alloy 825 in 0.5-M chloride (the approximate concentration of chloride in seawater is 0.55 M) at 20 °C is 60 mV_{SCE} (Sridhar and Dunn, 1994). Since the repassivation potential is expected to decrease with an increase in temperature and the corrosion potential in chlorinated seawater has been measured to be around 200 mV_{SCE} (Shaw et al., 1993), this in-service failure is consistent with the use of repassivation potential as a determining factor for localized corrosion. In stagnant, aerated 3 percent NaCl solution at 60 °C, Bernhardsson and Mellström (1983) found that type 316L SS underwent crevice

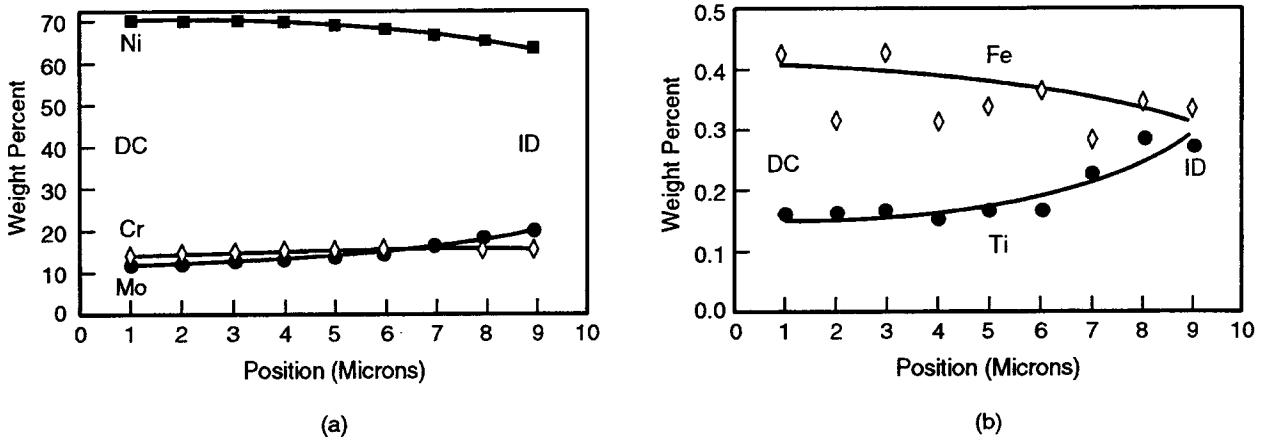

Figure 3-8. Element segregation pattern in quenched weld metal of alloy C-4 between the dendrite center (DC) and the interdendritic (ID) areas. Specimens were welded autogenously using gas tungsten arc welding (GTAW) process (Cieslak et al., 1986a).

corrosion after 2 months while alloy 825 did not. Although these are still relatively short-term tests, the results are consistent with even shorter-term repassivation potential values. For example, Okayama et al. (1987) report a value of -360 mV_{SCE} for repassivation potential of type 316 SS and -100 mV for alloy 825 in 3 percent NaCl at 80 °C and is expected to be slightly higher at a lower temperature. The corrosion potential in aerated chloride solution at 95 °C has been reported to be about -280 mV_{SCE} and is anticipated to increase slightly with a decrease in temperature due to higher solubility of oxygen. Again, from these values of corrosion and repassivation potentials, the observed crevice corrosion of type 316L SS and absence of crevice corrosion in alloy 825 in aerated NaCl is not surprising.

Protection against corrosion in highly oxidizing pulp and paper bleach plant washer fluids using controlled potential has been reported (Laliberté and Garner, 1981). In this case, the material is typically a type 317L SS and the corrosion potential in chlorine washers are in the range of 100–500 mV_{SCE} depending upon residual chlorine. This is far higher than the potential at which crevice corrosion was observed in potentiostatic tests (considered to be roughly equal to the repassivation potential). For type 317L SS in this environment (typically 1,000–5,000 ppm Cl^- and pH 2) the repassivation potential was measured to be about -30 mV_{SCE}. In these cases, cathodic protection by maintaining the potential at -500 mV_{SCE} has resulted in successful performance of the washer drums for over 10 yr.

In filtered, natural seawater (mean temperature 25.2 °C), Kain (1993) observed crevice corrosion on type 316L SS after 60 days, but no crevice corrosion on alloy 59 (61 percent Ni, 22 percent

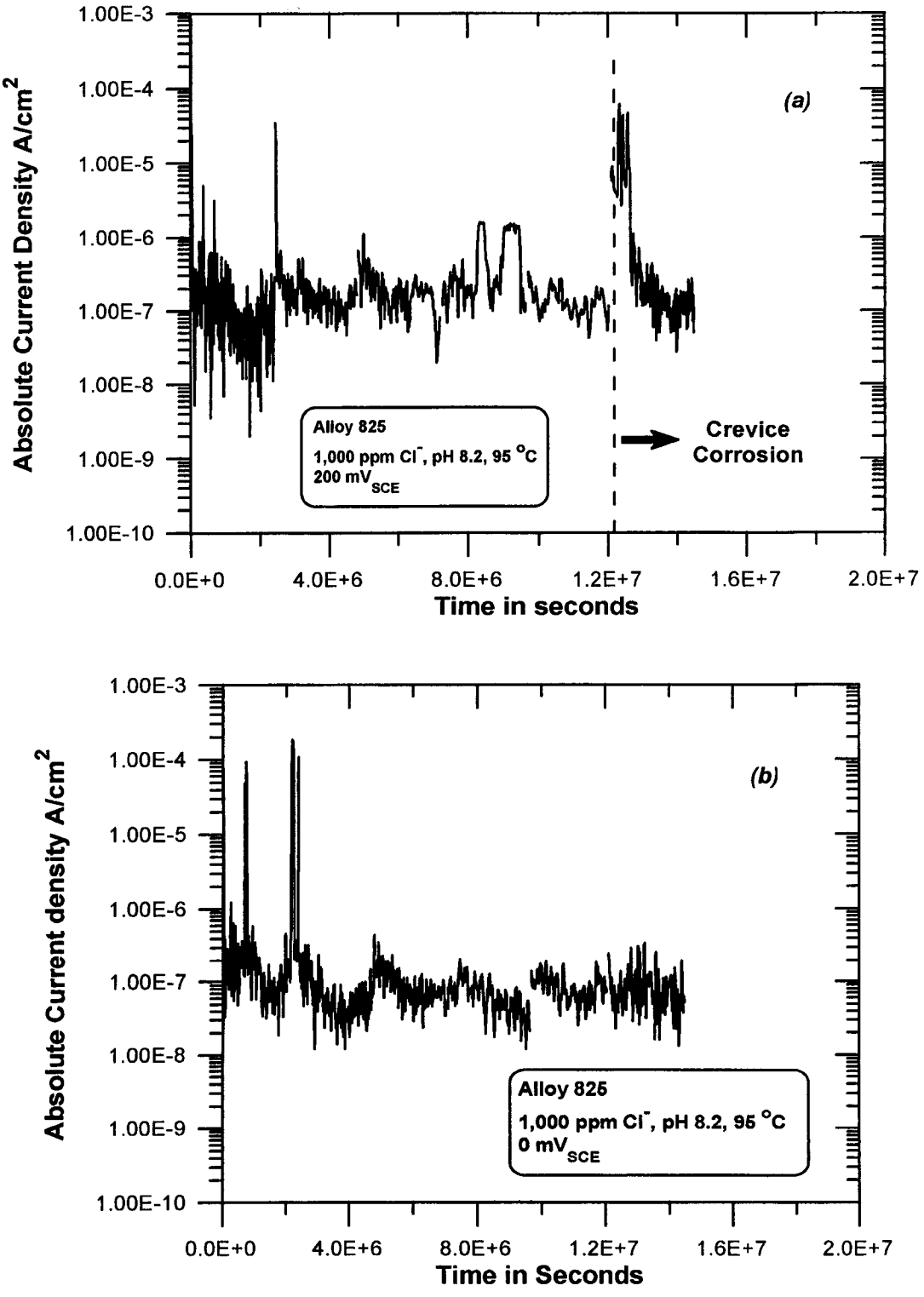

Figure 3-9. Results of long-term tests on alloy 825 in a solution containing 1,000 ppm Cl^-, 85 ppm HCO_3^-, 20 ppm SO_4^{2-}, 10 ppm NO_3^-, and 2 ppm F^- at 95 °C at two applied potentials of 200 mV_{SCE} and 0 mV_{SCE}. Mill-finished surfaces were exposed initially.

Cr, 15 percent Mo). Slight crevice corrosion was observed on alloy C-276. He measured a corrosion potential in the range of 200–300 mV_{SCE}. In natural seawater, microbiologically enhanced cathodic reduction of oxygen is believed to be responsible for the high corrosion potentials. Again, the observed crevice corrosion of type 316L SS is consistent with the measured repassivation potential at this temperature of 0 mV_{SCE} (Asphahani, 1980). A large number of Fe-Ni-Cr-Mo alloys were tested in natural, filtered seawater at 30 °C for 30 days by Hack (1982). The specimens were fitted with crevice washers of PTFE. In this limited duration test, alloys C-276 and 625 suffered no localized corrosion, while type 316 SS and alloy 825 suffered significant crevice corrosion. The repassivation potential for alloy 825 in 0.5 M Cl^- is -60 mV_{SCE} (Sridhar and Dunn, 1994) which is lower than the corrosion potentials reported for these alloys in natural seawater. An evaluation of all the published data on the repassivation potentials of alloy 825 and type 316/316L SS indicates that if the chloride concentration becomes higher than approximately 0.5 M, alloy 825 may not be significantly better than type 316L SS in localized corrosion resistance (Sridhar et al., 1993b).

Postlethwaite et al. (1988) have conducted both cyclic polarization and natural immersion tests on alloys C-276 and 625 in various chloride solutions. They report on the visual observation of localized corrosion on the specimens after these tests as a function of chloride concentration and test temperature (Figure 3-10). The authors did not report repassivation potentials or corrosion potentials. Okayama et al. (1987) report a repassivation potential for alloy C-276 in 3 percent NaCl at 80 °C of -20 mV_{SCE} while the corrosion potential under aerated conditions is expected to be about -280 mV_{SCE}. Hence, the lack of observation of localized corrosion by Postlethwaite et al. (1988) in 3 percent NaCl at temperatures up to 140 °C is consistent with the available data. It must also be noted that the cyclic polarization tests performed to date at the CNWRA on alloy C-22 in solutions containing up to 4M Cl^- (about 23 percent NaCl) and 95 °C have indicated no localized corrosion. From Figure 3-10, this would suggest that alloy C-22 is superior to alloy C-276 in localized corrosion resistance, an observation corroborated by field experience.

Laboratory studies of the effect of alloying elements on the repassivation potential in a 3-percent NaCl solution at 80 °C have been reported by Okayama et al. (1987). This remains one of the most extensive and systematic studies of the repassivation potential as a function of alloying elements. However, some of the conclusions of this report contradict previously reported data and may point to the effect of test technique. For example, the repassivation potential reported by these authors for alloy 625 is slightly lower than that for alloy 825, although most localized corrosion data published to date based on both laboratory and field experience would suggest the opposite (e.g., Hack, 1982). Okayama et al. (1987) also report that they could not initiate localized corrosion on alloy C-276 in 3 percent NaCl at 80 °C and hence used concentrated HCl to initiate localized corrosion prior to measuring repassivation potential in 3 percent NaCl. Use of a similar procedure on alloy C-4 (in which they were able to initiate pits in NaCl solution) did not seem to alter the repassivation potential.

However, the repassivation potentials Okayama et al. (1987) report for these alloys (-20 mV_{SCE} for alloy C-276 and 0 mV_{SCE} for alloy C-4) are surprisingly low, suggesting that these alloys would readily suffer localized corrosion in this environment if moderately oxidizing conditions are present. However, 1-yr tests in NaCl brine under γ irradiation (Smialos et al., 1990) did not indicate susceptibility to localized corrosion for alloy C-4. Hence, the test technique for measuring the repassivation potential, and the application of this potential to predict the performance of highly alloyed materials such as alloy C-4, need further evaluation. Long-term exposure studies on alloy C-4 and other austenitic SS have also been performed in salt repositories for time periods of up to 5 yr (Smialos et al., 1990; Schwartzkopf et al., 1992; Sorensen and Molecke, 1992). Unfortunately, in none of these tests were the corrosion potentials measured, nor were independent measurements of repassivation potential

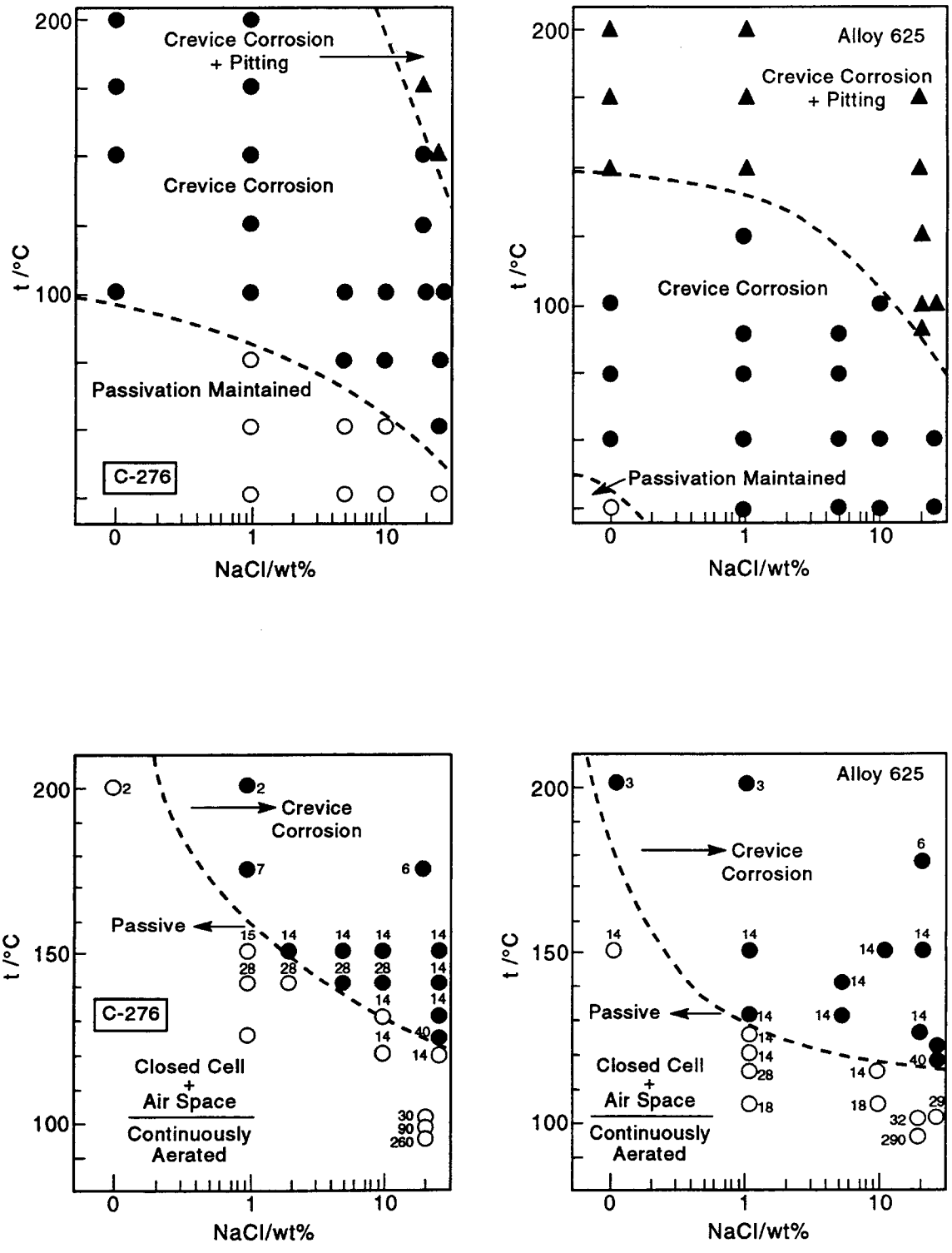

Figure 3-10. Visual observations of localized corrosion on alloy C-276 subjected to either cyclic polarization tests or immersion tests in natural environments as a function of chloride and temperature (Postlethwaite et al., 1988)

carried out. Hence, it is difficult to incorporate these findings in the current long-term predictive scheme. Nevertheless the findings of these investigations can be important in considering the effect of environments arising from evaporative concentration of groundwater, as modeled by Walton (1993).

In laboratory tests of alloy C-4 specimens immersed in Q-brine (see Table 2-7 for composition of Q-brine) at 90 °C and with a specimen surface/volume ratio of 1 cm^2/5 ml for 1 yr, Smialos et al. (1990) found pitting and crevice corrosion at γ dose rate of 10 Gy/hr (1,000 rad/hr) and higher. The rate of pit growth was found to increase from 20 μm/yr at 10 Gy/hr to 1 mm/yr at 1,000 Gy/hr. No localized corrosion was observed in the unirradiated solution (saturated oxygen concentration was 3.7 ppm at 25 °C). Since the corrosion potential in the irradiated solution is expected to be much higher than in the unirradiated and aerated solutions, the observation of localized corrosion is in qualitative agreement with the findings of Postlethwaite et al. (1988) on alloy C-276. In another series of tests in the Asse salt mine (Smialos et al. 1990), specimens of alloy C-4 were placed on the borehole wall and heated to a maximum temperature of 210 °C while subjected to γ radiation from a Co-60 source. No localized corrosion was observed in tests lasting 700 days. The lower corrosion rate can be attributed to the high temperature (above the boiling point) and the small volume of the migrating brine. In a later test, Schwartzkopf et al. (1992) reported that cast steel explosively clad with alloy C-4 and exposed to Q-brine in *in situ* heater tests in the Asse salt mine showed extensive but shallow pits on alloy C-4 after 18 months. The maximum depth of pits was about 15 μm.

Sorensen and Molecke (1992) reported results of coupon tests conducted over a 5-yr period in WIPP brine at 90 °C. They did not measure corrosion potential of the specimens, but found localized corrosion and SCC on type 304L SS, localized corrosion on type 316L SS, and no corrosion on alloy 625 (a Ni-21.55Cr-9 percent Mo-3.5 percent Nb alloy).

3.2.2 Stress Corrosion Cracking

There is an extensive literature on SCC of SS and nickel-base alloys which has been reviewed by many authors in books and proceedings of specialized conferences. An updated review of this vast literature is out of the scope of this report. Information on SCC relevant to the Yucca Mountain repository conditions is presented in this section as a continuation of a previous review on the subject (Cragnolino and Sridhar, 1992). Particular consideration is given to Fe-Ni-Cr-Mo alloys with a high nickel content because they were not included in the previous report which was essentially confined to the candidate alloys listed in the SCP.

As discussed previously (Sridhar et al., 1993a,b), one of the species found in groundwater that may play an important role in the degradation of Fe-Ni-Cr-Mo alloys under repository conditions is the chloride anion. Indeed, SCC of Fe-Ni-Cr-Mo alloys in the presence of chloride anions was the main topic in the previous review on SCC (Cragnolino and Sridhar, 1992). It was concluded that both types 304L and 316L SS are significantly more susceptible to SCC than alloy 825. Most of the data reviewed refer to types 304 and 316 SS rather than the low-carbon grades, but it was concluded that the differences associated with the carbon content are not significant for materials in the mill- or solution-annealed condition. Although there are data indicating that type 316 SS is more resistant to cracking in chloride solutions than type 304 SS, the difference in the behavior of these two materials was considered marginal for container applications.

Among the SS, only duplex and some superferritic SS offer significantly more resistance to SCC in chloride solutions (Sedriks, 1992) than the austenitic alloys currently considered as candidate container materials. However, duplex and ferritic SS are not being considered for containers and therefore the alternate materials are essentially limited to single phase Fe-Ni-Cr-Mo alloys with a sufficiently high nickel content. The beneficial effect of nickel on the SCC resistance of Fe-Ni-Cr alloys was originally established by Copson (1959) for Fe-18Cr-xNi alloys in boiling (145 °C) 42 percent $MgCl_2$ using wire specimens under constant loading. Alloys containing more than 45 percent Ni did not fail in 30 days testing. Speidel (1981) confirmed these results in terms of K_{Iscc} and crack velocity using fracture mechanics specimens of commercial alloys exposed to 22-percent NaCl solution at 105 °C. However, Staehle et al. (1970) found that commercial alloys containing 32–53 percent Ni, among them alloy 825, fail in boiling (155 °C) 45 percent $MgCl_2$ after more extended exposure times than that for type 304 SS. The failure time was about 10 times longer for alloy 825 than that for the SS. The susceptibility to SCC of alloy 825 has been confirmed by conducting slow strain rate tests in 40 percent $MgCl_2$ at 120 °C (Cragnolino et al., 1994). The elongation to failure was found to be about 6–8 times greater than that for type 316L SS under the same experimental conditions, which include a strain rate of 2.7×10^{-7} s^{-1}. Transgranular cracking was observed on the fracture surface, accompanied by numerous secondary cracks. These comparative observations indicate that even though alloy 825 is far more resistant to SCC than austenitic SS of the 300 series, it is still susceptible in concentrated chloride solutions.

Chiang and Streicher (1985) also evaluated the SCC susceptibility of alloy 825 in boiling $MgCl_2$ solutions using U-bend specimens, as shown in Table 3-3. Cracking occurred more readily with a finger-type condenser, presumably as a result of air intrusion into the flask. However, the addition of oxygen did not affect the failure time with the Allihn condenser at the intermediate temperature. On the other hand, no cracking was observed in the 50-percent $MgCl_2$ solution at the highest temperature tested (170 °C) and this was attributed to the decrease in the oxygen content of the solution as a result of increasing temperature and salt concentration. It is apparent from these results that more studies are necessary to evaluate the effect of potential, rather than oxygen content alone, on the SCC of alloy 825 in concentrated chloride solutions.

SCC occurs in alloys with higher Ni contents only at higher temperatures, as shown in Figure 3-11, in which the critical cracking temperature for several Ni-base alloys is plotted as a function of the Ni content for tests conducted in 20.4 percent $MgCl_2$ (Kolts, 1982). Tests were conducted for a week in autoclaves using two-point bend specimens which were examined visually at the end of that period. Figure 3-11 also includes some superaustenitic SS for comparison. In general, the critical temperature at which SCC was observed depends mainly on the nickel content and not in the chromium and molybdenum contents. No significant effect of cold-work up to 50 percent was observed on the SCC susceptibility. The higher SCC resistance of alloy C-276 and C-4 with respect to alloy 825 is clearly shown in the figure. On the other hand, commercial nickel and alloy 600 are resistant to SCC at about 285 °C. It is worthwhile to note, however, that alloy 600 is susceptible to intergranular SCC in deaerated pure water above 300 °C. Tests were also conducted in $CaCl_2$ and NaCl solutions at the same total chloride ion concentration. The crack morphology was transgranular in all environments tested. It was found that the severity of the environment increases in the sequence $CaCl_2$ < NaCl < $MgCl_2$, which is in disagreement with other observations (Latanision and Staehle, 1969) indicating that NaCl is the least severe of the three environments as a result of the higher pH of its solution.

Limited studies have been conducted on the behavior of high nickel-base alloys under simulated repository conditions. Helie and Plante (1986) conducted potentiostatic slow strain rate tests of alloys 625, C-276, and C-4 in simulated brines and in simulated groundwaters as found in contact either with granite

Table 3-3. SCC of mill annealed alloy 825 in boiling $MgCl_2$ solutions. Tests performed according to Standard Practice American Society for Testing and Materials G-36 using two different types of condensers (Chiang and Streicher, 1985).

$MgCl_2$ wt%	Temperature °C	Time to failure, hr		
		Finger Condenser	Allihn Condenser No purge	Allihn Condenser Oxygen purge
42	145	155	1,100	—
45	155	—	80	80
50	170	50[(a)]	1,000[(a)]	—
[(a)] no cracking				

or clay at 90 and 170 °C. They found that all the alloys were susceptible to SCC at potentials lower than the corrosion potential in acidified solutions derived from those environments, with the exception of the argillaceous solutions. As an example, Figure 3-12 shows the results obtained at 90 °C with alloy C-276 in an acidified granitic solution in which the chloride concentration was 0.5 M. The corrosion potential of alloy C-276 in a neutral granitic solution was found to be -0.29 V_{SCE}, suggesting that cracking may occur if localized acidification is promoted under crevice conditions. Cracking was found to be even more severe in the simulated brine which contained approximately 27 percent $MgCl_2$. Since cracking only occurred at cathodic potentials, hydrogen embrittlement rather than anodic SCC seems to be the cause of the environmentally assisted cracking. These results, however, indicate a susceptibility higher than expected if comparisons in terms of chloride concentration and temperature are made with other results published in the literature. The information provided by Helie and Plante (1986) regarding the experimental conditions is limited. For example, cathodic current densities corresponding to the applied potentials are not provided. Without additional information, any comparative discussion of the data is not possible.

Although it is not an environment directly related to the conditions expected at the proposed Yucca Mountain repository site, the addition of thiosulfate ($S_2O_3^{2-}$) anion to chloride containing solutions illustrates the possibility of having metastable sulfur oxyanions that may enhance SCC susceptibility of nickel-base alloys. Thiosulfate can be generated as an intermediate product in the biological reduction of sulfate by sulfate-reducing bacteria (Cragnolino and Tuovinen, 1984). Tsujikawa et al. (1993) have suggested that chloride solutions containing thiosulfate can be used to simulate brines saturated with H_2S, which are typical of sour gas and oil wells. Tests were conducted in 20-percent NaCl solution with the pH adjusted to 4.0 and the addition of 0.001–0.1 M of $S_2O_3^{2-}$ using the slow strain rate technique or constant loading conditions at 75 °C. Under constant loading or dynamic straining alloy 825 was found to be resistant to SCC whereas type 316L SS failed by transgranular cracking. Cold-worked specimens exhibited the same trend as the annealed ones under constant loading conditions.

Additional information on the SCC of nickel-base alloys in other environments, including high temperature water and concentrated chloride solutions containing H_2S and CO_2, has been reviewed in detail by Sridhar and Cragnolino (1992). Resistance to SCC for the Fe-Ni-Cr-Mo alloys with high nickel

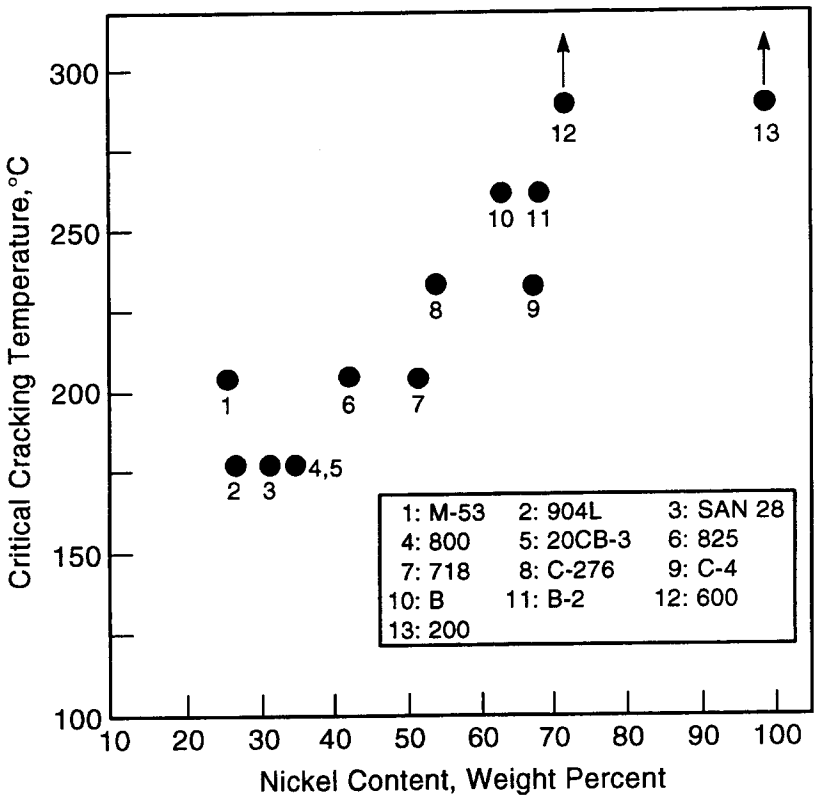

Figure 3-11. Effect of Ni on the critical SCC temperature of Fe-Ni-Cr-Mo alloys in 20.4-percent $MgCl_2$ solution deaerated with nitrogen. Adopted and modified from Kolts (1982).

content (>40 percent) increases with increasing molybdenum content in the sulfide containing environments, whereas in high temperature water the behavior improves with increasing chromium content.

From the information available it can be concluded that the increase in the nickel content of Fe-Ni-Cr-Mo alloys introduces a significant improvement in the resistance to SCC in hot concentrated chloride solutions. Alloy 825 seems to be far more resistant to cracking than type 316L SS in concentrated acidic chloride solutions, at least at temperatures around 120 °C. At higher temperatures and in the presence of other aggressive species, such as reduced sulfur compounds, alloy 825 becomes susceptible to transgranular cracking.

3.2.3 Hydrogen Embrittlement/Damage

The literature on the effects of hydrogen on materials, even for a narrow class of materials such as Fe-Ni-Cr-Mo alloys, is vast. A critical review of the literature on this topic is beyond the scope of this report. The sources of hydrogen and the hydrogen embrittlement susceptibility, under anticipated repository conditions, of SCP design candidate Fe-Ni-Cr-Mo alloys have been reviewed earlier (Sridhar et al., 1991). These sources are reviewed here with respect to the corrosion resistant inner layer of a multiple barrier waste package system. A review of hydrogen effects on carbon steel under anticipated repository conditions is provided in Chapter 2. Essentially, three sources of hydrogen can be expected:

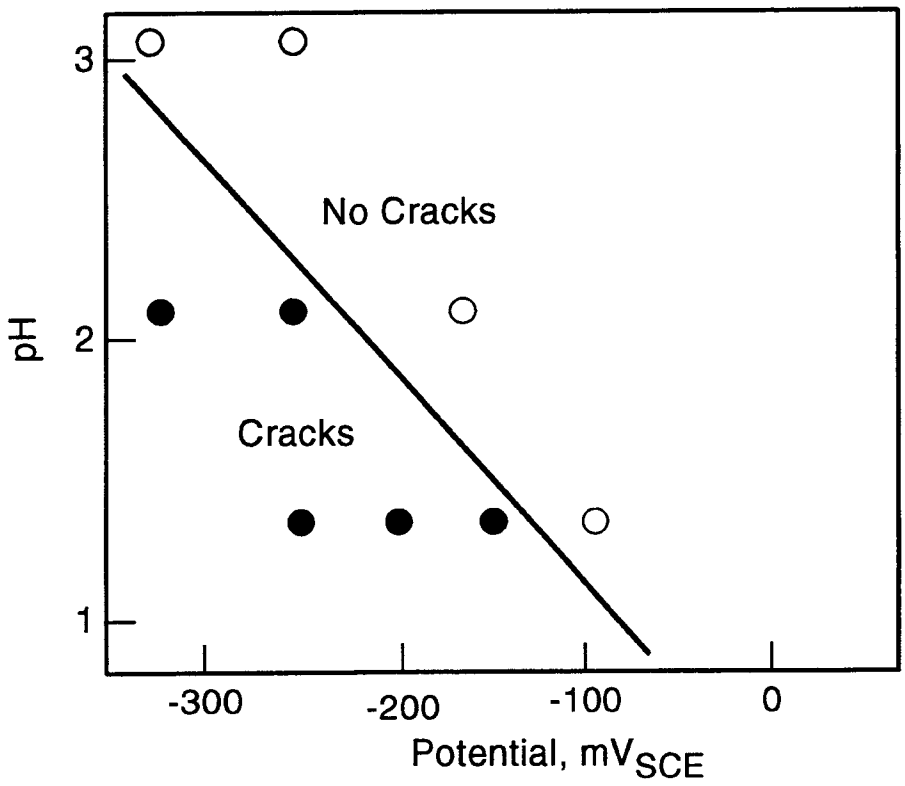

Figure 3-12. Effect of potential and pH on the environmentally assisted cracking of alloy C-276 as measured in slow strain rate tests in a simulated granitic solution at 80 °C (Helie and Plante, 1986)

(i) Galvanic coupling between the carbon steel/cast iron outer barrier and the inner corrosion resistant alloy barrier can cause the latter to be cathodically polarized and be subject to hydrogen evolution and ingress. In this case, a breach in the outer barrier is assumed and the influx of groundwater contacts both barriers. The area ratio that controls the galvanic current density is uncertain, depending upon the extent of wetting by the aqueous phase and the degree of contact between the two barriers. The worst case scenario from the point of view of hydrogen charging of the inner barrier occurs if the two barriers are in intimate contact, and the area of the steel is much larger than that of the alloy. This is illustrated in Figure 3-13(a). On the other hand, this scenario is also most beneficial in terms of protection from localized corrosion. In the other extreme, groundwater can fill the annular space of the two loosely fitting barriers as shown in Figure 3-13(b). In this case, the extent of galvanic effect will be less because the area ratio will be close to one. The effect of galvanic coupling between alloy C-276 and carbon steel on the intake of hydrogen is shown in Figure 3-14 where the hydrogen permeation rate is indicative of the dissolved concentration of hydrogen concentration in the alloy (Armacanqui and Harasyn, 1990). It should be noted that the permeation current increases markedly upon the addition of NaCl which leads to pitting of the carbon steel.

(ii) Radiolysis of the aqueous environment within a pit or a crevice can result in the formation of hydrogen free radicals. This has been discussed previously (Sridhar et al.,

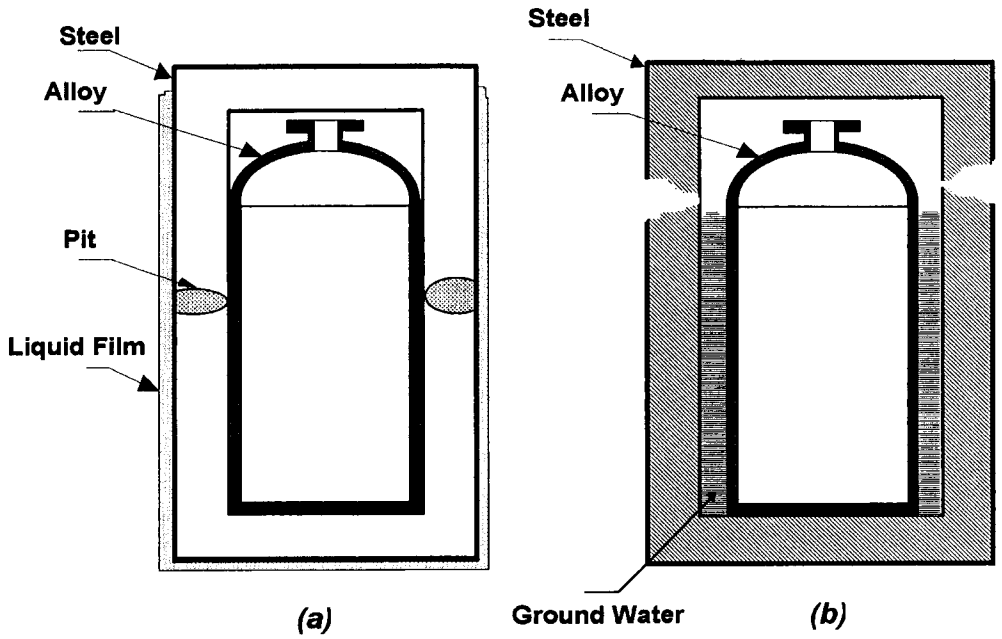

Figure 3-13. A schematic diagram showing two types of galvanic coupling between the outer steel barrier and the inner alloy barrier. The orientation of the waste package is not indicated in this figure.

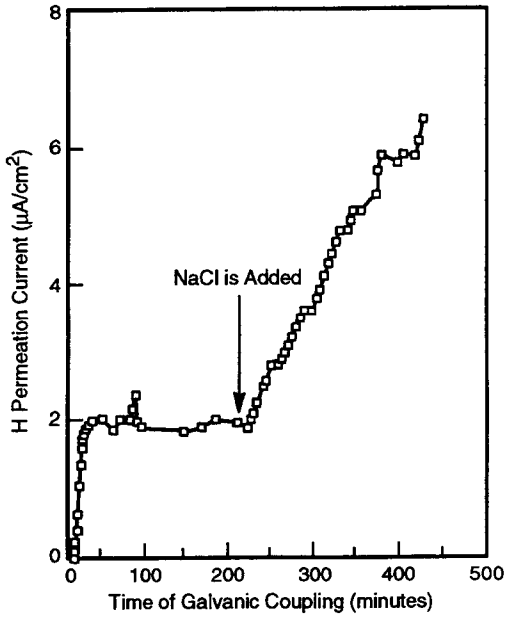

Figure 3-14. The hydrogen permeation current in alloy C-276 when galvanically coupled to AISI 1010 carbon steel in 0.005N H_2SO_4 at 83 °C. Area ratio was 1:1. Alloy C-276 was 20 μm thick (Armacanqui and Harasyn, 1990).

1991). However, the thick-walled containers in the proposed MPC/MPU designs are expected to minimize radiolysis of the external environment. Hence this is not expected to be an important source of hydrogen.

(iii) Microbiologically influenced generation of hydrogen has been shown to occur on carbon steel (Walch et al., 1989; Ford et al., 1990), but not on other substrates.

Generally, the hydrogen embrittlement susceptibility of Fe-Ni-Cr-Mo alloys goes through a minimum at intermediate Ni content. This has been especially well illustrated for the Ni-Fe binary system under cathodically charged hydrogen (Sridhar and Cragnolino, 1992). Minimum embrittlement was observed in the range of 40–50 percent Ni. In commercial alloys, type 304L SS (10 percent Ni) is more susceptible to hydrogen embrittlement than type 316L SS (12 percent Ni) and alloy 825 (42 percent Ni), but alloy C-4 (64 percent Ni) is more susceptible than alloy 825. The data generated in the IWPE program are consistent with this trend (Sridhar et al., 1991). Hence, for the candidate materials for MPC (type 316L SS and alloy 825), hydrogen embrittlement may not be an important failure mode warranting detailed investigation at present. In the case of welded type 316L SS, the occurrence of ferrite in the weld as mentioned in Section 3.1 may affect its tendency to be embrittled by hydrogen. Unfortunately, this is an area that has received scant attention.

The essential questions related to the hydrogen embrittlement of Ni-Cr-Mo alloys (such as alloy C-4) are the roles of microstructure and temperature. Coupled to these questions is the effect of test technique. Some of these aspects have been discussed in previous reviews (Sridhar et al., 1991; Sridhar and Cragnolino, 1992). It has been well established that short- and long-range ordering greatly exacerbates the hydrogen embrittlement of alloys C-276, C-4, and C-22. This is illustrated in Figure 3-15 for alloy C-276 (Sridhar et al., 1980). This effect is especially severe for cold-worked material. As mentioned before, the low-temperature aging of these alloys also produces segregation of phosphorus to grain boundaries and the increased embrittlement has been attributed to the segregation of phosphorus (Berkowitz and Kane, 1980). However, even in the ordered condition, the hydrogen embrittlement susceptibility of C-type alloys decreases markedly with an increase in temperature and no significant embrittlement is noted in relatively short-term tests above about 100 °C (Sridhar et al., 1991). This suggests that even for the Ni-Cr-Mo alloys, hydrogen embrittlement may not be an important failure mode under repository thermal conditions. The main uncertainty in this conclusion relates to the test time, since test data for time periods longer than 1 yr have not been reported. As mentioned previously, the results from Helie and Plant (1986) contradict this general trend and may need further investigation.

As indicated for hydrogen embrittlement of carbon steel at high temperatures, the mechanistic basis for the lowering of hydrogen embrittlement susceptibility relates to the temperature dependence of the accumulation of hydrogen at trap sites. This has been demonstrated by Hicks and Altstetter (1992) for two Ni-base alloys (625 and 718) and a precipitation hardenable SS. The data for alloy 718 are presented in Figure 3-16. Hence, further evaluation of the temperature effect of embrittlement of these alloys must be made in terms of critical hydrogen concentration/fugacity.

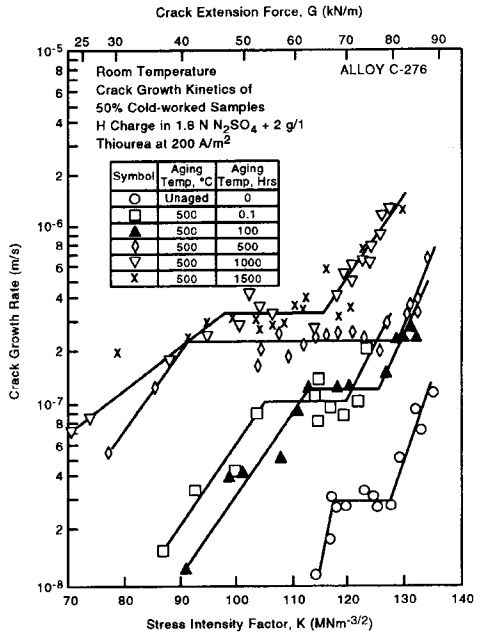

Figure 3-15. Effect of low-temperature aging on the hydrogen-induced cracking of alloy C-276 (Sridhar et al., 1980)

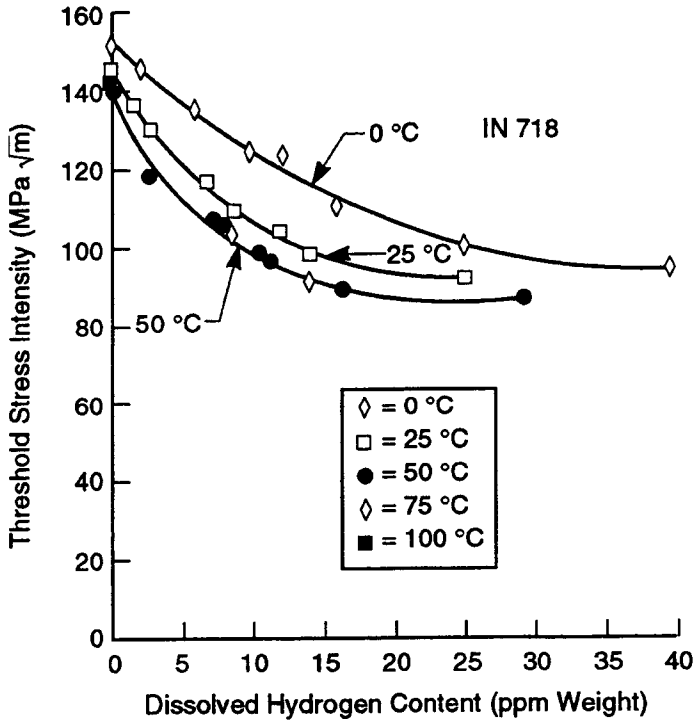

Figure 3-16. Threshold stress intensity factor versus dissolved hydrogen concentration for alloy 718 (18% Cr, 18% Fe, 3% Mo, 5% Nb, 1% Ti, 0.04% C) (Hicks and Altstetter, 1992)

4 SUMMARY AND RECOMMENDATIONS

4.1 SUMMARY

The candidate materials for HLW disposal containers have undergone significant changes since the SCP design. One important change in the direction of the DOE waste package program is the consideration of MPC a baseline design in the waste handling, transportation, interim storage, and disposal systems. It is also proposed that either unique or common overpacks will be used for transportation, storage, and disposal. Hence, various performance issues related to MPC candidate materials and appropriate disposal overpacks are considered in this report. The critical performance issues related to various classes of materials and components of waste packages are summarized in Table 4-1.

4.1.1 Carbon Steels and Cast Irons

The performance issues with respect to carbon steel and cast irons are divided into mechanical embrittlement, corrosion, and environment assisted cracking (SCC and hydrogen effects). The mechanical embrittlement can arise from long-term exposure to temperatures in the 200–300 °C range. The fundamental mechanism for such an embrittlement is phosphorus segregation to the grain boundaries. The literature on reactor pressure vessel steels was reviewed for this purpose, where the rise in ductile-brittle transition temperature was correlated to the grain boundary phosphorus concentration. It has also been shown in the literature that large grain sizes such as in the HAZs of weldments may exacerbate the embrittlement due to P segregation. The data for cast irons and ductile iron are sparse in this regard. Hence, it is recommended, that the relevance of this mechanism of embrittlement be examined more fully for the types of steel that may be proposed for disposal and transportation overpacks.

Corrosion of carbon steel and cast irons has been well characterized for many applications and environments. The long-term atmospheric corrosion tests of these materials have enabled the prediction of the corrosion allowance necessary for the lifetime of an engineered structure. The accuracy of long-term predictions appears to be enhanced by the use of more complex power-linear equations in comparison to simple logarithmic power functions. Accurate long-term prediction of the corrosion allowance is possible because the conditions during exposure remain constant with the exception of some small seasonal variations.

Corrosion rates in aqueous solutions, both with and without the presence of a passive film, are controlled by the cathodic reaction. In solutions that do not contain aggressive anions, the corrosion rate for steels and cast irons decreases with the presence of a passive film. Increasing the thickness of the passive film decreases the corrosion rate. Variations in the stability, stoichiometry, and structure of oxides formed both in solution and as a result of thermal exposure, have been shown to be responsible for the range of protection afforded by the passive films.

For solutions containing aggressive ions, the regions of immunity, passivity, and localized corrosion may be represented by potential pH. These diagrams may be calculated on the basis of thermodynamic data for pure elements or experimentally determined. The conditions for the localized corrosion of carbon steels and cast irons in aqueous environments containing bicarbonate and chloride have been examined by these means. The apparent possibility of localized corrosion in several proposed repository sites has led several investigators to study the propagation of pits in simulated groundwaters. These investigations have concluded that reactive wall pit models were found to better represent actual

Table. 4-1. Summary of performance issues related to various material classes in alternate conceptual designs

Component	Materials	Critical Performance Issues
MPC	Type 316L SS	1. Thermal aging leading to low fracture toughness in duplex weld metal due to α' precipitation 2. Sensitization due to thermal aging of base metal and weld metal 3. Localized corrosion and SCC
	Alloy 825	1. Thermal aging of base metal and weldment in terms of σ phase precipitation and embrittlement 2. Sensitization due to thermal aging 3. Localized corrosion and SCC 4. Hydrogen embrittlement due to galvanic effects
Single-Layer Overpack	Wrought Steel	1. Thermal aging leading to increase in DBTT due to P segregation. Exacerbated by weld, HAZ 2. Hydrogen embrittlement and hydrogen attack 3. SCC in HCO_3^-/CO_3^{2-} environment 4. MIC 5. Occurrence of localized corrosion
	Cast Steel/Ductile Iron	1. Thermal aging effect on DBTT (no published data) 2. Same environmental effects as wrought steel 3. MIC
	Alloy 825	Same effects as in MPC
	Alloy C-4	1. Hydrogen embrittlement due to galvanic effect and thermal aging 2. Embrittlement due to long-term aging of welds — M_6C, Ni_2Cr LRD 3. Prediction of localized corrosion

inservice pitting data than nonreactive wall pit models. In addition, empirically derived pit propagation rate equations have been used to calculate the necessary corrosion allowance for the waste package. These equations are similar in form to those used to describe atmospheric corrosion. Other investigations have concluded that crevice corrosion will occur prior to pitting corrosion.

Despite the extensive investigation of carbon steel and cast irons for use in a wide variety of applications including that of HLW disposal, there are several uncertainties about the performance of these materials under repository conditions. As stated above, the pit propagation rates in solutions that favor the formation of passive films have been studied. Crevice propagation rates have not been examined with sufficient detail to allow comparison to pit propagation rates. Pitting and crevice corrosion in vapor has only received limited study. Corrosion in the vapor phase may be significant in a hot repository. The limited data that are available suggest that the rate of both uniform corrosion and crevice corrosion decreases with time. However, the ratio of crevice corrosion to uniform corrosion increases with time. As a result the material allowance must be based on accurate knowledge of the crevice corrosion propagation rate. Bentonite, a proposed buffer material to surround the HLW packages for geologic disposal, has been shown to increase the pH of the groundwater and facilitate the initiation of crevice corrosion on carbon steel. The presence of extensive cementations material from repository construction can also increase the pH. At present, it is unknown whether the results of interactions between other possible backfill materials such as crushed tuff will cause detrimental changes in water chemistry. In addition, the nature and severity of the crevice formed by the contact of crushed tuff with the waste container surface is unknown.

The initiation and propagation of pitting and crevice corrosion on steel or cast iron outer barriers will be a function of the unique set of conditions specific to the repository design and location. Most investigations have not focused on the effects of dry oxidation on the localized corrosion rate. Dry oxidation may be relevant in a hot repository located above the water table. During the first several hundred years, the heat generated by radioactive decay of spent fuel may create conditions under which only dry oxidation may occur. With sufficient areal mass loading, the temperature of the carbon steel or cast iron container will be above 250 °C, causing oxidation of the material at a parabolic rate. As a result, water intruding into the repository will contact waste containers with a thick oxide scale formed over a period of perhaps several hundred years. Oxides formed under dry oxidation at 250 °C has been shown to be more susceptible to breakdown than oxides formed at either higher or lower temperatures. In addition, the presence of a mill scale or a thick oxide film has been shown to increase the pit propagation rate. Calculations of the material allowance needed from the measured corrosion rate after subjecting the test materials directly to aqueous, or in a few cases, vapor environments for relatively short terms, may significantly underpredict the material necessary requirements.

The localized corrosion of carbon steel in salt brines has been speculated to be a result of impurities in the metal. Information on the initiation, propagation, and repassivation of localized corrosion in this environment is scarce. Several investigators have proposed an upper limit on pit depth as a result of the increasingly large IR drop. However, it is unclear if this will be a limiting factor for localized corrosion along inclusion stringers.

Variations on the initiation and propagation of localized corrosion as a result of welding, and to a lesser extent other fabricating operations have been reported. The type of welding process used has also been shown to have a significant effect on the corrosion rate. Assuming the waste package will be closed by welding, detailed investigations of localized corrosion processes for the proposed materials and welding operations are warranted. Galvanic and thermal effects adjacent to the welded regions may be

equally important to long-term performance. The nature of these effects will be specific to the type of material and closure method selected.

A consequence of the localized corrosion of the carbon steel or cast iron outer container will be the generation of hydrogen and locally acidic conditions. While hydrogen can be liberated during uniform corrosion, the rate of hydrogen evolved is much larger during localized corrosion. Detrimental effects on the corrosion resistant inner barriers of the waste containers, caused by the local alteration in the environment, have received very little attention. It may be concluded from this review that there are several unresolved issues surrounding the use of carbon steel or cast irons as a corrosion allowance outer barrier for HLW disposal containers. The performance of these materials will be dictated by the location and design of the repository as well as the intrinsic characteristics of the selected material. Resolution of these uncertainties may be achieved through focused investigations for a location and design specific facility. Such investigations should reveal the time dependent environmental effects on the propagation of any relevant localized corrosion processes and advance the capability of long-term performance predictions.

SCC of carbon steel may arise out of contact with a mildly alkaline environment containing bicarbonate and carbonate, but not carbonate alone. Anionic species such as silicate, chromate, and monohydrogenphosphate act as inhibitors of SCC, but, of these, only silicates are present in repository environments. Stress relief heat treatments have a beneficial effect on welded structures. Cracking has also been observed in oxygenated high-purity water at temperatures ranging from 100–288 °C. Cracks tend to initiate in the area close to welds, within the HAZ. There is a lack of data for cast steels, both in high temperature water and in carbonate/bicarbonate solutions.

Carbon steels are well known to suffer hydrogen induced cracking. Cracking due to atomic hydrogen depends upon the hydrogen fugacity and temperature, with higher hydrogen fugacity required to crack at higher temperatures. Cracking due to the reaction of hydrogen with carbon (hydrogen attack) is dictated by Nelson type pressure-temperature diagrams, and depends upon the alloying elements, temperature, and hydrogen fugacity. While the anticipated repository temperatures are relatively low for hydrogen attack, the current database extends only for relatively short periods of time (10,000 hr). Further evaluation of models relevant to this damage process is necessary. The most important source of hydrogen is the corrosion of steel. Other sources such as radiolysis and microbiologically influenced generation of hydrogen are less important because of the thickness of the steel overpacks and the high temperatures. Welding-generated hydrogen is believed to be less important because of the high pre-welding and post-welding temperatures anticipated due to decay heat. The large grain sizes in wrought steel weldments are believed to be detrimental to hydrogen embrittlement, and may indicate a similar problem for cast steel and ductile iron. However, there is a paucity of data on the cast steel and ductile iron. The data on hydrogen evolution on these alloys due to corrosion or radiolysis are insufficient to calculate the hydrogen fugacity or the dissolved hydrogen concentration.

4.1.2 Type 316L Stainless Steel

One important issue in the performance of type 316L SS MPC is the embrittlement of circumferential welds. Minimization of hot-cracking requires that these welds solidify as primary ferrite resulting in a duplex (ferrite-austenite) microstructure at room temperature. The presence of ferrite at repository temperature may result in the precipitation of embrittling σ and α' phases which reduce the fracture toughness of the material. Current data indicate that the latter is of greater concern under

repository thermal conditions.The precipitation of α' has been examined in great detail with respect to SS castings (such as CF-8M) used in nuclear power reactors. However, it has not received much attention in the weldments of type 316L SS. The long-term prediction methodology used in cast SS aging and embrittlement can be applied in this case. The embrittlement of MPC welds has implications in its use as a sealed canister of spent fuel in various waste handling systems.

The long-term low-temperature sensitization of type 316L SS has been examined before in terms of carbide precipitation. However, the effects of σ and Laves phases upon long-term aging at repository temperatures have not been examined. The formation of these phases can be accelerated by the presence of cold-work or ferrite in the welds.

The susceptibility of type 316L SS to SCC in chloride solutions is well known and is not reviewed in this report. The possibility of hydrogen entry and embrittlement through galvanic contact with the outer carbon steel overpack has been examined. It is suggested that the high repository temperatures combined with relatively low anticipated hydrogen concentrations make this failure mechanism a low-probability one. Unlike the case of carbon steels, hydrogen attack is also less likely because of the stability of the carbides.

The susceptibility of type 316L SS to localized corrosion was examined in terms of the applicability of repassivation potential to long-term prediction. Several cases from other waste disposal programs, marine, pulp and paper, and pollution control industries, were examined and the findings were shown to be consistent with repassivation potential being a conservative parameter for long-term prediction of localized corrosion.

4.1.3 Alloy 825

This alloy has been considered both in terms of MPC and disposal overpack. The composition of alloy 825 is such that σ phase precipitation, an embrittling process, is expected, but has not been shown by relatively short-term studies conducted thus far. Further investigation that is currently underway in the IWPE project (Task 3) is expected to shed some light on this. Unlike the case of type 316L SS, the weld metal does not contain any ferrite, but does have zones of higher Cr and Mo. These zones may precipitate σ phase faster than the base metal. Unlike the case of the lower iron-containing alloys such as alloy C-4, alloy 825 has not been shown to undergo long-range ordering. However, it is not known whether this is a kinetic limitation or a fundamental electronic limitation.

Alloy 825 is more resistant than type 316L SS towards SCC and hydrogen embrittlement. It appears that in alloy 825, concentrated chloride solutions, and temperatures above 120 °C are required to promote SCC. In the IWPE project (Task 2), the environmental and mechanical conditions required to promote cracking are being investigated. In particular, the relationship between repassivation potential for crevice corrosion and the conditions for SCC initiation should be determined. Alloy 825 is more resistant to hydrogen embrittlement than the high nickel alloys such as alloy C-4. However, it is susceptible to localized corrosion and its resistance to localized corrosion in concentrated chloride environments such as seawater is only slightly better than that of type 316L SS. Examples of localized corrosion of alloy 825 in a variety of chloride containing environments have been cited in this report. Their behavior is consistent with the repassivation potential measured in appropriate environments in short-term tests being the critical potential. Galvanic coupling of alloy 825 with carbon steel is expected to lower the corrosion potential and mitigate the tendency towards localized corrosion.

4.1.4 Alloy C-4 and Related Alloys

While alloy C-4 is being considered in connection with the disposal overpack, related alloys such as alloys C-276 and C-22 were also evaluated. The main precipitation reaction that may be of concern in terms of repository thermal conditions is the long-range ordering of the Ni_2Cr type. Presence of cold-work may increase the kinetics of ordering of these alloys. While this ordering reaction has been shown to be detrimental towards hydrogen embrittlement resistance, data on fracture toughness are insufficient to make any conclusion regarding the long-term mechanical stability of these alloys.

These alloys are highly resistant to localized corrosion and SCC in chloride environments. However, in $MgCl_2$ brines, crevice corrosion has been observed on alloy C-4. The data on repassivation potential of these alloys are sparse and the available data are conflicting with the data on long-term performance. Hence, the method of obtaining repassivation potential and the applicability of this concept to these alloys needs further evaluation. The role of surface Cr depletion may become more significant in these alloys than in alloy 825 and needs further investigation.

These alloys are more susceptible to hydrogen embrittlement than alloy 825, especially in the long-range ordered condition. Galvanic coupling with carbon steel has been shown to generate significant amounts of dissolved hydrogen. However, the essential question is the hydrogen embrittlement susceptibility under relatively high temperatures anticipated in the repository. It is anticipated that under the repository thermal conditions, hydrogen embrittlement may not be an important failure mode, but this conclusion is based on relatively short-term data.

4.2 RECOMMENDATIONS

The present review, while not exhaustive, indicates several areas where further experimental investigation will be necessary. These are divided into thermomechanical embrittlement and environmental related processes. However, this division is arbitrary and there are many areas of synergism. Further, in the case of steel overpacks, a clear material specification is not available at this time and efforts should be focused on a more detailed evaluation of existing data. The recommendations are listed under several key technical uncertainties (KTUs) although in some cases, more than one KTUs may be applicable.

Prediction of Thermomechanical Effects

- The low-temperature embrittlement of type 316L weldments due to α' precipitation must be examined in light of similar studies on duplex SS castings of similar composition but higher ferrite content. The changes in room temperature toughness must be related to toughness at repository/MPC temperatures.

- The effect of phosphorus segregation to grain boundaries of cast steels/irons on embrittlement must be explored in comparison with the already widely available data on wrought, low-alloy steels.

Prediction of Environmental Effects

- The hydrogen concentration and fugacity due to corrosion or microbial reactions of steel or cast iron in repository environments must be quantified to evaluate the possibility of

hydrogen embrittlement or attack. The type and extent of microbial action must be investigated with repository relevant conditions, if carbon steel is specified as an overpack.

- The effect of repository environmental conditions on the localized corrosion and SCC of carbon steels or cast irons should be evaluated further.

- The sensitization studies of type 316L SS and alloy 825 should be extended to an evaluation of σ and Laves phase (for the former).

- The galvanic effect between carbon steel and the corrosion resistant alloys must be studied with a focus not only on localized corrosion, but also hydrogen evolution and permeation in the corrosion-resistant alloy. The possibility of hydrogen embrittlement of the corrosion-resistant alloys at repository temperatures must be explored.

- The SCC resistance of cast iron and cast steels in carbonate/bicarbonate environments should be studied, if these are specified as disposal overpacks.

- The effect of relatively high temperature on the type and extent of microbial activities and their effect on corrosion and cracking must be investigated.

Extrapolation of Short-Term Laboratory Results

- The applicability of repassivation potential and the measurement techniques must be examined for the alloy C-4-type high Ni alloys.

5 REFERENCES

Abraham, T., H. Jain, and P. Soo. 1986. *Stress Corrosion Cracking Tests on High-Level Waste Container Materials in Simulated Tuff Repository*. NUREG/CR-4619. Washington, DC: Nuclear Regulatory Commission.

Accary, A. 1985. *Corrosion Behavior of Container Materials for Geological Disposal of High-Level Radioactive Waste*. EUR 9836 EN. Luxembourg: Commission of the European Communities.

Advani, A.H., L.E. Murr, D.G. Atteridge, and R. Chelakara. 1991. Mechanisms of deformation-induced grain boundary chromium depletion (sensitization) development in type 316 stainless steels. *Metallurgical Transactions A*. 22A(12): 2,917–2,934.

Ahn, T.M., and P. Soo. 1984. *Container Assessment—Corrosion Study of High-Level Waste Container Materials*. Quarterly Progress Report July–September 1984. Washington, DC: Nuclear Regulatory Commission.

Akashi, M., T. Fukuda, and H. Yoneyama. 1990. A corrosion localization assessment of the mild steel used for nuclear waste package. *Symposium Proceedings of Scientific Basis for Nuclear Waste Management XIII*. V.M. Oversby and P.W. Brown, eds. Pittsburgh, PA: Materials Research Society 176: 525–532.

Alavi, A., and R.A. Cottis. 1987. The determination of pH, potential, and chloride concentration in corroding crevices on 304 stainless steel and 7475 aluminum alloy. *Corrosion Science* 27(5): 443–451.

American Iron and Steel Institute. 1985. *Plates; Rolled Floor Plates: Carbon, High Strength Low Alloy, and Alloy Steel Products Manual*. Washington, DC: American Iron and Steel Institute.

American Iron and Steel Institute. 1986. *Alloy, Carbon and High Strength Low Alloy Steels: Semifinished for Forging; Hot Rolled Bars and Cold Finished Bars, Hot Rolled Deformed and Plain Concrete Reinforcing Bars: Steel Products Manual*. Washington, DC: American Iron and Steel Institute.

Anantatmula, R.P. 1985. Effect of Grande Ronde Basalt groundwater composition and temperature on the corrosion of low-carbon steel in the presence of basalt-bentonite packing. *Symposium Proceedings of Scientific Basis for Nuclear Waste Management VIII*. C.M. Jantzen, J.A. Stone, and R.C. Ewing, eds. Pittsburgh, PA: Materials Research Society 44: 273–278.

Anzai, H., J. Kuniya, and I. Masaoka. 1992. Evaluation of hydrogen-assisted cracking behavior of low-alloy steel in the range 95 °C to 350 °C. *Metallurgical Transactions* 23A: 1,291–1,298.

Armacanqui, M.E., and D.E. Harasyn. 1990. Galvanic currents and hydrogen permeation currents caused by galvanic coupling. *Corrosion* 46(5): 320–321.

ASM International. 1987. *Metals Handbook*. Materials Park, OH: ASM International 9(13): 1–14.

ASM International. 1988. Forming and Forging. *Metals Handbook*. Metals Park, OH: ASM International 19(14): 616–623.

Asphahani, A.I. 1980. Localized corrosion of high performance alloys. *Materials Performance* 19(8): 9–21.

Baird, J.D. 1963. Strain aging of steel—A critical review. *Iron and Steel* 36: 186–457.

Beavers, J.A., N.G. Thompson, and A.J. Markworth. 1987a. Pit propagation of carbon steel in groundwater. *Advances in Localized Corrosion: Proceedings of the Second International Conference on Localized Corrosion*. H.S. Isaacs, U. Bertocci, J. Kruger, and S. Smialowska, eds. Houston, TX: NACE International: 165–174.

Beavers, J.A., N.G. Thompson, A.J. Markworth, H.J. Cialone, B.S. Majumdar, and J.K. McCoy. 1987b. *Long-Term Performance of Container Materials for High-Level Waste*. NUREG/CR-4955. Washington, DC: Nuclear Regulatory Commission.

Beavers, J.A., N.G. Thompson, and C.L. Durr. 1992. *Pitting, Galvanic, and Long-Term Corrosion Studies on Candidate Container Alloys for the Tuff Repository*. NUREG/CR-5709. Washington, DC: Nuclear Regulatory Commission.

Berkowitz, B.J., and R.D. Kane. 1980. The effect of impurity segregation on the hydrogen embrittlement of a high-strength nickel base alloy in H_2S environments. *Corrosion* 36(1): 24–29.

Bernhardsson, S., and R. Mellström. 1983. Performance of a highly alloyed stainless steel in marine environments. Paper No. 72. *CORROSION/83*. Houston, TX: NACE International.

Bhakta, P., and A.A. Solomon. 1987. Pitting corrosion of low-carbon steel nuclear waste canisters. *Advances in Localized Corrosion: Proceedings of the Second International Conference on Localized Corrosion*. H.S. Isaacs, U. Bertocci, J. Kruger, and S. Smialowska, eds. Houston, TX: NACE International: 445–451.

Bird, H.E.H., B.R. Pearson, and P.A. Brook. 1988. The breakdown of passive films on iron. *Corrosion Science* 28(1): 81–86.

Birnbaum, H.K. 1990. Mechanisms of Hydrogen-Related Fracture of Metals. *Environment Induced Cracking of Metals*. R.P. Gangloff and M.B. Ives, eds. Houston, TX: NACE International: 21–29.

Brooks, J.A., and A.W. Thompson. 1991. Microstructural development and solidification cracking susceptibility of austenitic stainless steel welds. *International Materials Reviews* 36(1): 16–44.

Bullen, D.B., and G.E. Gdowski. 1988. *Survey of Degradation Modes of Candidate Materials for High-Level Radioactive Waste Disposal Containers. Volume 1. Phase Stability*. UCID–21362. Livermore, CA: Lawrence Livermore National Laboratory.

Buscheck, T.A., and J.J. Nitao. 1992. The impact of thermal loading on repository performance at Yucca Mountain. *Proceedings of the Third Annual International High-Level Radioactive Waste Management Conference.* La Grange Park, IL: American Nuclear Society: 1,003–1,017.

Chiang, Y-L., and M.A Streicher. 1985. The effect of condenser design on stress corrosion cracking of stainless steels in boiling chloride solutions. Paper No. 353. *CORROSION/85.* Houston, TX: NACE International.

Choi, H., F.H. Beck, Z. Szklarska-Smialowska, and D.D. MacDonald. 1982. Stress corrosion cracking of ASTM A508 Cl 2 steel in oxygenated water at elevated temperatures. *Corrosion* 38(3): 136–144.

Chung, H.M. 1992. Aging and life prediction of cast duplex stainless steel components. *International Journal of Pressure Vessel & Piping* 50: 179–213.

Chung, H.M., and O.K. Chopra. 1989. Accelerated aging embrittlement of cast duplex stainless steel—Activation energy for extrapolation. *Proceedings of the Fourth International Symposium on Environmental Degradation of Materials in Nuclear Power Systems—Water Reactors.* D. Cubicciotti, ed. Houston, TX: NACE International: 3-47–3-65.

Ciaraldi, S.W. 1992. Stress-corrosion cracking of carbon and low-alloy steels (yields strengths less than 1,241 MPa). *Stress-Corrosion Cracking. Materials Performance and Evaluation.* R.H. Jones, ed. Materials Park, OH: ASM International: 41–61.

Cieslak, M.J., T.J. Headley, and A.D. Romig. 1986a. The welding metallurgy of Hastelloy alloys C-4, C-22, and C-276. *Metallurgical Transactions A* 17A: 2,035–2,047.

Cieslak, M.J., G.A. Knorovsky, T.J. Headley, and A.D. Romig. 1986b. The use of new PHACOMP in understanding the solidification microstructure of nickel base alloy weld metal. *Metallurgical Transactions A* 17A: 2,107–2,116.

Copson, H.R. 1959. Effect of composition on stress corrosion cracking of some alloys containing nickel. *Physical Metallurgy of Stress Corrosion Cracking.* T.N. Rhodin, ed. New York, NY: Interscience Publishers: 247–269.

Cragnolino, G., and N. Sridhar. 1991. *A Review of Localized Corrosion of High-Level Nuclear Waste Container Materials—I.* CNWRA 91-004. San Antonio, TX: Center for Nuclear Waste Regulatory Analyses.

Cragnolino, G., and N. Sridhar. 1992. *A Review of Stress Corrosion Cracking of High-Level Nuclear Waste Container Materials—I.* CNWRA 92-021. San Antonio, TX: Center for Nuclear Waste Regulatory Analyses.

Cragnolino, G., and N. Sridhar. 1993. *Long-Term Stability of High-Level Nuclear Waste Container Materials I—Thermal Stability of Alloy 825.* CNWRA 93-003. San Antonio, TX: Center for Nuclear Waste Regulatory Analyses.

Cragnolino, G., and O. Tuovinen. 1984. The role of sulphate-reducing and sulphur-oxidizing bacteria in the localized corrosion of iron-base alloys—A review. *International Biodeterioration* 20: 9–26.

Cragnolino, G., D. Dunn, and N. Sridhar. 1994. Unpublished results from IWPE project. San Antonio, TX: Center for Nuclear Waste Regulatory Analyses.

Davies, J.A., and P.A. Brook. 1992. The breakdown of passivity on mild steel. *Corrosion Science* 33(2): 315–316.

de Meybaum, B.R., and E.S. Ayllon. 1980. Characterization of atmospheric corrosion products on weathering steels. *Corrosion* 36(7): 345–347.

Doering, T.W. 1993. Robust waste package concept (multibarrier). *Proceedings of the Fourth Annual International High-Level Radioactive Waste Management Conference.* La Grange Park, IL: American Nuclear Society: 551–557.

Donovan, J.A. 1977. Factors controlling nitrate cracking in mild steel. *Proceedings of the Conference on Environmental Degradation of Engineering Materials.* M.R. Louthan and R.P. McNitt, eds. Blacksburg, VA: Virginia Polytechnic Institute and State University: 185–198.

Dunn, D.S., N. Sridhar, and G.A. Cragnolino. 1993. The effect of surface conditions on the localized corrosion of a candidate high-level nuclear waste container material. *Corrosion Control for Low-Cost Reliability. Proceedings of the 12th International Corrosion Congress.* Houston, TX: NACE International 5B: 4,021–4,030.

El-Dahshan, M.E., F.M. Al-Habdan, and F.A. Abdulaleem. 1988. Case study of corrosion in desalination plants. *Key Engineering Materials. Tenth International Congress on Metallic Corrosion.* Aedermannsdorf, Switzerland: Trans Tech Publications: 735–743.

Escalante, E., and W.P. Iverson. 1978. The protection of steel piles by nonmetallic coatings in seawater. *Materials Performance* 17(10): 9–15.

Farmer, J.C., R.D. McCright, and J.N. Kass. 1988. *Survey of Degradation Modes of Candidate Materials for High-Level Radioactive-Waste Disposal Containers.* UCID–21362. Livermore, CA: Lawrence Livermore National Laboratory.

Flasche, L.H., and H.S. Ahluwalia. 1993. Localized corrosion of the unmixed zone in nickel-base alloy weldments. *Proceedings of the 12th International Corrosion Congress.* Houston, TX: NACE International: 4: 2,907–2,925.

Flis, J. 1979. Stress corrosion cracking of Armco iron in phosphate solutions. *Corrosion Science* 19: 151–164.

Ford, F.P. 1983. Stress corrosion cracking of iron-base alloys in aqueous environments. *Treatise on Materials Science and Technology Volume 25. Embrittlement of Engineering Materials.* C.L. Briant and S.K. Banerji, eds. New York, NY: Academic Press: 235–274.

Ford, T.E., P.C. Searson, T. Harris, and R. Mitchell. 1990. Investigation of microbiologically produced hydrogen permeation through palladium. *Journal of Electrochemical Society* 137(4): 1,175–1,179.

Gainer, L.J., and G.R. Wallwork. 1980. Effect of alloy element additions on the pitting corrosion of mild steel. *Corrosion* 36(7): 348–355.

Gangloff, R.P., and M.B. Ives, eds. 1990. *Environment Induced Cracking of Metals*. Houston, TX: NACE International.

Garofalo, F., and G.V. Smith. 1955. The effect of time and temperature on various mechanical properties during strain aging of normalized low carbon steels. *Transactions of the American Society for Metals* 47: 957–983.

Geesey, G. 1993. *A Review of the Potential for Microbially Influenced Corrosion of High-Level Nuclear Waste Containers*. CNWRA 93-014. San Antonio, TX: Center for Nuclear Waste Regulatory Analyses.

Gill, T.P.S., M. Vijayalakshmi, P. Rodriguez, and K.A. Padmanabhan. 1989. On microstructure-property correlation of thermally aged type 316L stainless steel weld metal. *Metallurgical Transactions A* 20A(6): 1,115–1,124.

Glass, R.S., G.E. Overturf, R.A. van Konynenburg, and R.D. McCright. 1986. Gamma radiation effects on corrosion—I. Electrochemical mechanisms for the aqueous corrosion processes of austenitic stainless steels relevant to nuclear waste disposal in tuff. *Corrosion Science* 26(8): 577–590.

Glassley, W.E. 1990. Geochemical Interactions. *Presentation to the Nuclear Waste Technical Review Board. January 18–19, 1990.* Livermore, CA: Lawrence Livermore National Laboratory.

Gordon, G.M. 1977. Physical metallurgy of Fe-Cr-Ni alloys. *Stress Corrosion Cracking and Hydrogen Embrittlement of Iron Base Alloys*. R.W. Staehle, J. Hochman, R.D. McCright, and S.E. Slater, eds. Houston, TX: NACE International: 893–945.

Hack, H.P. 1982. Crevice corrosion behavior of 45 molybdenum-containing stainless steels in seawater. Paper No. 65. *CORROSION/82*. Houston, TX: NACE International.

Hack, H.P., and D.W. Taylor. 1979. Seawater corrosion of fasteners in various structural materials. *Reviews on Coatings and Corrosion*. Tel-Aviv, Israel: Scientific Publications Division, Freund Publication House: 177–210.

Hart, P.H.M., and A.R. Jones. 1982. The prediction of safe welding conditions for C-Mn steels. *Current Solutions to Hydrogen Problems in Steels*. C.G. Interrante and G.M. Pressouyre, eds. Materials Park, OH: ASM International: 137–141.

Helie, M., and G. Plante. 1986. HLW container corrosion in geological disposal conditions. *Symposium Proceedings of Scientific Basis for Nuclear Waste Management IX*. L.O. Werme, ed. Pittsburgh, PA: Materials Research Society: 50: 445–452.

Heubner, U., and M. Köhler. 1992. Das zeit-temperatur-ausscheidungs- und das zeit-temperatur-sensibilisierungs-verhalten von hochkorrosions beständigen nickel; -chrom-molybdän-legierungen. *Werkstoffe und Korrosion* 43: 181–190.

Hickling, J., and D. Blind. 1986. Strain-induced corrosion cracking of low-alloy steels in LWR systems—Case histories and identification of conditions leading to susceptibility. *Nuclear Engineering and Design* 91: 305–330.

Hicks, P.D., and C.J. Altstetter. 1992. Hydrogen-enhanced cracking of superalloys. *Metallurgical Transactions* 23A: 237–249.

Hoar, T.P., and J.R. Galvele. 1970. Anodic behavior of mild steel during yielding in nitrate solutions. *Corrosion Science* 10: 211–224.

Hodge, F.G., and R.W. Kirchner. 1976. An improved Ni-Cr-Mo Alloy for corrosion service. *Corrosion* 32(8): 332–336.

Hodge, F.G., and H.S. Ahluwalia. 1993. The influence of long-term low temperature aging on the performance of candidate high-nickel alloys for the nuclear waste repository. *Proceedings of the 12th International Corrosion Congress*. Houston, TX: NACE International 5B: 4,031–4,046.

Hollaway, W.R., R. Rozier, D.A. Nitti, and J.R. Williams. 1993. A multi-purpose unit concept to integrate storage, transportation, and the engineered barrier system. *Proceedings of the Fourth Annual International High-Level Radioactive Waste Management Conference.* La Grange Park, IL: American Nuclear Society: 1: 824–831.

Hurst, P., P. Banks, G. Pemberton, and A.S. Raffel. 1986. Stress corrosion behavior of A533B and A508-III steels and weldments in high temperature water environments. *Proceedings of the Second International Symposium on Environmental Degradation of Materials in Nuclear Power Systems—Water Reactors*. La Grange Park, IL: American Nuclear Society: 645–656.

Interrante, C.G., and G.M. Pressouyre, eds. 1982. *Current Solutions to Hydrogen Problems in Steels.* Materials Park, OH: ASM International.

Isaacs, H.S. 1987. The pitting of iron in dilute chloride and sulfate solutions. *Advances in Localized Corrosion: Proceedings of the Second International Conference on Localized Corrosion.* H.S. Isaacs, U. Bertocci, J. Kruger, and S. Smialowska, eds. Houston, TX: NACE International: 221–226.

Ives, M.B., and S.C. Srivastava. 1987. Nonmetallic inclusions as sites for the initiation of localized corrosion in steels. *Advances in Localized Corrosion: Proceedings of the Second International Conference on Localized Corrosion.* H.S. Isaacs, U. Bertocci, J. Kruger, and S. Smialowska eds. Houston, TX: NACE International: 295–302.

Jaske, C.E., and V.N. Shah. 1989. Life assessment procedure for LWR cast stainless steel components. *Proceedings of the Fourth International Symposium on Environmental Degradation of Materials in Nuclear Power Systems—Water Reactors*. D. Cubicciotti, ed. Houston, TX: NACE International: 3-66–3-83.

Jenkins, L.R., and R.D. Forrest. 1990. Ductile iron, in properties and selection: Irons, steels, and high-performance alloys. *ASM Handbook*. Metals Park, OH: ASM International: 1(10).

Jurek, J., and Z. Szklarska-Smialowska. 1976. Susceptibility of the oxide film formed on steel in air at 100–400 °C to local breakdown in borate buffer solutions containing Cl^- anions. *Corrosion* 32(8): 309–312.

Kain, R.M. 1993. Seawater testing to assess the crevice corrosion resistance of stainless steels and related alloys. *Proceedings of the 12th International Corrosion Congress*. Houston, TX: NACE International 3B: 1,889–1,900.

Kargol, J.A., and B. Ladna. 1982. The roles of ordering and impurity segregation on the hydrogen assisted crack propagation in nickel base alloys. *Scripta Metallurgica* 16: 191–195.

Kerrisk, J.F. 1987. *Groundwater Chemistry at Yucca Mountain, Nevada, and Vicinity*. LA-10929-MS. Los Alamos, NM: Los Alamos National Laboratory.

Kim, I.S., and S.S. Kang. 1993. Temperature and loading rate dependence of deformation and fracture characteristics of the SA508 pressure vessel steel in the upper shelf region. *Proceedings of the Sixth International Symposium on Environmental Degradation of Materials in Nuclear Power Systems—Water Reactors*. R.E. Gold and E.P. Simonen, eds. Pittsburgh, PA: The Minerals, Metals, and Materials Society (TMS): 139–144.

Kim, Y.J., and R.A. Oriani. 1987. Corrosion properties of the oxide film formed on grade 12 titanium in brine under gamma radiation. *Corrosion* 43(2): 85–97.

Klein, H.J., C.R. Brooks, and E.E. Stansbury. 1970. The establishment of long-range order in Ni_2Cr using electron microscopy. *Physica Status Solidi* 38: 831–836.

Knauss, K.G., T.J. Wolery, and K.J. Jackson. 1990. A new approach to measuring pH in brines and other concentrated electrolytes. *Geochimica et Cosmochimica Acta* 54: 1,519–1,523.

Kolts, J. 1982. Temperature limits for stress corrosion cracking of selected stainless steels and nickel-base alloys in chloride-containing environments. Paper No. 241. *CORROSION/82*. Houston, TX: NACE International.

Kolts, J., J. Murali, and M.W. Joosten. 1987. Polarization behavior of steel and selected corrosion-resistant alloys in laboratory environments containing CO_2. *Advances in Localized Corrosion: Proceedings of the Second International Conference on Localized Corrosion*. H.S. Isaacs, U. Bertocci, J. Kruger, and S. Smialowska, eds. Houston, TX: NACE International: 453–458.

Kosaki, A., and H. Komada. 1993. Corrosion life-time assessment of carbon steel and stainless alloys for geological disposal facility. *Proceedings of the Fourth Annual International High-Level Radioactive Waste Management Conference*. La Grange Park, IL: American Nuclear Society 1: 1,754–1,760.

Kowaka, M. 1990. *Metal Corrosion Damage and Protection Technology*. New York, NY: Allerton Press: 149–287.

Laliberté, L.H., and A. Garner. 1981. Corrosion protection of bleach plant washers by electrochemical potential control. *Tappi, The Journal of the Technical Association of Pulp and Paper Industry* 64(1): 47–51.

Langelier, W.F. 1936. The analytical control of anti-corrosion water treatment. *Journal of the American Water Works Association* 1,500–1,521.

Larson, F.R., and J. Miller. 1952. A time temperature relationship for rupture and creep stresses. *Transactions of the American Society Mechanical Engineers* 74: 765–771.

Latanision, R.M., and R.W. Staehle. 1969. Stress corrosion cracking of iron-nickel-chromium alloys. *Fundamental Aspects of Stress Corrosion Cracking*. R.W. Staehle, A.J. Forty, and D. van Rooyen, eds. Houston, TX: NACE International: 214–300.

Legault, R.A., and A.G. Preban. 1975. Kinetics of the atmospheric corrosion of low-alloy steels in an industrial environment. *Corrosion* 31(4): 117–122.

Lehman, L.P., and T.H. Kosel. 1985. The influence of phosphorus on the kinetics of ordering in Ni_2Cr. *High-Temperature Ordered Intermetallic Alloys*. C.C. Koch, C.T. Liu, and N.S. Stoloff, eds. Pittsburgh, PA: Materials Research Society 39: 147–154.

Lenz, E., and N. Wieling. 1986. Strain-induced corrosion cracking of low-alloy steels in LWR systems—Interpretation of susceptibility by means of a three dimensional (T, ϵ, dissolved oxygen) diagram. *Nuclear Engineering and Design* 91: 331–344.

Leslie, W.C. 1961a. The quench-aging of low-carbon iron and iron-manganese alloys: An electron transmission study. *Acta Metallurgica* 9: 1,004–1,022.

Leslie, W.C. 1961b. The control of annealing texture by precipitation in cold-rolled iron. *Transactions of American Institute of Mining. Metallurgical and Petroleum Engineers (AIME)* 221: 752–758.

Liu, S., and J.E. Indacochea. 1990. Weldability of steels, in properties and selection: Irons, steels, and high-performance alloys. *ASM Handbook*. Metals Park, OH: ASM International: 1(10).

Luo, J.L., Y.C. Lu, and M.B. Ives. 1992. The use of microelectrodes to determine the local conditions within active pits. Paper No. 233. *CORROSION/92*. Houston, TX: NACE International.

Magdowski, R.M., and M.O. Speidel. 1988. Clean steels for steam turbine rotors—their stress corrosion cracking resistance. *Metallurgical Transactions A* 19A: 1,583–1,596.

Marsh, G.P., K.J. Taylor, I.D. Bland, C. Westcott, P.W. Tasker, and S.M. Sharland. 1985. Evaluation of the localized corrosion of carbon steel overpacks for nuclear waste disposal in granite environments. *Symposium Proceedings of Scientific Basis for Nuclear Waste Management IX.* L.W. Werme, ed. Pittsburgh, PA: Materials Research Society: 59: 421–428.

Marsh, G.P., I.D. Bland, and K.J. Taylor. 1988. Statistical study of pit propagation in carbon steel under nuclear waste disposal conditions. *British Corrosion Journal* 23: 157–164.

Masaoka, I., I. Takase, and S. Ikeda. 1982. Criteria for hydrogen attack of 1/2Mo steel and Cr-Mo steel weldments at high temperature and pressure. *Current Solutions to Hydrogen Problems in Steels.* C.G. Interrante and G.M. Pressouyre, eds. Materials Park, OH: ASM International: 249–255.

Matthews, S.J. 1976. *Thermal Stability of Solid Solution Strengthened High Performance Alloys.* Report No. 8979. Kokomo, IN: Haynes International, Inc.

McCright, R.D. 1988. *An Annotated History of Container Candidate Material Selection.* UCID-21472. Livermore, CA: Lawrence Livermore National Laboratory.

McCright, R.D., and H. Weiss. 1985. Corrosion behavior of carbon steels under tuff repository environmental conditions. *Symposium Proceedings of Scientific Basis for Nuclear Waste Management VIII.* C.M. Jantzen, J.A. Stone, and R.C. Ewing, eds. Pittsburgh, PA: Materials Research Society: 44: 287–294.

McCuen, R.H., and P. Albrecht. 1994. Composite modeling of atmospheric corrosion penetration data. *Application of Accelerated Corrosion Tests to Service Life Prediction of Materials.* ASTM STP 1194. G. Cragnolino and N. Sridhar, eds. Philadelphia, PA: American Society for Testing and Materials: 65–102.

McKubre, M.C.H., S.C. Leach, and L.E. Eiselstein. 1983. *Crevice Corrosion of Lattice Support Alloys in Secondary Environments of Nuclear Steam Generators.* EPRI NP-3045. Palo Alto, CA: Electric Power Research Institute.

McLean, D. 1958. *Grain Boundaries in Metals.* Oxford, England: Clarendon Press.

Misawa, T., T. Kyuno, W Suetaka, and S. Shimodaira. 1971. The mechanism of rusting and the effect of Cu and P on the rust formation of low alloy steels. *Corrosion Science* 11: 35–48.

Mishra K.G., and C.R. Das. 1987. Corrosion of welded steel specimens in industrial steel plant atmospheres. *British Corrosion Journal* 22(3): 195–198.

Mizuno, T., S. Pednekar, Z. Szklarska-Smialowska, and D.D. Macdonald. 1984. Corrosion and stress corrosion cracking of carbon steels in oxygenated, high purity water at elevated temperatures. *Proceedings of the International Symposium on Environmental Degradation of Materials in Nuclear Power Systems—Water Reactors.* Houston, TX: NACE International: 395–422.

Moody, N.R., and A.W. Thompson, eds. 1990. *Hydrogen Effects on Materials Behavior.* Warrendale, PA: The Minerals, Metals & Materials Society.

NACE International. 1993. *Use of Corrosion Resistant Alloys for Resistance to Environmental Cracking in Oilfield Environments*. Draft NACE Publication 1F192. Houston, TX: NACE International.

Nakayama, G., and M. Akashi. 1992a. The critical condition for the initiation of localized corrosion of mild steels in contact with bentonite used for nuclear waste package. *Symposium Proceedings of Scientific Basis for Nuclear Waste Management XV*. C.G. Sombret, ed. Pittsburgh, PA: Materials Research Society: 257: 415–422.

Nakayama, G., and M. Akashi. 1992b. Critical conditions for initiation of localized corrosion of mild steels in contact with bentonite used in geological disposal packages of nuclear waste. *Symposium Proceedings of Scientific Basis for Nuclear Waste Management XVI*. C.G. Interrante and R.T. Pabalan, eds. Pittsburgh, PA: Materials Research Society: 294: 329–334.

Nelson, G.A. 1949. Hydrogenation Plant Steels. *Proceedings of the American Petroleum Institute* 29M(III): 163–172.

Nelson, G.A. 1965. Operating limits and incubation times for steel in hydrogen service. *Proceedings of the American Petroleum Institute* 45M(III): 190–195.

Nelson, G.A. 1966. When to use low alloy steel for hydrogen service. *Hydrocarbon Proceedings* 45(5): 201–204.

Nelson, J.L., R.E. Westerman, and F.S. Gerber. 1984. Irradiation-corrosion evaluation of metals for nuclear waste package applications in grande ronde basalt groundwater. *Symposium Proceedings of Scientific Basis for Nuclear Waste Management VII*. G.L. McVay, ed. Pittsburgh, PA: Materials Research Society: 26: 121–128.

Newhouse, D.L. 1972. *Temper Embrittlement of Alloy Steels*. ASTM STP 499. Philadelphia, PA: American Society for Testing and Materials.

Okayama, S., Y. Uesugi, and S. Tsujikawa. 1987. The effect of alloying elements on the repassivation potential for crevice corrosion of stainless steels in 3% NaCl solution. *Corrosion Engineering* 36: 157–168.

Ondrejcin, R.S. 1979. Stress corrosion cracking test with slow strain rate and constant current. *Stress Corrosion Cracking—The Slow Strain Rate Technique*. ASTM STP 665. G.M. Ugiansky and J.H. Payer, eds. Philadelphia, PA: American Society for Testing and Materials: 203–221.

Ondrejcin, R.S., S.P., Rideout, and J.A. Donovan. 1979. Control of stress corrosion cracking in storage tanks containing radioactive waste. *Nuclear Technology* 44: 297–306.

Oriani, R.A., J.P. Hirth, and M. Smialowski, eds. 1985. *Hydrogen Degradation of Ferrous Alloys*. Park Ridge, NJ: Noyes Publications.

Oversby, V.M. 1985. *The Reaction of Topopah Spring Tuff with J-13 Water at 150 °C—Samples from Drill Cores USW G-1, USW GU-3, USW G-4, and UE-25h#1*. UCRL-53629. Livermore, CA: Lawrence Livermore National Laboratory.

Pabalan, R.T., and W. Murphy. 1991. Geochemical modeling. *Report on Research Activities for Calendar Year 1990.* W.C. Patrick, ed. NUREG/CR-5817. Washington, DC: Nuclear Regulatory Commission: 2-24–2-25.

Parkins, R.N. 1975a. Stress corrosion cracking of ferritic steels. *NATO Advanced Study Institute on Stress Corrosion Cracking*. Copenhagen, Denmark: North Atlantic Treaty Organization: 1–26.

Parkins, R.N. 1975b. Inhibition of structurally dependent localized corrosion processes. *Proceedings of the Fourth European Symposium on Corrosion Inhibitors*. Ferrara, Italy: University of Ferrara: 595–614.

Parkins, R.N. 1977. Environmental aspects of stress corrosion cracking in low strength ferritic steels. *Stress Corrosion Cracking and Hydrogen Embrittlement of Iron Base Alloys*. R.W. Staehle, J. Hochman, R.D. McCright, and J.E. Slater, eds. Houston, TX: NACE International: 601–624.

Parkins, R.N. 1980. Predictive approaches to stress corrosion cracking failure. *Corrosion Science* 20: 147–166.

Parkins, R.N. 1985. Prevention and control of stress corrosion cracking—An overview. Paper No. 348. *CORROSION/85*. Houston, TX: NACE International.

Parkins, R.N., and R. Usher. 1962. The effect of nitrate solutions in producing stress corrosion cracking in mild steel. *Proceedings First International Congress on Metallic Corrosion*. London, U.K.: Butterworths: 296–302.

Parkins, R.N., P.W. Slattery, W.R. Middleton, and M.J. Humphries. 1973. Effects of quenching and tempering upon the stress corrosion cracking of ferritic steels. *British Corrosion Journal* 8: 117–123.

Parkins, R.N., N.J.H. Holroyd, and R.R. Fessler. 1978. Stress corrosion cracking of C-Mn steel in phosphate solutions. *Corrosion* 34: 253–262.

Parkins, R.N., P.W. Slattery, and B.S. Poulson. 1981. The effects of alloying additions to ferritic steels upon stress corrosion cracking resistance. *Corrosion* 37: 650–664.

Patrick, W.C. 1986. *Spent Fuel Test—Climax: An Evaluation of the Technical Feasibility of Geologic Storage of Spent Nuclear Fuel in Granite*. Final Report UCRL-53702. Livermore, CA: Lawrence Livermore National Laboratory.

Payer, J.H., W.E. Berry, and R.N. Parkins. 1979. Application of slow strain rate technique to stress corrosion cracking of pipeline steel. *Stress Corrosion Cracking. The Slow Strain Rate Technique*. G.M. Ugiansky and J.H. Payer, eds. ASTM STP 665. Philadelphia, PA: American Society for Testing and Materials: 222–234.

Phillips, V.A. 1963. An electron microscopic study of quench-aging and strain aging in a dilute Fe-C-N alloy. *Transactions of the American Society for Metals*. 56: 600–617.

Pitman, S.G. 1987. Evaluation of the susceptibility of ASTM A216 Grade WCA mild steel to stress corrosion cracking in simulated salt repository environments. *Symposium Proceedings of Scientific Basis for Nuclear Waste Management X.* J.K. Bates and W.B. Seefeldt, eds. Pittsburgh, PA: Materials Research Society: 84: 239–249.

Postlethwaite, J., R.J. Scoular, and M.H. Dobbin. 1988. Localized corrosion of molybdenum-bearing nickel alloys in chloride solutions. *Corrosion* 44(4): 199–203.

Poulson, B.S., and R.N. Parkins. 1973. Effects of Ni additions upon the stress corrosion of ferritic steels in a chloride environment. *Corrosion* 29: 414–422.

Pourbaix, M. 1974. *Atlas of Electrochemical Equilibria in Aqueous Solutions*. Houston, TX: NACE International.

Pruthi, D.D., M.S. Anand, and R.P. Agarwala. 1977. Diffusion of chromium in Inconel 600. *Journal of Nuclear Materials* 64: 206–210.

Pyun, S.I., C. Lim, and R.A. Oriani. 1992. The role of hydrogen in the pitting of passivating films on pure iron. *Corrosion Science* 33(3): 437–444.

Raghavan, M., B.J. Berkowitz, and J.C. Scanlon. 1981. Analytical microscopic analysis of precipitates in hastelloy alloy C-276. *39th Annual Meeting of the Electron Microscopy Society of America.* G.W. Bailey, ed. Baton Rouge, LA: Claitor's Publishing Division: 280–281.

Raghavan, M., B.J. Berkowitz, and J.C. Scanlon. 1982. Electron microscopic analysis of heterogeneous precipitates in Hastelloy C-276. *Metallurgical Transactions A* 13A: 979–984.

Ravindran, K., and A.G. Gopalakrishna Pillai. 1984. Observations of the inter-relation of marine corrosion and fouling in a tropical environment. *Marine Corrosion and Fouling, Marine Biology, 6th International Congress*. Athens, Greece: National Technical University of Athens: 6: 370–383.

Reed, D.T., and R.A. van Konynenburg. 1990. Progress in evaluating the corrosion of candidate high-level waste container metals in irradiated air-steam mixtures. *Proceedings of the Topical Meeting on Nuclear Waste Packaging—Focus '91*. La Grange Park, IL: American Nuclear Society: 185–192.

Reed, D.T., and R.A. van Konynenburg. 1991. Corrosion of copper-based materials in irradiated moist-air systems. *Symposium Proceedings of Scientific Basis for Nuclear Waste Management XIV.* T.A. Abrajano, Jr. and L.H. Johnson, eds. Pittsburgh, PA: Materials Research Society 212: 317–325.

Sasaki, N., H. Ishikawa, T. Teshima, and K. Fujiwara. 1992. Effects of dissolved oxygen content on the propagation of localized corrosion of carbon steel in synthetic seawater. *Mechanical Behavior of Materials—VI.* New York, NY: Pergamon Press: 627–632.

Schumaker, M., ed. 1979. *Seawater Corrosion Handbook.* Parkridge, NJ: Noyes Data Corporation.

Schwartzkopf, W., E. Smialos, and R. Koster. 1992. *In-situ* corrosion on cast-steel high-level waste containers plated with titanium/nickel alloys. *Symposium Proceedings of Scientific Basis for Nuclear Waste Management XV.* C.G. Interrante and R.T. Pabalan, eds. Pittsburgh, PA: Materials Research Society: 257: 423–430.

Scully, J.R., and H.P. Hack. 1984. Galvanic corrosion prediction using long and short term polarization curves. Paper No. 34. *CORROSION/84.* Houston, TX: NACE International.

Sedriks, A.J. 1992. Stress-corrosion cracking of stainless steels. *Stress-Corrosion Cracking. Materials Performance and Evaluation.* R.H. Jones, ed. Materials Park, OH: ASM International: 91–130.

Shalaby, H.M., S. Attari, W.T. Riad, and V.K. Gouda. 1992. Erosion-corrosion behavior of some cast alloys in seawater. *Corrosion* 48(3): 206–217.

Shastry, C.R., J.J. Friel, and H.E. Townsend. 1988. Sixteen-year atmospheric corrosion performance of weathering steel in marine, rural, and industrial environments. *Degradation of Metals in the Atmosphere.* ASTM STP 965. S.W. Dean, Jr. and T.S. Lee, eds. Philadelphia, PA: American Society for Testing and Materials: 5–15.

Shaw, B.A., P.J. Moran, and P. Gartland. 1993. Crevice corrosion of a nickel-based superalloy in natural and chlorinated seawater. *Proceedings of the 12th International Corrosion Congress.* Houston, TX: NACE International 3B: 1,915–1,928.

Shewmon, P.G. 1976. Hydrogen attack of carbon steel. *Metallurgical Transactions* 7A: 279–286.

Short, D.W., D.L. Ruffner, and L.J. Jardine. 1992. Engineered barrier system and waste package design concepts for a potential geologic repository at Yucca Mountain. *Proceedings of the Topical Meeting on Nuclear Waste Packaging—Focus'91.* La Grange Park, IL: American Nuclear Society: 113–124.

Simpson, J.P., R. Schenk, and B. Knecht. 1985. Corrosion rate of unalloyed steels and cast irons in reducing granitic groundwaters and chloride solutions. *Symposium Proceedings of Scientific Basis for Nuclear Waste Management IX.* L.W. Werme, ed. Pittsburgh, PA: Materials Research Society: 50: 429–436.

Smialos, E., W. Schwartzkopf, R. Koster, B. Fiehn, and G. Halm. 1990. *Corrosion Testing of Selected Packaging Materials for Disposal of High-Level Waste Glass in Rock Salt Formations.* KfK 4723 (EUR–13672). Karlsruhe, Germany: Kernforschungszentrum Krlsruhe GmbH.

Smith, J.J., and R.A. Farrar. 1993. Influence of microstructure and composition on mechanical properties of some AISI 300 series weld metals. *International Materials Reviews* 38(1): 25–51.

Sorensen, N.R., and M.A. Molecke. 1992. Summary of the WIPP materials interface interactions test—Metal corrosion. *Workshop on In-situ Tests on Radioactive Waste Forms and Engineered Barriers. Corsendok. Belgium.* SAND92–1921C. Albuquerque, NM: Sandia National Laboratories.

Speidel, M.O. 1981. Stress corrosion cracking of stainless steels in NaCl solutions. *Metallurgical Transactions A* 12A: 779–789.

Speidel, M.O., and R.M. Magdowski. 1988. Stress corrosion cracking of nuclear reactor pressure vessel and piping steels. *International Journal of Pressure Vessels and Piping* 34: 119–142.

Speller, F.N. 1951. *Corrosion, Causes and Prevention.* 3rd Edition. New York, NY: McGraw-Hill.

Spinks, J.W.T., and R.J. Woods. 1990. *Introduction to Radiation Chemistry.* 3rd Edition. New York, NY: John Wiley & Sons.

Sridhar, N., and G.A. Cragnolino. 1992. Stress-corrosion cracking of nickel-base alloys. *Stress-Corrosion Cracking. Materials Performance and Evaluation.* R.H. Jones, ed. Materials Park, OH: ASM International: 131–179.

Sridhar, N., and G.A. Cragnolino. 1993. Applicability of repassivation potential for long-term prediction of localized corrosion of alloy 825 and type 316L stainless steel. *Corrosion* 49(11): 885–894.

Sridhar, N., and D.S. Dunn. 1994. Effect of applied potential on changes in solution chemistry inside crevices on type 304L stainless steel and alloy 825. Paper No. 347. *CORROSION/94.* Houston, TX: NACE International.

Sridhar, N., J.A. Kargol, and N.F. Fiore. 1980. Effect of low-temperature aging on hydrogen-induced crack growth in a nickel-base superalloy. *Scripta Metallurgica* 14: 1,257–1,260.

Sridhar, N., B.E. Wilde, C. Manfredi, S. Kesavan, and C. Miller. 1991. *Hydrogen Absorption and Embrittlement of Candidate Container Materials—I.* CNWRA 91-008. San Antonio, TX: Center for Nuclear Waste Regulatory Analyses.

Sridhar, N., J.C. Walton, G.A. Cragnolino, and P.K. Nair. 1993a. *Engineered Barrier System Performance Assessment Codes (EBSPAC) Progress Report—October 1, 1992, through September 25, 1993.* CNWRA 93-021. San Antonio, TX: Center for Nuclear Waste Regulatory Analyses.

Sridhar, N., G.A. Cragnolino, and D.S. Dunn. 1993b. *Experimental Investigations of Localized Corrosion of High-Level Waste Container Materials.* CNWRA 93-004. San Antonio, TX: Center for Nuclear Waste Regulatory Analyses.

Sridhar, G., J. Hong, Y. Zou, J.C. Britt, and K.L. Murty. 1993c. Dynamic strain aging and radiation effects in A490 Steel. *Proceedings of the Sixth International Symposium on Environmental Degradation of Materials in Nuclear Power Systems—Water Reactors.* R.E. Gold and E.P. Simonen, eds. Pittsburgh, PA: The Minerals, Metals, and Materials Society (TMS). 145–152.

Staehle, R.W. 1991. Combining design and corrosion for predicting life. *Life Prediction of Corrodible Structures.* R.N. Parkins, ed. Houston, TX: NACE International. To be published.

Staehle, R.W., J.J. Royuela, T.L. Raredon, E. Serrate, C.R. Morin, and R.W. Farrar. 1970. Effect of alloy composition on stress corrosion cracking of Fe-Cr-Ni base alloys. *Corrosion* 26: 451–486.

Staehle, R.W., J. Hochmann, R.D. McCright, and J.E. Slater, eds. 1977. *Stress Corrosion Cracking and Hydrogen Embrittlement of Iron Base Alloys*. Houston, TX: NACE International.

Stawström, C., and M. Hillert. 1969. An improved depleted-zone theory of intergranular corrosion of 18-8 stainless steel. *Journal of the Iron and Steel Institute* 207(1): 77–85.

Stephenson, E.T., and M. Cohen. 1961. The effect of prestraining and retempering on AISI type 4340. *Transactions of the American Society for Metals*. 54: 72–83.

Sundararajan, G., and P.G. Shewmon. 1980. The hydrogen attack of high strength low alloy steels. *Metallurgical Transactions* 11A: 509–516.

Sutcliffe, J.M., R.R. Fessler, W.K. Boyd, and R.N. Parkins. 1972. Stress corrosion cracking of carbon steel in carbonate solutions. *Corrosion* 28: 313–320.

Szklarska-Smialowska, Z. 1986. *Pitting Corrosion of Metals*. Houston TX: NACE International: 201–236.

Szklarska-Smialowska, Z., and J. Jurek. 1976. Ellipsometric studies on iron oxide film growth at 100–350 °C. *Corrosion* 32(7): 294–296.

Tawancy, H.M. 1981. Long-term aging characteristics of some commercial nickel-chromium-molybdenum alloys. *Journal of Materials Science* 16: 2,883–2,889.

Tawancy, H.M., R.B. Herchenroeder, and A.I. Asphahani. 1983. High-performance alloys of the Ni-Cr-Mo-W system. *Journal of Metals* 35: 37–43.

Telander, M.R., and R.E. Westerman. 1993. *Hydrogen Generation by Metal Corrosion in Simulated Waste Isolation Pilot Plant Environments: Progress Report for the Period November 1989 Through December 1992*. SAND92–7347. Albuquerque, NM: Sandia National Laboratories.

Thompson, N.G., and J.A. Beavers. 1990. Effect of groundwater composition on the electrochemical behavior of carbon steel: *A Statistical Experimental Study. Corrosion in Natural Waters*. ASTM STP 1086. C.H. Baloun, ed. Philadelphia, PA: American Society for Testing and Materials: 101–121.

Townsend, H.E., and J.C. Zoccola. 1982. Eight-year atmospheric corrosion performance of weathering steel in industrial, rural, and marine environments. *Atmospheric Corrosion of Metals*. ASTM STP 767. S.W. Dean, Jr. and E.C. Rhea, eds. Philadelphia, PA: American Society for Testing and Materials: 45–59.

Tsujikawa, S., A. Miyasaka, M. Ueda, S. Ando, T. Shibata, T. Haruna, M. Katahira, Y. Yamane, T. Aoki, and T. Yamada. 1993. Alternative for evaluating sour gas resistance of low-alloy steels and corrosion-resistant alloys. *Corrosion* 49: 409-419.

Tsujino, B., and S. Miyase. 1982. The galvanic corrosion of steel in sodium chloride solution. *Corrosion* 38(4): 226–230.

Turnbull, A. 1983. The solution composition and electrode potential in pits, crevices, and cracks. *Corrosion Science* 23(8): 833–870.

Turnbull, A., and M.K. Gardner. 1982. Electrochemical polarization studies of BS 4360 50D steel in 3.5% NaCl. *Corrosion Science* 22(7): 661–673.

Uhlig, H.H., and R.W. Revie. 1985. *Corrosion and Corrosion Control.* New York, NY: John Wiley and Sons.

U.S. Department of Energy. 1988. *Site Characterization Plan for the Yucca Mountain Site, Nevada Research and Development Area, Nevada.* DOE/RW–0199. Washington, DC: U.S. Department of Energy.

U.S. Department of Energy. 1993a. *MPC Implementation Program Conceptual Design Phase. Volume I—MPC Conceptual Design Summary Report.* DOC ID: A20000000–00811–5705–00001. WBS: 3.1.07. Washington, DC: U.S. Department of Energy, Office of Civilian Radioactive Waste Management.

U.S. Department of Energy. 1993b. *A Preliminary Evaluation of Using Multi-Purpose Canisters Within the Civilian Radioactive Waste Management System. Revision 0.* CRWMS M&O Document No. A00000000-AA-07-00002. Vienna, VA: TRW Environmental Safety Systems, Inc.

van Konynenburg, R.A. 1986. *Radiation Chemical Effects in Experiments to Study the Reaction of Glass in an Environment of Gamma-Irradiated Air, Groundwater, and Tuff.* UCRL-53719. Livermore, CA: Lawrence Livermore National Laboratory.

Van Luik, A., D. Stahl, and D. Harrison. 1993. Progress in waste package and engineered barrier system performance assessment and design. *Symposium Proceedings of Scientific Basis for Nuclear Waste Management XVI.* C.G. Interrante and R.T. Pabalan, eds. Pittsburgh, PA: Material Research Society: 294: 663–674.

Vatter, I.A., C.A. Hippsley, and S.G. Druce. 1993. Review of thermal ageing data and its application to operating reactor pressure vessels. *International Journal of Pressure Vessel and Piping* 54: 31–48.

Vitovec, F.H. 1982. Modeling of hydrogen attack of steel in relation to material and environmental variables. *Current Solutions to Hydrogen Problems in Steels.* C.G. Interrante and G.M. Pressouyre, eds. Materials Park, OH: ASM International: 236–241.

Walch, M., T.E. Ford, and R.Mitchell. 1989. Influence of hydrogen-producing bacteria on hydrogen uptake by steel. *Corrosion* 45(9): 705–709.

Walton, J.C. 1993. Effects of evaporation and solute concentration on presence and composition of water in and around the waste package at Yucca Mountain. *Waste Management* 13: 293–301.

Wei, R.P., and M. Gao. 1985. Chemistry, microstructure and crack growth response. *Hydrogen Degradation of Ferrous Alloys*. R.A. Oriani, J.P. Hirth, and M. Smialowski, eds. Park Ridge, NJ: Noyes Publications.

Weinstein, D. 1982. *BWR Environmental Cracking Margins for Carbon Steel Piping*. EPRI NP-2406. Palo Alto, CA: Electric Power Research Institute.

Weiss, B., and R. Stickler. 1972. Phase instabilities during high temperature exposure of 316 austenitic stainless steel. *Metallurgical Transactions A* 3A(4): 851–866.

Westerman, R.E., and S.G. Pittman. 1985. Corrosion of candidate iron-base waste package structural barrier materials in moist salt environments. *Symposium Proceedings of Scientific Basis for Nuclear Waste Management VIII*. C.M. Jantzen, J.A. Stone, and R.C. Ewing, eds. Pittsburgh, PA: Materials Research Society: 44: 279–285.

Westerman, R.E., J.L. Nelson, S.G. Pitman, and W.L. Kuhn. 1984. Evaluation of iron-base materials for waste package containers in a salt repository. *Symposium Proceedings of Scientific Basis for Nuclear Waste Management VII*. G.L. McVay, ed. Pittsburgh, PA: Materials Research Society 26: 427–436.

Westerman, R.E., J.H. Haberman, S.G. Pitman, and J.S. Perrin. 1986. Corrosion of iron-base waste package container materials in salt environments. *Proceedings of the 1986 Joint ASME/ANS Nuclear Power Conference, Session: High-Level Radioactive Waste Disposal and Storage Containers I*. La Grange Park, IL: American Nuclear Society: 174–178.

Westerman, R.E., S.G. Pitman, and J.H. Haberman. 1987. *Corrosion Testing of 304L Stainless Steel in Tuff Groundwater Environments*. UCRL-21005. Livermore, CA: Lawrence Livermore National Laboratory.

Wilde, M.H., and B.E. Wilde. 1993. Some observations on the mechanism of corrosion to be encountered in nuclear waste repositories located in tuffaceous rock. *Corrosion Science* 34(3): 433–443.

Williams, P.I., and R.G. Faulkner. 1987. Chemical volume diffusion coefficients for stainless steel corrosion studies. *Journal of Materials Science* 22: 3,537–3,542.

Wilson, D.V., and B. Russell. 1960. The contribution of precipitation in low carbon steels. *Acta Metallurgica* 8: 468–479.

Yunker, W.H. 1990. *Corrosion Behavior of Copper-base Materials in a Gamma-irradiated Environment, Final Report*. WHC-EP-0188. Richland, WA: Westinghouse Hanford Co.

Yurioka, N., and H. Suzuki. 1990. Hydrogen assisted cracking in C-Mn and low-alloy steel weldments. *International Materials Reviews* 35(4): 217–251.